POLITECNICO
MILANO 1863

SCUOLA DI INGEGNERIA INDUSTRIALE
E DELL'INFORMAZIONE

Executive Summary of the Thesis

CFD modeling of ammonia fueled internal combustion engines

Laurea Magistrale in Mechanical Engineering - Ingegneria Meccanica

Author: Davide Bonaiti

Advisor: prof. Tommaso Lucchini

Co-advisor: Andrea Schirru

Academic year: 2021-2022

1. Introduction

Every day politics and mass media talk about the climate change. One of the main cause of climate change is identified in the CO_2 emissions due to human activity, in particular activities linked to hydrocarbon fuels. Many alternative fuels have been proposed proposed as substitutes for hydrocarbon fuels. The most attractive alternative fuels are hydrogen and ammonia because of their null carbon content and because of their combustion without CO_2 emissions, as demonstrated in Equations (1)(2). Ammonia is more suitable than hydrogen as fuel for internal combustion engine (ICE) because of its low price and because ammonia production facilities, storage system and distribution infrastructure are more developed with respect to the ones of hydrogen.

$$2H_2 + 0_2 \Rightarrow 2H_2O + heat \quad (1)$$

$$4NH_3 + 30_2 \Rightarrow 2N_2 + 6H_2O + heat \quad (2)$$

Moreover, ammonia energy density is higher than the hydrogen one. Therefore, at constant energy amount, energy transport through ammonia is easier with respect to the use of hydrogen [1].
The use of ammonia as ICE fuel dates back to 1822 [2] but it was set aside over the years because of the propensity for gasoline and diesel. In fact, the use of ammonia features some challenges because of ammonia thermochemical properties. Ammonia is indeed considered as a non-flammable fluid because of its low cetane number, its high auto-ignition temperature and the large energy amount required for ammonia auto-ignition. After a short revival during the '60s [3], ammonia is back as a tool to reach the increasingly strict limitations for CO_2 emissions. Therefore the idea of ammonia as ICE fuel is not a total novelty but its applications is quite new for engine field: only a few experimental data are available and CFD modeling of ammonia combustion is at the beginning.
The implementation of ammonia as ICE fuel is tested for both spark ignition (SI) and compression ignition (CI) engines with acceptable performances [4][5]. However, CI engine features higher efficiency then SI engine then studies focus on CI applications for ammonia. The best solution for both overcoming the ignition problems of ammonia and exploiting the higher efficiency of CI engine consists in diesel dual fuel (DDF) engine: an injection of a fuel with high cetane number (e.g. diesel) ignites another fuel with low cetane number (e.g. methane, hydrogen or ammonia).

The purpose of this work is the simulation of ammonia combustion in DDF engines. Simulations employs the CFD tools developed by Politecnico di Milano and implemented in the Lib-ICE code, a library based on OpenFOAM. The CFD solvers were validated for many operating conditions, especially diesel and diesel-methane applications. However, this work makes such solvers face new operating conditions because they are tested for alternative fuels combustion.
This study focuses on two different ammonia DDF engines: the first case is an high pressure direct injection (HPDI) DDF engine with ammonia directly injected inside the cylinder; the second one is a DDF engine with port injection of ammonia. Different injections strategies lead to different combustion mode for ammonia: the first case features a diffusive combustion and the second case is characterized by a premixed combustion. Different computational strategies are then adopted for dealing with the two modes. The simulation of HPDI engine relies on the tabulated kinetics approach while an hybrid solver based on tabulated kinetics and Weller combustion model is adopted for the second case.

2. Tabulated kinetics approach for combustion modeling

The basic concept of tabulated kinetics model is to process results of auto-ignition calculations in a homogeneous reactor to generate lookup tables in which chemical composition and reaction rates are stored. This method relies on a chemical mechanism with thermochemical initial conditions specified by the user. Calculations are performed in a constant pressure homogeneous reactor for an user-defined range of thermochemical conditions [6][7].
The reaction rate $\dot{\omega}_i$ of chemical species i is defined in Equation (3), being Y_i the mass fraction of chemical species i, p the pressure value and T the temperature. The reaction rates are computed for each specified condition.

$$\frac{dY_i}{dt} = \dot{\omega}_i(Y_1, Y_2, \ldots, Y_n, p, T) \tag{3}$$

At each time step, two stages are performed:

1. the evaluation of progress variable C;
2. the computation of the chemical composition using the virtual species approach.

In this approach, the progress variable C is defined as the heat released by combustion. C is thus determined by Equation (4) as the difference between the current and the initial value of the reactor enthalpy of formation h_{298}. Equation (4) involves all the N_s chemical species included in the user-specified mechanism.

$$C = \sum_{i=1}^{N_s} h_{298,i} \cdot Y_i(t) - \sum_{i=1}^{N_s} h_{298,i} \cdot Y_i(0) \tag{4}$$

The definition of C for each time i is important because it is the variable that uniquely defines each thermochemical quantity and it is suitable for a transport equation. Once each reactor calculation has been performed, the chemical composition and the reaction rate related to the progress variable are stored in tables as function of the discrete values of the normalized progress variable c_i. During calculations, tables are updated with values of c, values of reaction rate and values of the chemical composition. The definition of c_i is specified in Equation (5), where C_{max} and C_{min} are respectively the maximum values of the progress variable C found after the auto-ignition event and the minimum value found at initial conditions.

$$c_i = \frac{C_i - C_{min}}{C_{max} - C_{min}} \tag{5}$$

To simplify the species storage and to gain tables characterised by an acceptable size, only seven species - called virtual species - are tabulated (N_2, O_2, $fuel$, CO_2, CO, H_2O, H_2) and their composition is obtained for any values of c.
During the CFD domain solution, the table is accessed when the transport equations are solved for mixture fraction, enthalpy, unburned gas temperature and for the progress variable. A simplified approach for modeling dual-fuel combustion assumes ignition as governed by local thermodynamic conditions and by the progress variable diffusion. Such approach relies on the use of separate tables for any fuel, without the need of intricate mechanism and with acceptable size tables.

3. Simulating premixed combustion with Weller model

After being port injected, a fuel diffuses in all the cylinder before its ignition caused by diesel

ignition. This dual fuel mode requires a computational approach able to manage the previous diffusive combustion of diesel plus the premixed combustion of ammonia. Such model relies on the one-equation Weller model [8].
The combustion model of Weller is founded on the solution of a transport equation for a combustion regress variable b, which helps numerical stability in flame propagation description. In addition, the model counts on an algebraic expression of the flame wrinkling factor Ξ to control the reaction rate. The ignition event is described through a deposition model, performing transition from laminar to turbulent using a semi-empirical model [9].
The regress variable b represents the unburned gas fraction in each computational cell. The b transport equation is obtained conditionally averaging the continuity equation on the unburned gas state.

$$\frac{\partial \rho \tilde{b}}{\partial t} + \nabla \cdot \left(\rho \tilde{\mathbf{U}} \tilde{b}\right) - \nabla \cdot \left(\mu_t \nabla \tilde{b}\right) = \tag{6}$$

$$= \rho_u \tilde{S}_u \tilde{\Xi} |\nabla \tilde{b}| + \dot{\omega}_{ign}$$

$$\Xi = \frac{S_t}{S_u} \tag{7}$$

$$\Sigma = \Xi |\nabla \tilde{b}| \tag{8}$$

being μ_t the turbulent viscosity, S_u the unstrained laminar flame speed, ρ and ρ_u the mixture and the unburned mixture density, $\dot{\omega}_{ign}$ is the ignition source term and $\rho_u \tilde{S}_u \tilde{\Xi} |\nabla \tilde{b}|$ is the reaction rate due to turbulent flame propagation. The flame wrinkling factor Ξ is the ratio between turbulent flame speed S_t and the unstrained one S_u, as defined in Equation (7). Equation (8) exposes the dependence between Ξ and the flame surface density Σ.
The regress variable b is set to 1 in any CFD cell until the combustion starts. This setup allows to solve fully implicitly the Equation (6), thanks to the exploitation of differential operator properties.

4. Simulation of high-pressure dual-fuel engine

The first engine case involves the experimental data gathered by Frankl et al.[10][11] by testing a full optical accessible single cylinder engine in Bowditch design, derived from a four strokes marine MTU 4000 diesel engine.
Tests are performed by fueling the engine with diesel-methane and diesel-hydrogen. The fuels are injected by a dual fuel injector produced by Woodward L'Orange, which can introduce independently inside the cylinder two fuels at high pressures, up to 1800 bar for the pilot fuel and maximum 500 bar for the main fuel. This injector has a quite complex geometry which allows to exploit engine symmetry to only three parts. The CFD domain includes three pilot injections and three injections of the main fuel. The injector holes diameters are computed using formulas available in literature [12].
A Lagrangian approach suits the diesel injection because it allows to consider the liquid flow as a discontinuity phase, with the flow fragmentation in many particles. After evaporation, diesel is considered as n-heptane because of their similar thermochemical properties. However, the Lagrangian approach is not suitable for a gaseous phase injection because the gaseous injected flow cannot be characterized as an heterogeneous flow of particles.

4.1. Virtual injector model

The alternative approach is found in the so-called virtual injector model. The basic concept of this injection modeling is the addition of a source term in the finite volume equation for a cells group defined by the user. The main advantage of this injection model is the possibility to keep into account all the physical phenomena involved in a gaseous flow, such as shock waves and under-expansions [13], and without simulating the flow inside the injector.
The cell group to implement the virtual injector model is specified by the user through the definition of a group of cells in the CFD domain. The correct cell group setup for this case is composed by three separated cell groups because this choice reduces some unexpected recirculation effects.

4.2. Diesel-methane simulation

First of all, diesel-only simulations are performed with the Representative Interactive Flamelet (RIF) approach to define some initial conditions: a lower compression ratio, equal to 15.5, and IVC pressure value fixed to 4.5 bar al-

low to fit the pressure value at the start of diesel injection in the diesel-methane case.
In the diesel-methane case, the injected masses are equal to 30 mg/cycle of diesel and 320 mg/cycle of methane. The dual-fuel simulation relies on the tabulated kinetics approach.

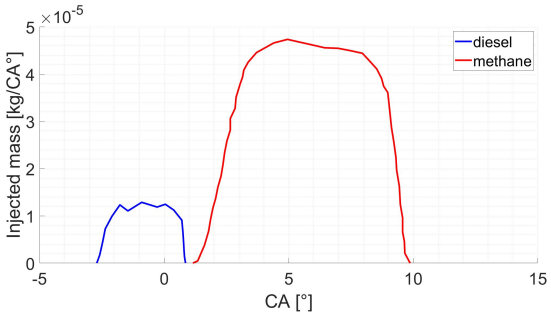

Figure 1: MTU 4000 diesel marine engine: diesel and methane injections laws

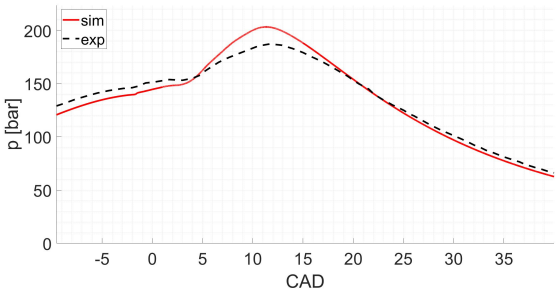

(a) Pressure curves: experimental and simulated.

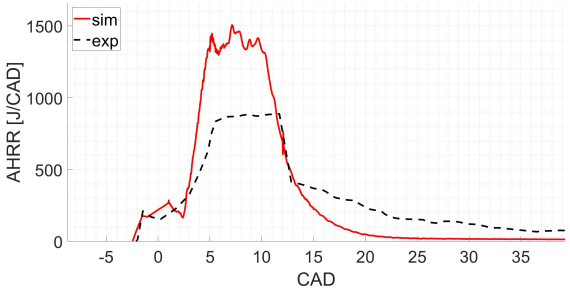

(b) AHRR curves: experimental and simulated.

Figure 2: Methane DDF simulation: pressure and AHRR.

The simulation setup for the diesel-methane configuration implies the adoption of three outer correctors to avoid some inaccuracies in the mass calculation. This setting has the drawback of long computational time, up to 120 hours.
Figure 2a presents a comparison between simulated pressure and experimental one. The results are good, despite a simulated pressure overestimation (around 8.5%). Figure 2b shows the experimental and the simulated apparent heat release rate (AHRR); both of them are calculated through a post-processing from pressure curves. Simulation present a faster combustion with respect to the experimental: simulated AHRR presents larger peak and a shape similar to the methane injection law, pointing out a almost instantaneous combustion for methane.

4.3. Diesel-hydrogen simulation

Simulation of diesel-hydrogen application is characterized by the lack of some injection data. First of all, the injected masses and the injection laws are not specified: masses are computed from the experimental AHRR curves available in literature [11]. In addition, the diesel injection law is assumed equal to the one of the previous diesel-methane case and the hydrogen injection law is calculated from SOI, injection pressure, masses and injector hole diameter.

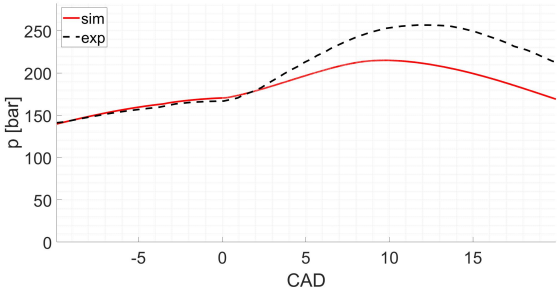

Figure 3: Hydrogen DDF simulation: simulated and experimental pressure curves.

Figure 3 shows simulated pressure curve: a too large underestimation (16%) is performed by simulation. New attempts are done with new assumptions about hydrogen injection parameters but there is no configuration able to match the experimental data: pressure is always overestimated by simulation. The error might depend on inaccuracies of hydrogen modeling or on some assumption about injection. However, the idea to validate the model using diesel-methane and diesel-hydrogen cases then simulate diesel-ammonia case in not feasible.

5. Diesel-ammonia simulation with premixed ammonia

The second case consists of a CAT 3401 engine fueled with diesel and port injected ammo-

nia. The experimental results are taken from the work done by Yousefi et al.[14]. Different conditions are tested: firstly various ammonia energy fractions (0%, 20% and 40%) then different starts of injection (SOI) are performed at ammonia energy ratio fixed to 40%. The ammonia energy fraction is defined as in Equation 9.

$$\%NH_3 = \frac{\dot{m}_{NH_3} \cdot LHV_{NH_3}}{\dot{m}_d \cdot LHV_d + \dot{m}_{NH_3} \cdot LHV_{NH_3}} \cdot 100 \quad (9)$$

The port injection of ammonia leads to a premixed-like combustion of ammonia that is ignited by the diesel combustion. A specific simulation solver is then adopted: after the modeling of diesel combustion with tabulated kinetics, the model switch to the Weller combustion model to perform calculations of ammonia premixed combustion.
The simulation with null ammonia energy fraction is performed by a RIF approach and it is useful to set some initial conditions. The compression ratio is fixed to 16.5 and the initial pressure is equal to 1.32 bar. This first simulation is characterized by a ignition delay too large to be related to a simulation error about diesel ignition. A delay of 8° CAD is then considered as hydraulic delay for all the conditions.

5.1. Simulations with different ammonia energy fractions

The first diesel-ammonia simulations are performed for cases with two different ammonia energy fractions (20% and 40%) and the results are very promising. Figure 4 and Figure 5 show the resulting pressure and AHRR curves.
Experimental pressure curves for both cases are matched quite well by simulations but a larger overestimation (up to 6%) is obtained for the case with 40% ammonia energy fraction. Despite this overestimation, the global result is acceptable for a first simulation with ammonia. Figure 5b suggests that combustion in simulated cases is slightly faster than experiment: at about 20-25° aTDC the experimental curve shows higher AHRR, meaning larger fuel quantity is still burning.
The pressure curves of the three different ammonia energy fractions are compared in Figure 6. The effects of the bad flammability properties of ammonia is detected because larger ammonia energy fractions (which means larger ammonia amount and less diesel mass) leads to longer ignition delay. Pressure peak of 0% and 40% ammonia cases are very similar but this fact is related to pressure overestimation of case with 40% ammonia.

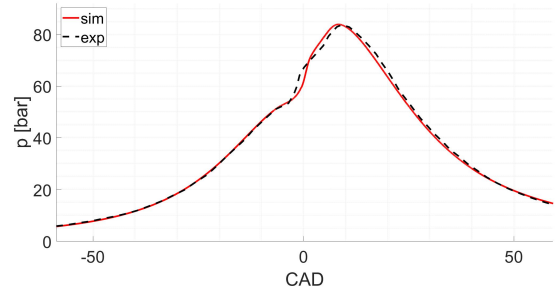

(a) Pressure curves: experimental and simulated.

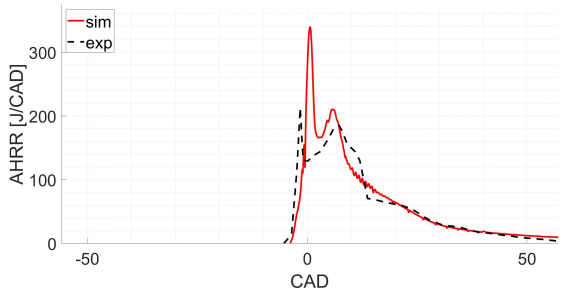

(b) AHRR curves: experimental and simulated.

Figure 4: CAT 3401: 20% ammonia energy fraction case.

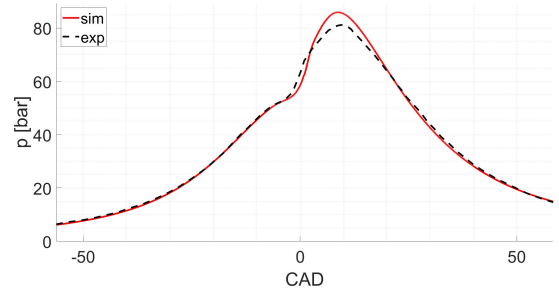

(a) Pressure curves: experimental and simulated.

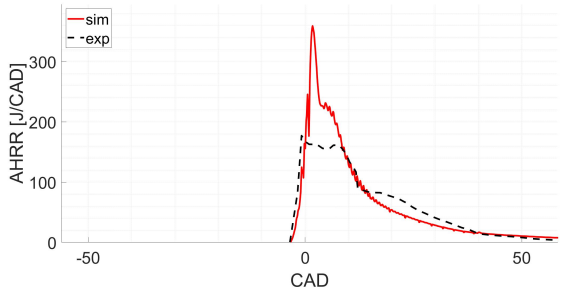

(b) AHRR curves: experimental and simulated.

Figure 5: CAT 3401: 40% ammonia energy fraction case.

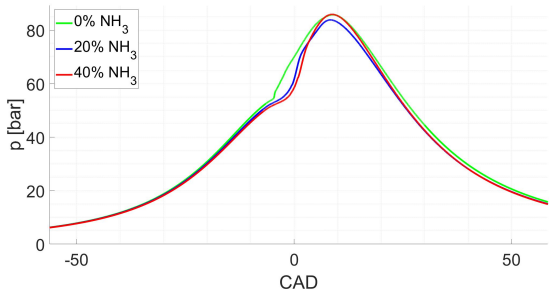

Figure 6: CAT 3401: simulated pressure curves for 0%,20% and 40% ammonia energy fraction cases.

The analysis of the combustion event shows a quite strange behaviour for both diesel-ammonia cases. The normalized progress variable c is adopted to represent the combustion event. With a focus on the 40% case, the transition from diffusive to premixed combustion ends at 0.855° aTDC. Just after the end of the transition, at 1° aTDC, a second ignition event happen near the injector, as shown in Figure 7.

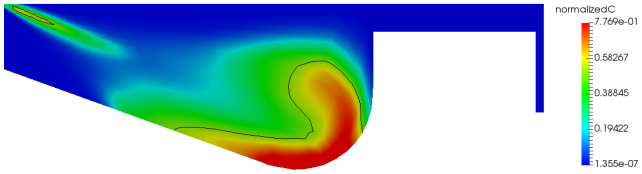

Figure 7: Normalized progress variable at 1° aTDC. A second ignition can be noticed near the injection hole. The dark line is $c = 0.5$.

5.2. Simulations with different SOI

Diesel-ammonia simulations are run at different diesel SOI with the ammonia energy ratio fixed to 40%. Simulations results are good because the experimental curves are generally well matched, as shown in Figure 8. More precisely, the peak pressure error, defined in Equation 10, generally decreases as the SOI is advanced (see Figure 9).

$$p_{error} = 100 \cdot \frac{max(p_{sim}) - max(p_{exp})}{max(p_{sim})} \quad (10)$$

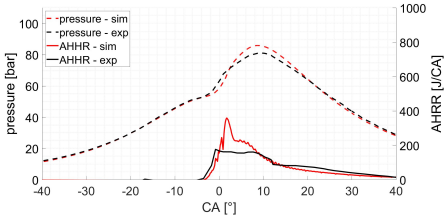

(a) SOI at 14.2° bTDC.

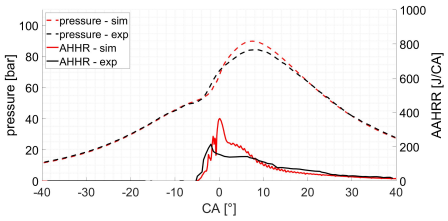

(b) SOI at 16° bTDC.

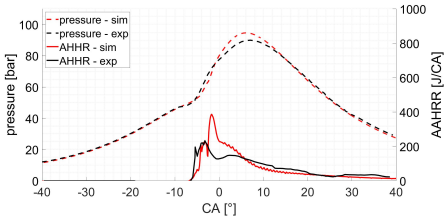

(c) SOI at 18° bTDC.

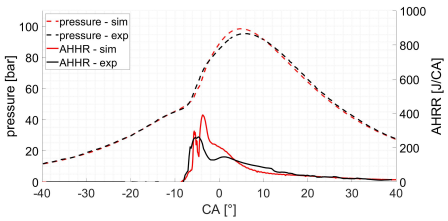

(d) SOI at 20° bTDC.

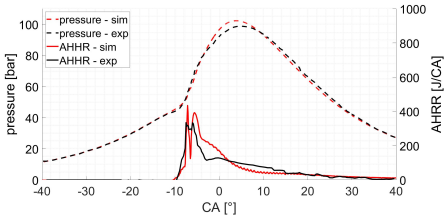

(e) SOI at 22° bTDC.

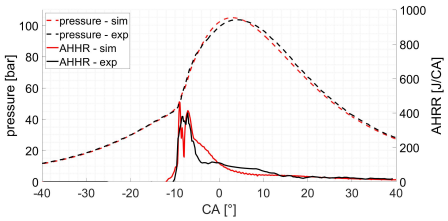

(f) SOI at 24° bTDC.

Figure 8: CAT 3401: SOI advancing.

In conventional diesel engine, advancing the SOI implies advanced start of combustion, higher cylinder peak pressure and higher efficiency because of better diesel-air premixing. This improvement of diesel, ammonia and air mixing as the SOI is advanced can be related to the peak pressure error decrease.
Figure 10 compares the trend of a gross efficiency computed for experimental tests and simulations: the generally increasing trend of efficiency as the SOI is advanced is matched also by the simulations.

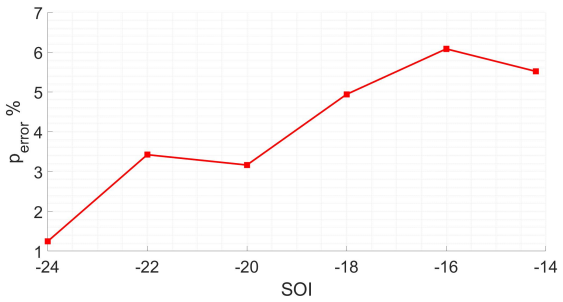

Figure 9: Pressure peak value error and corresponding SOI.

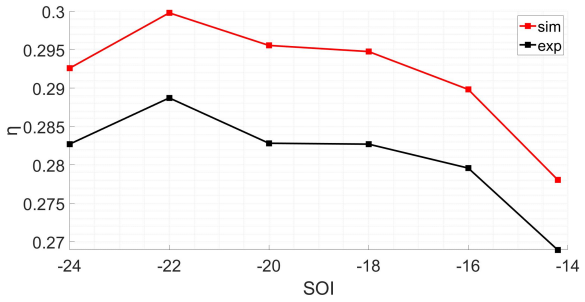

Figure 10: Gross efficiency values: experimental and simulated ones at corresponding SOI.

6. Conclusions

The purpose of this work is the simulation of diesel-ammonia combustion in internal combustion engines.
The first case relies on a four strokes marine MTU 4000 diesel engine, in dual fuel mode, with direct injection of each fuel. The simulations are carried out with the tabulated kinetics approach and the adopted model achieves good results for the diesel-methane case. Unfortunately, simulations for diesel-hydrogen mode cannot reach acceptable results. The case is then put aside because the diesel-ammonia simulation cannot rely on a reliable diesel-hydrogen simulation setup.
The second engine configuration is a Caterpillar 3401 diesel engine with port injection of ammonia and a diesel pilot injection. The resulting ammonia combustion is a premixed-like one and this combustion mode is modeled by the use of an hybrid model between the tabulated kinetics approach and the Weller combustion model. Different conditions are simulated: different ammonia energy inputs (0%, 20% and 40%) at constant total energy input and different diesel SOI at ammonia energy input fixed to 40%.
For a first attempt with a tough fuel such as ammonia, the simulations results are very promising. However, some aspects need further attention:

- Simulations match quite well the experimental data, with tiny differences in pressure curves. However, ignition event needs a deeper analysis because of the unexpected presence of two different premixed combustion events inside the cylinder, one of them close to the injector.
- The CFD solver behaves good in both 20% and 40% cases but simulation of the 40% ammonia case features a pressure overestimation larger than the 20% ammonia case. Further studies are required to understand how the ammonia percentage (then the ammonia quantity) affects the simulation of diesel-ammonia combustion and if the specific ammonia properties are accurately matched by the model.
- Higher efficiency is one of the main benefits of SOI advance. Simulations are able to detect this increasing trend.
- Diesel SOI advance improves the diesel mixing with the homogeneous ammonia-air mixture; it then leads to an higher pressure peak. The solver features smaller peak pressure error at longer SOI advance. Therefore, it should be useful to understand if a better mixing of diesel in an homogeneous ammonia-air mixtures affects the simulation reliability.
- A complete ammonia combustion analysis should involve also pollutant and GHG emissions to determine the best operating condition. This work does not include ex-

haust emissions analysis because of the time limitations of the project but it can be considered as a preliminary step. Analysis and simulation of exhaust emissions should be done in future.

References

[1] C. Zamfirescu and I. Dincer, "Ammonia as a green fuel and hydrogen source for vehicular applications," *Fuel Processing Technology*, vol. 90, no. 5, pp. 729–737, 2009. [Online]. Available: https://www.sciencedirect.com/science/article/pii/S0378382009000241

[2] J. S. Cardoso, V. Silva, R. C. Rocha, M. J. Hall, M. Costa, and D. Eusébio, "Ammonia as an energy vector: Current and future prospects for low-carbon fuel applications in internal combustion engines," *Journal of Cleaner Production*, vol. 296, p. 126562, 2021. [Online]. Available: https://www.sciencedirect.com/science/article/pii/S0959652621007824

[3] W. Cornelius, L. W. Huellmantel, and H. R. Mitchell, "Ammonia as an engine fuel," *SAE Transactions*, vol. 74, pp. 300–326, 1966. [Online]. Available: http://www.jstor.org/stable/44460524

[4] E. S. Starkman, H. K. Newhall, R. Sutton, T. Maguire, and L. Farbar, "Ammonia as a spark ignition engine fuel: Theory and application," *SAE Transactions*, vol. 75, pp. 765–784, 1967. [Online]. Available: http://www.jstor.org/stable/44563674

[5] E. S. Starkman, G. E. James, and H. K. Newhall, "Ammonia as a diesel engine fuel: Theory and application," *SAE Transactions*, vol. 76, pp. 3193–3212, 1968. [Online]. Available: http://www.jstor.org/stable/44562852

[6] T. Lucchini, G. D'Errico, A. Onorati, A. Frassoldati, A. Stagni, and G. Hardy, "Modeling non-premixed combustion using tabulated kinetics and different fame structure assumptions," *SAE International Journal of Engines*, vol. 10, no. 2, pp. 593–607, 2017. [Online]. Available: https://www.jstor.org/stable/26285068

[7] T. Lucchini, A. Della Torre, G. D'Errico, and A. Onorati, "Modeling advanced combustion modes in compression ignition engines with tabulated kinetics," *Applied Energy*, vol. 247, pp. 537–548, 2019. [Online]. Available: https://www.sciencedirect.com/science/article/pii/S0306261919307081

[8] L. Sforza, T. Lucchini, G. Gianetti, and G. D'Errico, "Development and validation of si combustion models for natural-gas heavy-duty engines," 09 2019.

[9] R. Herweg and R. R. Maly, "A fundamental model for flame kernel formation in s. i. engines," in *International Fuels & Lubricants Meeting & Exposition*. SAE International, oct 1992. [Online]. Available: https://doi.org/10.4271/922243

[10] S. Gleis, S. Frankl, D. Waligorski, M. Prager, and G. Wachtmeister, "Investigation of the high-pressure-dual-fuel (hpdf) combustion process of natural gas on a fully optically accessible research engine," 08 2019.

[11] S. Frankl, S. Gleis, S. Karmann, M. Prager, and G. Wachtmeister, "Investigation of ammonia and hydrogen as co2-free fuels for heavy duty engines using a high pressure dual fuel combustion process," *International Journal of Engine Research*, vol. 22, no. 10, pp. 3196–3208, 2021. [Online]. Available: https://doi.org/10.1177/1468087420967873

[12] G. Ferrari, *Motori a combustione interna*. Esculapio, 2016. [Online]. Available: https://books.google.it/books?id=UOoWxwEACAAJ

[13] Q. Zhou, "Brief review on direct gaseous fuel injection modeling," 2020.

[14] A. Yousefi, H. Guo, S. Dev, B. Liko, and S. Lafrance, "Effects of ammonia energy fraction and diesel injection timing on combustion and emissions of an ammonia/diesel dual-fuel engine," *Fuel*, vol. 314, p. 122723, 2022. [Online]. Available: https://www.sciencedirect.com/science/article/pii/S0016236121025886

POLITECNICO
MILANO 1863

SCUOLA DI INGEGNERIA INDUSTRIALE
E DELL'INFORMAZIONE

CFD modeling of ammonia fueled internal combustion engines

Tesi di Laurea Magistrale in
Mechanical Engineering - Ingegneria Meccanica

Author: **Davide Bonaiti**

Student ID: 944425
Advisor: prof. Tommaso Lucchini
Co-advisors: Andrea Schirru
Academic Year: 2021-22

Abstract

Ammonia is one of the main alternatives for a carbon-free energy future because of its thermo-chemical properties and its carbon-free characteristics. A partially substitution with ammonia of common fuels, for reducing CO_2 emissions in heavy-duty applications, relies on a deeper knowledge of ammonia combustion and on the development of new research tools. Higher efficiency is a basic requirement for lowering greenhouse gases (GHG) and pollutant emissions. Compression ignition (CI) engines are characterised by higher efficiency with respect to spark ignition (SI) engines, therefore future developments in alternative fuels field focus on CI engine. Because of bad flammability properties of ammonia, the most suitable solution to keep the CI benefits and to use ammonia is an ammonia diesel dual fuel (DDF) engine. This thesis work aims to simulate ammonia DDF combustion for internal combustion engine applications and to provide a better understanding of ammonia DDF engines performances. Simulations are performed by the use of CFD solvers developed by Politecnico di Milano for DDF applications and implemented in Lib-ICE code, a OpenFOAM based library developed by ICEGroup.
This work considers two engines: a MTU 4000 modified engine in high pressure direct injection (HPDI) configuration simulated by a tabulated kinetic approach and a CAT 3401 engine with port injected ammonia approached by the use of the Weller combustion model. Unfortunately, this first case encounters many problems during the initial condition setup and it is set aside. The second case is successful and the results are compared with some experimental data available in literature, with a focus on the engine performances and neglecting the exhaust gases emission analysis. Keeping the same total energy input, different conditions are simulated: the ammonia energy input is increased in three steps (0%, 20% and 40%) and, at 40%, the start of diesel injection (SOI) is advanced. The general result is very promising because pressure and apparent heat release rate (AHRR) curves are quite well matched. Future studies should be done to improve the model parameters, to understand the ignition event and to validate the model for exhaust emissions.

Keywords: internal combustion engines, CFD, OpenFoam, dual fuel engines, alternative fuels, ammonia.

Abstract in lingua italiana

L'ammoniaca è una delle proposte principali per un futuro energetico carbon-free grazie alle sue proprietà termochimiche e alla sua combustione senza emissioni di CO_2. Una maggiore conoscenza della combustione dell'ammoniaca e lo sviluppo di nuovi strumenti di ricerca sono la base per una parziale sostituzione dei combustibili fossili nelle applicazioni heavy-duty, al fine di ridurre le emissioni di CO_2. Un maggior rendimento è un requisito fondamentale per ridurre le emissioni di inquinanti e di gas serra e i motori ad accensione spontanea sono caratterizzati da un maggior rendimento rispetto ai motori ad accensione comandata. Per questa proprietà, le ricerce per futuri sviluppi si concentrano su questa tipologia. A causa della scarsa infiammabilità dell'ammoniaca, la soluzione più adatta per mantenere i benefici di un motore ad accensione spontanea alimentato con l'ammoniaca è una configurazione di tipo dual fuel diesel-ammoniaca.
Lo scopo di questa tesi è la simulazione della combustione diesel-ammoniaca in motori dual fuel. Per fare ciò, si avvale di due diversi risolutori CFD sviluppati dal Politecnico di Milano per applicazioni diesel-metano e implementati nel codice Lib-ICE, una libreria basata su OpenFOAM sviluppata dal gruppo di ricerca ICEGroup.
Due motori sono presi in considerazione: un motore derivato dal modello MTU 4000 con iniezione diretta di ammoniaca e un motore CAT 3401 con l'iniezione indiretta di ammoniaca. Purtroppo, il primo caso è abbandonato per alcuni problemi nella definizione delle condizioni iniziali. Il secondo caso, invece, ottiene risultati positivi che sono confrontati con dei dati sperimentali presenti in letteratura, concentrandosi soprattutto sulle prestazioni del motore. Diverse condizioni a pari input energetico sono simulate: vari input energetici legati all'ammoniaca (0%, 20% e 40%) e, al 40%, l'inizio dell'iniezione diesel è anticipato. I risultati ottenuti sono molto promettenti perchè le risultanti curve di pressione e di AHRR sono simili a quelle sperimentali. Studi più dettagliati rimangono tuttavia necessari per un raffinamento dei parametri del modello, per una completa comprensione dell'accensione e per uno studio delle emissioni dei gas di scarico.

Keywords: motori a combustione interna, CFD, OpenFoam, motori dual fuel, combustibili alternativi, ammoniaca.

Contents

Introduction

The transportation industry is one of the most important sector for the global economy: every day millions of people and goods travel all around the word ensuring the living standard of mankind. However, the transportation is mainly based on hydrocarbon fuels. This dependence makes transportation industry one of the main cause for the greenhouse effect, for the global warming and for other climate issues [1].
National governments and international treaties, e.g. the Paris Agreement, impose ever stricter limitation to the greenhouse gases (GHG) emissions to reduce effects of the global warming. The light-duty transportation industries are focusing on the electric vehicles to reduce GHG emissions but this possibility is not suitable for the heavy-duty transportation sector because of many technical problems [2].
The first possibility to reduce GHG is the improvement of engines efficiency. Therefore more attentions is given to compression ignition (CI) engines than to the spark ignition (SI) engines. Moreover, the heavy-duty transportation industry generally prefers CI engines not only because of their high thermal efficiency but also because of their high load operability. Same happens for power generation and marine vehicles [2].
Conventional CI engines have disadvantages of large amount of soot and NO_X emissions and, during the last years, great efforts to improve combustion technologies and exhaust treatments have enabled to reduce them. However, despite all the improvement for pollutant emissions, the problem of GHG emissions remains because GHG are related to the carbon content of the fuel itself, specially regarding CO_2 emissions [3]. Therefore alternative fuels with low or null carbon content are searched with the aim of CO_2 emissions reduction through a complete or partial fuel substitution. Nevertheless, because of the lack of time for a complete fuel renewal, research focuses on applications with a partial fuel substitution, leading to dual fuel configurations.
A growing interest has been given to ammonia in the last years because of its excellent properties as hydrogen carrier and as carbon-free fuel. The ammonia null carbon quantity is the main characteristic that allows to reduce CO_2 emissions from internal combustion engines because it leads to a carbon-free combustion. Therefore, ammonia could help to match the increasingly strict CO_2 and GHG emissions requirements imposed by laws

and government because of its thermochemical properties. However, only a few studies concerning ammonia combustion have been done [2]. Engine design are usually supported by detailed numerical model [4] therefore the importance of this CO_2 emissions reduction makes engine manufacturers and researchers in need of new precise tools to investigate effects and benefits of using ammonia as a fuel.
Research in internal combustion engine (ICE) field is problematic because of the large number of parameters and variables that affect the final results. Different experimental settings to cover all the possible operating conditions means long time to have results and a wide use of resources, primarily economic. A reliable combustion numerical model might be the best solution to reduce time and resources waste because it will allow to exclude the worst possibilities simply by the use of a computation tool and to focus only on the most promising setup. Therefore, both experimental costs and time drops because tests are done only in a few conditions, using specific fuels and specific engine geometries. Moreover, the change of one or more conditions can be simulated without the need of a new experimental setup. A reliable combustion model also allows to repeat test at the same conditions, working as a virtual test bench which is not affected by external conditions. Furthermore, with a combustion model it is possible to achieve data for all the quantities in all the combustion chamber, not only in a few points where sensors are placed.
Many numerical combustion models are available for the most common fuel but ammonia is a quite new fuel and it presents some differences with respect to traditional fuels. Therefore a model validation is needed to ensure that the model can properly handle ammonia. This lack of reliable numerical models for ammonia combustion in ICE needs to be filled to speed up research in ammonia fueled engines field. The main challenges for these numerical models are the limited availability of experimental data and the poor flammability properties, e.g. higher auto-ignition temperature and low flame speed.
This work aims to propose a computational model for ammonia combustion in ICEs. The focus is on two ammonia diesel dual fuel (DDF) engines which differs for ammonia injection strategy: the first case is characterized by direct injection of ammonia; the second case performs port injection of ammonia. The two different injection strategies lead to different combustion modes, therefore two different numerical models are adopted. The case characterized by direct injection of ammonia is simulated by the use of the tabulated kinetics approach; the case with premixed ammonia relies on a hybrid approach which uses the tabulated kinetics to manage the combustion of diesel then it switches to Weller combustion model to compute the ammonia premixed combustion. These two numerical models were developed by Politecnico di Milano for methane DDF engines [5][6][4].
First of all, the two cases are simulated in specific operating conditions by very reliable

solvers, such as diesel-only configuration simulated with the Representative Interactive Flamelet (RIF) approach [7][8]. This first step is necessary to catch the correct initial conditions. After that, other dual fuel modes, if available, are simulated for a solver validation before use the two models, developed for diesel-methane applications, for diesel-ammonia configuration. However, simulations settings stumble on some lacks of experimental setup data which are solved by some assumptions. The gross validation of the two models is based on the comparison with data found in literature [2][3]. Furthermore, the validation focuses only on the engine performance, specially pressure curves, while neglecting the exhaust emissions calculations.

1 | Concerning ammonia

1.1. Why ammonia?

In the last years, fossil fuels are increasingly at the heart of the energy debate because of their effects on human health. In fact, human health is damaged by pollutants and human lifestyle all around the world is affected by climate changes. Despite the continuous improvement in combustion and exhaust after-treatment technologies, fossil fuels still produce large amounts of greenhouse gas (GHG), especially carbon dioxide (CO_2), because of their natural carbon content. This problem is related to the nature of fossil fuels, therefore different kinds of fuels can provide a real breakthrough in this field: in particular a solution could be the use of fuel with null or almost null carbon content. This concept is the main reason why every day we hear more and more about hydrogen as a promising fuel for the future.

$$2H_2 + 0_2 \Rightarrow 2H_2O + heat \tag{1.1}$$

Hydrogen seems to be a great solution because of its high heating value and because of its clean combustion, which in fact produces only water as shown in Equation (1.1). However, the use of hydrogen as engine fuel have its weaknesses to be taken into account. First, because of its low density, it is difficult to store hydrogen, especially on a vehicle; moreover, the cost of hydrogen is relative high (5 \$/kg or 35 \$/GJ). Furthermore, a logistic structure for hydrogen production, storage and distribution around the world using a suitable storage medium [9] is missing nowadays. Compared to conventional fuels used for transportation, hydrogen has a low energy content per unit of volume and this property increases the volume quantity to be moved. Moreover, hydrogen could be the cause of safety issues due to its volatility and large flammability limits.
Nowadays hydrogen is the most famous alternative fuel but other interesting solutions are taken into account. One of these alternatives consists in ammonia. This option is not a real novelty because ammonia was already used in the past as internal combustion engine fuel and many properties make ammonia a more attractive alternative to both fossil fuels and to hydrogen. Ammonia as a transportation fuel can reach properties very close

to gasoline ones, without the problems associated with CO_2 and pollutants production during combustion [10].

Fuel storage	**p (bar)**	**ρ (kg m^{-3})**	**LHV (MJ kg^{-1})**	**Energy density (GJ m^{-3})**	**Volumetric cost ($ m^{-3})**	**Energetic cost ($ GJ^{-1})**
Gasoline liquid tank	1	736	44.5	34.4	1000	29.1
CNG integrated storage system	250	188	50	10.4	400	38.3
Hydrogen metal hydrides	14	25	120	3.6	125	35.2
Ammonia pressurized tank	10	603	18.8	13.6	181	13.3

Table 1.1: Comparison between ammonia and other fuels properties [10][11].

Table 1.1 summarises some of the properties of the most common fuels in comparison with hydrogen and ammonia; here hydrogen mostly differs for its high volumetric cost and for its low energy density. Despite energy content of ammonia is much lower than the other fuels, especially when compared to gasoline, ammonia remains an interesting solution because of its low volumetric and energetic cost. Besides, ammonia main advantage is related to its nature: no carbon content means that ammonia combustion happens without CO_2 generation, as demonstrated in Equation (1.2) [1].

$$4NH_3 + 3O_2 \Rightarrow 2N_2 + 6H_2O + heat \tag{1.2}$$

Both low cost and no carbon content make ammonia one of the most attractive fuels for a clean energy future; furthermore other possible advantages emerge during research, such as those reported by Zamfirescu at al.[10]:

- ammonia has a high octane number, about 130, and therefore ammonia is a good fuel for internal combustion engines because of its ability to avoid detonation during compression;
- because of the low energy quantity required to thermally crack ammonia into hydrogen and nitrogen (about 14% of LHV) ammonia can be successfully used as an

hydrogen carrier;

- ammonia production and distribution infrastructures are already present and well established: yearly, more than 100 millions tons are produced worldwide and delivered to a vast market for a value of about 91-225 billion dollars per year [10];
- in case of crash or in case of damage to the fuel tank, ammonia can be safer than hydrogen thanks to 3 main characteristics: ammonia has a narrow flammability range, its strong odor makes ammonia detectable by nose at 5 ppm and ammonia density is lower than air density, which means that it dissipates faster in the atmosphere.

Ammonia low density is considered a good property from a safety point of view but it introduces the greatest problem concerning the use of ammonia as a fuel: usually ammonia is considered as a non-flammable fluid and unrelated to explosion danger. Due to its low flammability properties, in particular the low flame speed (see Table 1.2 and Table 1.3), ammonia is not properly suitable for a direct use in ICEs [10][12]. A special design is required for ammonia engines because ammonia ignition requires huge compression ratio value, around 40 [10], which is much higher than values for the current ICEs. To solve the problem of ammonia ignition, dual fuel diesel-ammonia or hydrogen-ammonia engines are considered. The use hydrogen-ammonia engines is an interesting option because hydrogen H_2 can be obtained by ammonia decomposition, thus avoiding a dedicated tank for hydrogen.

Property	**Ammonia**	**Gasoline**
Lower heating value [MJ/kg]	18.6	42.45
Octane rating	>130 RON	92.4 (R+M)/2
Stoichiometric A/F mass ratio	6.1	14.5
Flammable/equivalence ratio range	0.72-1.46	0.55-4.24 (JP-4)
Flame speed at stoichiometric [cm/s]	12	52 (JP-4)

Table 1.2: Features of ammonia and gasoline [13].

At last, the exhaust gases released by ammonia combustion should be properly controlled: an internal combustion engine fueled with ammonia emits large NO_X amount which is generated because of nitrogen excess in the combustion chamber. The NO_X amount can be minimized adjusting the fuel-air ratio and with exhaust after-treatment devices such as ammonia catalyst. Great attention should be paid also to the unburned ammonia released at exhaust because of it is possibly harmful to human health.

Property	Gasoline	Diesel	Natural gas	H_2	NH_3
Flammability limit [volume % in air]	1.4 - 7.6	0.6 - 5.5	5 - 15	4 - 75	16 - 25
Autoignition temperature [°C]	300	230	450	571	651
Peak flame temperature [°C]	1977	2053	1884	2000	1850

Table 1.3: Features of ammonia and other fuels [10].

1.2. Ammonia production, storage and distribution

Among all the chemical compounds, ammonia occupies the second place as the most-produced chemical compound with a production around 180 tons/year [1]. The basic idea behind ammonia synthesis is a catalytic reaction of nitrogen and hydrogen while the opposite reaction is called ammonia decomposition or cracking and it is used to deliver hydrogen from ammonia storage. Equations (1.4)(1.3) show the two chemical reactions.

$$N_2 + 3H_2 \Rightarrow 2NH_3 \qquad \Delta H = -92 \text{ kJ/mol} \tag{1.3}$$

$$2NH_3 \Rightarrow N_2 + 3H_2 \qquad \Delta H = +46 \text{ kJ/mol} \tag{1.4}$$

Industrial ammonia production is mainly based on the Haber-Bosch process, developed by the German Nobel prizes in chemistry Fritz Haber and Carl Bosch between XIX and XX century. The procedure consists on steam reforming of natural gas, consuming 3-5% world production of natural gas to provide around around 85% of the world ammonia demand [1]. The Haber-Bosch process, if powered by fossil fuel, is a fast and efficient way to generate ammonia but it releases a huge quantity of CO_2, around 1.4% world's CO_2 emissions. Moreover, this production process is very energy consuming (about 80 MWh/ton per) and it releases large quantities of NO_X requiring a selective non-catalytic reduction. The non-catalityc reduction not only increases the cost but also it invalidates one of the best characteristic of ammonia by making the fuel no more fully decarbonized. Luckily, there are other more sustainable methods to produce ammonia and Haber-Bosch process can be optimized and powered by renewable energy.
Ammonia production is classified in three different categories, according to the production process used:

- brown ammonia: produced exclusively from fossil fuels, in relationship with this kind of production high amount of CO_2 is generated;
- blue ammonia: produced from fossil fuels but carbon capture and storage (CCS) is added to the process;
- green ammonia: produced via sustainable electricity, air and water. Green ammonia production is obtained combining electrolysis-based hydrogen and the traditional ammonia synthesis loop and the final result is the carbon-free ammonia. A process schematization is done in Figure 1.1.

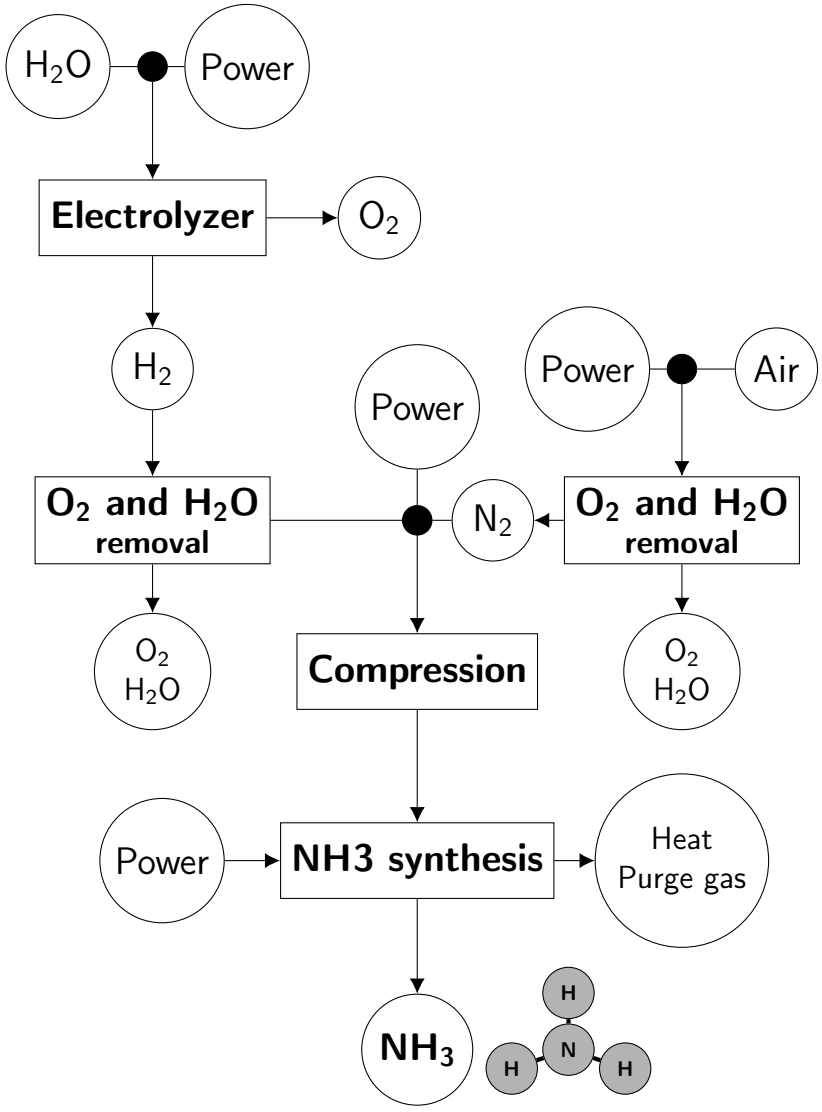

Figure 1.1: Schematization of green ammonia synthesis with hydrogen produced through electrolysis [1].

At the moment only 0.5% of ammonia production is achieved via water electrolysis pro-

cesses: a cost reduction and other process improvements can save the emission of over 360 million CO_2 tons worldwide. These improvements might be the turning point for the future of ammonia as a fuel, as mentioned by Miura et al.[14]:

> *"Using ammonia as an energy carrier was demonstrated to be competitive in terms of efficiency, CO2 emissions and supply cost for energy systems requiring fairly large numbers of storage days. (...) Further technical improvements and cost reduction associated with both conventional and unconventional ammonia production were found to be imperative for using ammonia in a normal energy system. The efficiency improvement of Haber-Bosch process needs to be pursued by exploring better utilization of process waste heat. New ammonia production techniques with the potential to be CO2-free, including direct ammonia synthesis from water and nitrogen, should be researched further, and these technologies should be validated in terms of future commercialization."*[14]

For the years to come the interest in green ammonia market is expected to constantly grow thanks to new technologies and commercial solutions, based for example on alkaline and proton-exchange membrane or on biomass-based hydrogen production, and other non-conventional methods which are at the beginning of their development. Moreover, as it is proved by the increasing number of carbon-free ammonia production plant programs all around the world, there is a big excitement about green ammonia. For example, Japan has one of the main roles in green ammonia program as a renewable energy solution and in 2014 it started a program called Energy Carries which promotes the use of ammonia as a tool for storing and for delivering energy [14].
Because of a such large market, ammonia infrastructure is large and widespread: the existing system is able to store and to distribute ammonia all around the world, even to our homes (though diluted) but especially for some industrial sectors. One large consumer of ammonia, for example, is the fertilizing industry. Therefore, a widespread distribution network has been built in the years based on ship transports, pipelines, railway and road trailers. Moreover, natural gas pipelines can be converted to liquid ammonia pipelines which helps making energy transport simpler if compared to hydrogen. With this background, from technological, economic and logistic point of view ammonia is more suitable than hydrogen to be implemented in power generation field [1].

2 | Ammonia in internal combustion engines

Ammonia has been considered as transportation fuel since the second half of XIX century, at that time it was used for trams and locomotives but not for private vehicles. During WWII, the lack of fossil fuels made Belgium authorities use ammonia to fuel public buses. Although at the end of the war the use of ammonia was set asides, it remained as emergency solution to be tested and improved.
Figure 2.1 reports the main steps concerning the evolution of the use of ammonia in transportation sector.

1822	Goldsworthy Gurney develops an ammonia engine for small locomotive
1869	Emile Lamm develops an ammonia motor
1870	Delaporte's ammonia engine
1894	MachMahon creates an ammonia motor for small trams
1905	Ammonia Casale Ltd develops the first small-scale motor
1933	Norsk Hydro company coverts a pick-up truck to run with ammonia
1942	Belgium's public buses converts buses to run with ammonia
1965	GM develops ammonia engines and fuel cells
1965	US Air Force and NASA use ammonia on the X-15 jet project
1972	University of Tennessee develops an ammonia-fuelled urban vehicle
1981	Canadian company develops an ammonia fuelled car
2007	American company converts a pick-up truck to run with ammonia
2010	Hydrofuel Inc. adapts multiple vehicles to run on ammonia
2013	KIER team develops the AmVeh ammonia fuelled car
2014	Marangoni tyre presents an ammonia fuelled sports-car

Figure 2.1: Use of ammonia in transportation sector over the years [15].

During the '60s, the US Army started to consider the idea of using ammonia as fuel for

military application for both CI and SI engines: the basic aim was to reduce the problem of military supply and to increase autonomy thanks to the possibility to synthesize ammonia on site.
A first work was published in 1965 by Cornelius at al.[16] at General Motors Corporation: after many tests on real engines performed at different compression ratios, both with and without supercharger, the basic result was that an ammonia-fueled spark-ignited engine can be developed with performance equivalent to the ones obtained in current automotive gasoline engines. Moreover, the addition of a small amount of hydrogen, that can be obtained by ammonia dissociation, to the ammonia is a requisite for a suitable part-load engine performance. Compared with a gasoline engine, an ammonia-fueled vehicle requires at least 2.8 times by volumes and 2.35 times by weight to drive equal distances, but there is not a serious issue concerning the main military applications. The following year, in 1966, Gray at al.[17] investigated the compatibility of ammonia and its combustion products with engineering material and lubricants used at the time in ICE. Even in this case basically no problems were found. Regardless, the main problem related to compatibility between ammonia and gasoline engines is the high compression ratio, which goes up to 35 to ignite ammonia, even though combustion can occur also with a compression ratio equal to 12 in presence of a pilot fuel. The energy level required by ammonia combustion is high and it is not lowered by any fuels additive. Therefore spark plugs and standards glow plugs, fail to initiate combustion while high temperature glow coils are suitable ignition sources. Some gases can be introduced into the intake manifolds to help the ignition, but large amounts are required: 10% hydrogen or 15 up to 20% acetylene. During the same year different concepts were achieved by Starkman et al.[12]: after a thermodynamic calculation to predict SI engine performance operating with ammonia at different conditions, the result was an indicated output reduced approximately to 70% but no more than 77% than with hydrocarbon (see Figure 2.2). In addition, they proved that ammonia can be successfully used as a SI engine fuel at the normal compression ratios under certain conditions which are the following: ammonia is introduced as a vapor and it is partly decomposed to nitrogen and hydrogen, whose concentration is a key factor for a successful operation. Other calculations predicted that introducing ammonia in the cylinder as a liquid, engine indicated output would exceed the hydrocarbon one.
During the '60s, ammonia was also considered for CI engine: Newhall [18] predicted the theoretical performance for ammonia in Diesel engine using one of the first digital computer program. In the event of a successful combustion, ammonia was expected to yield up to 10% more power output than hydrocarbon fuel at same operating condition, with a 20% greater efficiency, a 2.5 times specific fuel consumption and lower NO_X concentration at exhaust. A theoretical higher power output for ammonia fueled CI engine than hydro-

carbon fueled one was calculated also by Starkman et al.[19] tests on a real engine reveal the opposite result: at a comparable fuel-air ratio the real engine developed approximately 10% less power. About specific fuel consumption, for ammonia the consumption resulted 2.4 times higher than diesel fuel, value close to the computed increase 2.5. Among all the tests, the best performance was obtained injecting liquid ammonia at 150-180 CA bTDC using spark ignition. Also Pearsall at al.[20] performed some tests on a real CI engine: a Continental AVDS-1790, air cooled diesel engine mounted by combat tanks. The main tests investigated the feasibility of converting and operating CI engines with anhydrous ammonia fuel; obviously the performance improved using engines designed for ammonia. Basic design features for an ammonia fueled engine were found: the engine should be SI with a high energy ignition source, such as a magnet, and it should have a relatively high compression ratio, between 12 and 16. The presence of a spark plug in a CI engine is admitted due to difficulties found for ammonia ignition. During the '60s the main problems of ammonia combustion were already known and studied, as reported by Garabedian at al.[21] they are very high auto-ignition temperature, low flame speed, narrow flammability limits and high vaporization heat.
While the interest on the potential of ammonia as fuel declined at the end of '60s, this idea is becoming appealing in accordance with the current need for low-carbon content fuel.

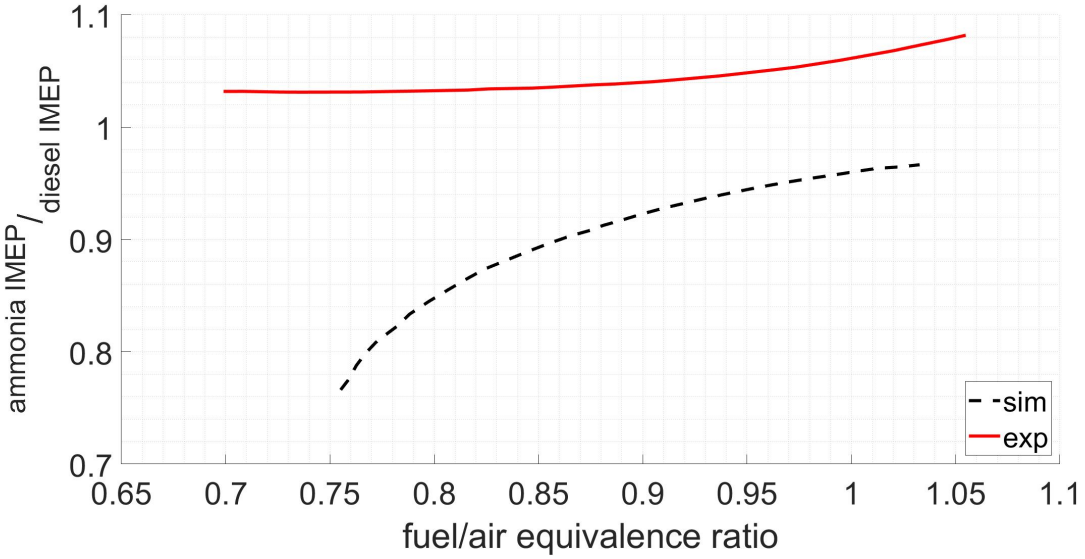

Figure 2.2: Ammonia fueled engine: predicted and experimental power output. Comparison at following conditions: compression ratio equal to 20, 1500 rpm, ammonia injected at 180° bTDC [12].

2.1. Ammonia compression ignition engines

At the end of the first decade of the 2000s, due to the increasing interest in low carbon content fuel to reduce greenhouse gases emissions, ammonia got back in the game: new studies and new tests were performed. In 2008 Reiter at al.[22] tested a John Deere 4045 engine with a dual fuel diesel- ammonia approach, introducing ammonia into the air intake system and initiating combustion with diesel directly injection. The main result of these tests was that ammonia can be successfully burned in a modern engine at various engine speeds and loads. This is possible because ammonia stoichiometric mixture has similar energy content per unit mass as stoichiometric mixture to other hydrocarbon fuels; diesel injection was used to provide the ignition energy needed for the in-cylinder mixture. A successful engine operation can be achieved with the replacement by ammonia for a total energy up to 95%. For better fuel economy energy replacement by ammonia is adjusted to 40-80% and for a good NO_X reduction ammonia energy ratio should not exceed 60%. A significant CO_2 emissions reduction is achieved and the cutting is nearly proportional to the ammonia energy ratio, hence CO_2 reduction is improved by using bio-diesel and ammonia combination.
Dual fuel approach was studied also by Gill et al.[23] who made a comparison of combustion and emissions characteristics of the sue of H_2 , NH_3 and dissociated NH_3 , achieving a significant CO_2 reduction replacing diesel with carbon-free fuel. Comparing pure ammonia to dissociated ammonia, at high load pure NH3 performs better than dissociated ammonia in terms of engine stability and brake thermal efficiency, while at low load they have similar performances. The main advantages of the use of dissociated ammonia are lower exhaust NH_3 emissions and lower fuel consumption but ammonia dissociation remains unfeasible on-board a vehicle.
The use of H_2 and NH_3 is also the base for a novel concept of ammonia engine which is expressed by Boretti [24]: ammonia burns diesel-like in a highly turbocharged, high compression ratio diesel engine and ignition relies on hydrogen injection. This design requires three injector (two main injector for NH_3 and H_2 and one H_2 jet ignition in a pre-chamber) and it can achieve high efficiencies, up to 46% with a power turbine or up to 44% without power turbine. The main issue is the unavailability of models that are able to deal with the dual fuel feeding of the in-cylinder and the jet ignition pre-chamber. A similar approach was considered using both port and direct injection of ammonia together with jet ignition of a gasoline-like fuel, such as gasoline, CH_4 , C_3H_8 or H_2: simulation results show the opportunity to achieve diesel-like power densities and efficiencies [25].
Dual fuel approach for ammonia in CI ignition is not limited to only diesel-NH_3: in the last years different mixing has been tested. Gros et al.[26] tested a Yanmar L70 V engine

fueled by NH_3-DME (20-80% and 40-60%), but engine load conditions were limited by ammonia proprieties such as high auto-ignition temperature and low flame speed. Since the presence of ammonia decreases combustion temperature, higher CO and HC emissions are achieved, soot emissions remains very low and the exhaust ammonia emissions are in order of a few hundred ppm; acting on injection pressure and injection law the system can be improved. Niki et al.[46] conduced a study regarding different injections laws effects that focused on reducing NH_3 and N_2O emissions with some experiment. NH_3 emissions are proportional to the mixed NH_3 in intake air: advancing diesel fuel injection, NH_3 and N_2O emissions reduce slightly, while a pilot diesel injection can reduce NH_3 emissions and simultaneously increase and N_2O. The multiple diesel injections would be one of the effective measures to reduce NH_3 and N_2O emission for ammonia-diesel dual-fuel engine but the analysis of CO_2 emissions does not concern only the engine performances. The low CO_2 emissions of an ammonia-diesel engine depend on the ammonia production system: ammonia might be one the cleanest fuels only if low-carbon methods for ammonia production and reducing NH_3 and N_2O emissions system will be developed.
In recent years, not only experiments but also some numerical simulation have been performed. For example Lasocki et al.[27] simulated a Perkins 1104C-E44T, a 3.3 4 cylinders engine, to investigate the effect of ammonia as primary fuel and a diesel pilot: a significant reduction of CO_2 and CO emissions are achieved, while different ammonia-diesel ratios affect efficiencies, power and torque. Other simulations were performed on ammonia in ICE but sometimes ammonia is not considered as fuel but only as tool to reduce NO_X emissions. Such kind of work was performed by Galdo et al.[28] on a Wärtsilä 6L 46 six cylinders engine. They applied a numerical model based on the so-called inert species method in order to investigate the NO_X reduction in a marine diesel engine due to ammonia injection: in this scenario a main role is played by injection timing and the optimum result is obtained injecting ammonia during the expansion stroke. Similar results were obtained [29] simulating a MAN D2840LE V10 engine fueled by diesel-hydrogen mix: the optimum CAD to reduce NO_X emissions is found at 43.2°, while basically no effects are experienced on HC, CO and CO_2 emissions.

2.2. Ammonia spark ignition engines

During the 2000s, there was a revival also of ammonia spark ignition engines, for which expectations were high, because of the same reasons of the revival of ammonia in CI engines, i.e. the possibility to reduce CO_2 emissions. Shawn et al.[30] tested an ammonia and gasoline dual fuel engine resulting in higher brake mean effective pressure and efficiency than a gasoline-only configurations. Ammonia bad combustibility allows to in-

crease compression ratio and supercharge but a combustion promoter is required: high amount of gasoline, up to 50%, can be replaced by ammonia but the same mix cannot work in all conditions. Indeed the required amount of gasoline is not fixed but depends on the load. At first ammonia-gasoline mix is not always the same, then different tanks must be used to store the two fuel. On the other hand compression ratio has weak effect on the combustion promoter requirement and the optimal compression ratio for the analyzed configuration is about 10, starting from a value of 9 for the gasoline fueled configuration. Ammonia knock resistance also allows to operate a downsized engine at high load with higher thermal efficiencies [30].

The need of combustion promoter for SI engines fueled with ammonia is an obstacle for the commercialization of ammonia as an alternative fuel in SI engines so some solution has been searched: the most popular chance is a mix of ammonia and hydrogen. Considering that both these elements have an higher octane number than gasoline a higher compression ratio can be used allowing to compensate for the intake air dilution. Ammonia-hydrogen mix results in a very suitable fuels blend for SI engines and the best performances regarding efficiency and mean effective pressure can be achieved with a 10%vol. of H_2 in the fuel [31]. The same hydrogen quantity is identified as the best one for all operating conditions while for neat ammonia the maximum speed is around 2000 rpm because of the slow combustion of ammonia-air mixture. The main problem for ammonia-hydrogen mixtures is the amount of NO_X emissions. In fact, a SCR is always required because, even if NO_X emissions are mainly composed by NO, the combustion can emit N_2O, one of the strongest greenhouse gas which has 300 times the CO_2 global warming effect. Similar results were obtained by experiments on 505 cm^3 Lombardini twin-cylinder [32]: the best range of hydrogen quantity for engine stability is 6-10%, depending mainly on the load, then on the engine speed. The same engine was tested in a particular settings: a catalytic reactor to produce H_2 from NH_3 using energy from exhaust gases. This specific layout is the most desired one because it allows to store only ammonia and produce hydrogen from ammonia to supply a dual fuel configuration. The main issues are related to the cold starts and the overproduction of H_2 , that is good for fuel economy and engine cyclic variability but it is problematic for NO_X emissions [33].

Another solution for the promotion of ammonia ignition can be ammonia-hydrocarbons fuel blends, similar to ethanol-gasoline fuel blends. The use of ethanol and methanol as fuel - or as fuel additives - proved to be a successful possibility because it resulted in good performances at high engine speed for ammonia rich fuels [34]. Increasing the ammonia percentage, engine performances remain constant or improve, especially at high engine speed. The optimum blend for the existing SI engines and ECU controls is identified in gasoline with 20% ethanol and 12.9% ammonia [35].

Special attention must be paid to NO_X emissions in spark ignition engines fueled by ammonia because of the nitrogen content of ammonia: NO_X emissions are lower than other hydrocarbon combustion at stoichiometric conditions but higher levels are achieved at lean conditions because of mechanisms of NO formation other than dissociated molecular nitrogen. Moreover, N_2O formation is sensitive to spark timing and to excess air ratio because of the temperature increase caused by late ignition. Unburned ammonia emissions are in the admitted range of 10-25 ppm and after-treatment simulation of SCR reveals that the addition of ammonia helps to treat nitrogen oxides emissions [36].

2.3. Advanced combustion modes with ammonia

New combustion methods are studied nowadays to achieve better efficiency and to comply with the increasingly stringent emission rules. These new combustion modes have been tested also for ammonia fueled ICE, combining the most advanced technologies in fuels and combustion.

A new combustion method developed for CI engines is the so called Homogeneous Charge Compression Ignition (HCCI): auto-ignition starts simultaneously at different locations in the combustion chamber, generating a quick heat release and a fast pressure rise in a short time, while the peak cylinder still remains low [37]. In a HCCI engine, ammonia can not be used in any conditions but should be mixed with hydrogen or methanol, hence usually pure ammonia is not a good candidate for HCCI (see Figure 2.3) [38]. Better results are obtained using hydrogen-ammonia blends: engines can operate with ammonia content up to 70 vol.% while higher compression ratio and higher intake pressure improve IMEP and efficiency results [39]. However there can be some issues related to the hydrogen tendency to ringing with high compression ratio.

Ammonia-hydrogen blends increase power density (because of larger combustion duration) and therefore they can improve brake efficiencies thanks to smaller mechanical and heat losses. Unfortunately HCCI ammonia fueled engines have drawbacks about NO_X emissions: hydrogen HCCI combustion is usually NO_X free because of low temperature but the presence of ammonia makes nitrogen radicals appear [39].

Specific strategies to promote ammonia ignition with different stages has been proposed, one of them consists on the use of an engine with compression ratio up to 35 that allows ammonia ignition and a pilot injection followed by pre-combustion to increase temperature and pressure thus to promote the main injection ignition. The start of injection timing is the main parameter to control combustion: if much advanced, combustion will be similar to HCCI condition. Unfortunately, because of the risk of misfiring due to low ammonia quantity, the HCCI-like configuration is stable at low loads only, which makes

the use of HCCI difficult for practical applications.

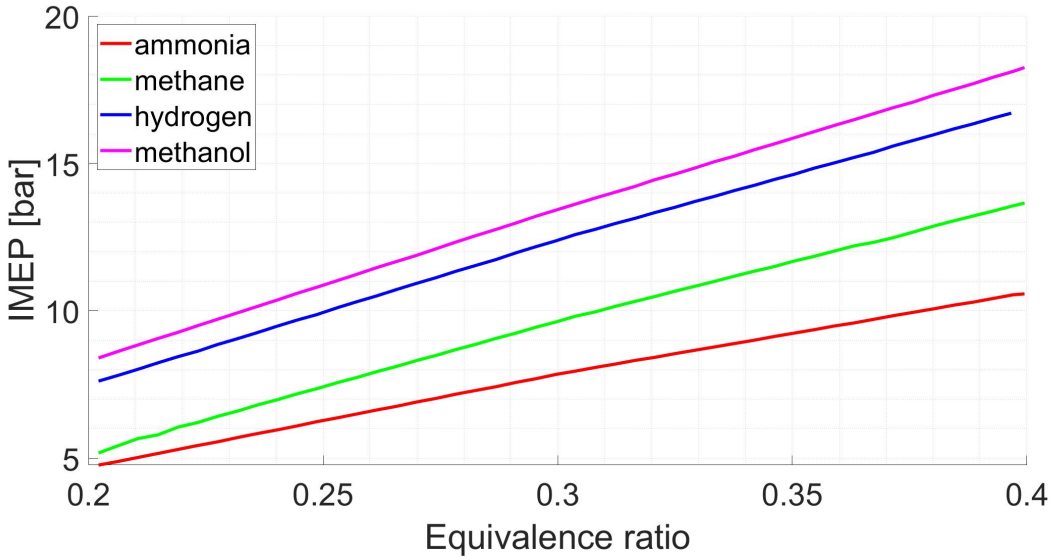

Figure 2.3: Modeling engine in HCCI mode: IMEP as a function of equivalence ratio. Operating conditions: compression ratio equal to 20, intake pressure equal to 2 bar [12].

Simulations with different mass and start of injection (SOI) for pilot injections have been conducted to understand the optimal configuration for the proposed strategy: for a fixed amount of total fuel, higher pilot injection quantity brings higher IMEP and useful SOI timing expands because of the higher temperature after pre-combustion. Increasing the main injection mass at fixed pilot injection quantity, the time interval suitable for the SOI becomes narrower; therefore it is harder for the engine to work. The main pollutant released by this engine is NO and SOI variation affects the total NO production; unfortunately the overall NO emission is higher than a typical engine therefore additional NO reduction method is needed [40].
Another fundamental concept for ammonia in-cylinder combustion is the use of a diesel pilot injection and of a main injection of liquid ammonia in a high pressure dual fuel configuration. Simulation and experimental results made by Frankl et al.[3] on diesel-hydrogen configuration allow to set numerical model to simulate diesel-ammonia configuration. According to this study an high injection pressure improves ammonia mixing throughout the cylinder allowing a mainly premixed combustion with wrinkled flames. Higher pilot diesel mass, preheating ammonia and higher injection pressure help ammonia vaporization, mixing and ignition but they do not necessarily lead to a faster combustion.
Many problems are connected to the use of ammonia as a fuel but luckily many technologies can be studied and can be validated in the future. New combustion technologies can improve combustion and emission performances of ammonia. Combustion researches

must be combined with improvement in advanced and cost-effective ammonia production systems with renewable resources: only this innovation composition can make ammonia a main component for the energy future.

3 | Dual fuel engines

3.1. Diesel-methane dual fuel engines

In the last decades, the global carbon dioxide emissions (CO_2) produced by transportation have been increasing and now great efforts are needed to reduce these CO_2 emissions. A leading role in transportation is played by diesel engines because of their high fuel efficiency and torque. However, besides the CO_2 emissions, other problems concern diesel engines, one of them is the emission of nitrogen oxides (NO_X) and particulate matter (PM). These emissions problems are related to the nature of diesel combustion process, characterized by locally rich and high temperature regions.
In the last years, environmental effects are the main obstacles for engines producers and manufacturers: to solve the widening environment and energy issues, many solutions have been proposed during the years. The main proposals concern alternative fuels, new in-cylinder combustion modes and technologies such as homogeneous compression charge ignition, premixed charge compression ignition and low temperature combustion. Unfortunately many challenges prevent the commercialization of these technologies in diesel engines: the main one is that the engine operating range is limited because the chemical kinetics influences auto-ignition by reducing range of speeds and loads [41].
Many alternative fuels have been searched and natural gas is considered one of the most promising because of its great appeal. The main advantages of methane are the following: a wide source, low price, low carbon-to-hydrogen ratio and clean combustion that helps in the engine emission improvement. For these aspects many studies are conducted on methane as a promising alternative fuel. The increasing interest and diffusion of natural gas in transportation field is proved by looking at the raising number of natural gas vehicles in the years, for example, from 2001 to 2007 the number had grown from 1.7 to 7 million [42].
Natural gas presents high auto-ignition temperature and this property makes it suitable for compression ignition engine. However, typical CI engines are not enough to auto-ignite methane, hence a source of controlled ignition is needed, usually provided by another high cetane number (CN) liquid fuel. Therefore, the main configuration able to implement

natural gas fuel in internal combustion engines is the natural gas-diesel dual fuel mode because it is a more practical and less expensive method than using only natural gas in a diesel engine. This fuel configuration has been studied and improved by many researchers as a promising way to reduce diesel consumption and to enhance engine performances by keeping low pollutant emissions. Currently new fuels are researched to substitute methane, such as hydrogen or ammonia; from now on methane is going to be the reference fuel to explain engine configurations, but the same strategies can be adopted for all the others [37].

A strategy to use methane in a compression ignition engine is the so called methane-diesel dual fuel (DF) engine: the concept is to use a pilot-fuel with high cetane number, such as a small amount of diesel, injected near the top dead center to initiate combustion and ignite a low reactivity fuel, such as methane. Great results have been obtained also using diesel and gasoline to take advantage of an existing infrastructure and engines can operate from low to high loads. The method adopted to introduce methane distinguishes engines in direct injected DF and port injected DF: both of them are promising solutions.

Nowdays, for direct injected DE engines, the most common applications rely on the port injected DF configuration. In such configuration methane is injected into the intake manifold and is premixed with air during compression; afterwards a small diesel pilot is used to initiate the combustion of a uniform methane-air mixture. The main benefit of this setting is the possibility to maintain diesel capability in case of lack of methane.

Nowadays the simpler and cheaper system for injecting the two fuels consists in the so-called "co-injector". This system is composed by only one needle and a single actuator for both the fuels. The basic concept for the co-injection is a single injection of both diesel and methane: a small diesel quantity enters the injector above the needle seat and, when the gas injection starts, methane carries diesel into the cylinder [42].

Another options is the presence of two different injectors, one for the main injection and one for the pilot injection. The last option is the use of a special injector which is able to handle separately both diesel and methane fuel. This setting allows unthrottled operation with little methane slip but particle and NO_X are problematic. In addition, a quite complex and expensive total system is needed to performs separate injection through a single injector. The main component of this injection system is the special high-pressure gaseous injector that can inject natural gas directly into the cylinder right before the end of the compression stroke. The injection structure is quite complex because it requires a dual-needle and dual-actuator fuel injector to deliver both diesel and gas directly in the combustion chamber through separate holes; an injector example is shown in Figure 3.1. The final result is very promising because it allows a better fuel economy. However, the implementation of a complex structure of injector and fuel supply system

has a major impact on the total cost, so that cost reduction becomes one of the main areas of improvement.

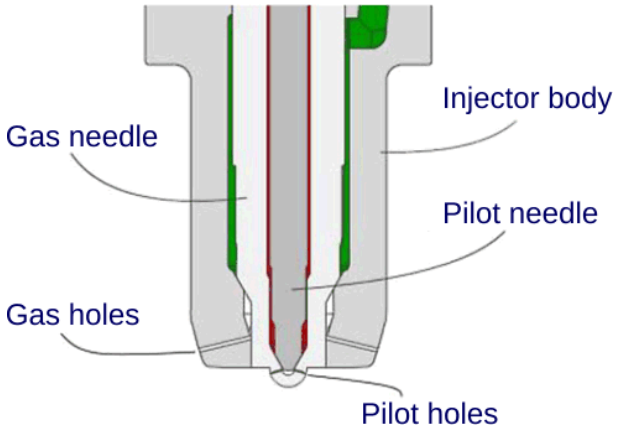

Figure 3.1: Schematic drawing of a HPDI dual fuel injector [43].

In case of direct injection of methane, there are two main configurations whose difference concerns the combustion modes, depending on the sequence of the two injections, the pilot injection of diesel and the main injection of methane. The first configuration is a diesel pilot injection followed by the main injection of natural gas is performed in high-pressure direct-injection (HPDI) configuration: a small pilot diesel amount is injected before the main injection in order to increase the temperature and to allow methane ignition. After the injection, methane burns in a diffusion flame, then the resulting natural gas combustion is mainly a diffused one, quite similar to diesel combustion. The second configuration is an injection sequence obtained by a first injection of natural gas and by a pilot injection of diesel to ignite a uniform air-methane mixture. The resulting combustion is a partially premixed compression ignition (PPCI), where natural gas combustion is mainly premixed combustion. Another difference refers to the indicated thermal efficiency which for PPCI can be lower than in HPDI mode, where efficiency values can go up to 49% in specific conditions [44].
The last option for diesel dual fuel engines is the hot surface assisted compression ignition strategy: natural gas is injected at the end of compression phase directly into the cylinder, close to a hot surface. This hot surface usually is a glow plug with a temperature range of 1200-1400 K.
Engines in DDF mode absorb properties of both CI and SI engines because such engines are a mix of CI and SI configurations. DDF combustion can be considered as composed by four parts. The four parts are listed below and they are indicated in Figure 3.2:

1. combustion of the diesel pilot;
2. combustion of methane in the premixed pilot-region;

3. flame propagation through the methane-air mixture;
4. possible bulk ignition of the end gas.

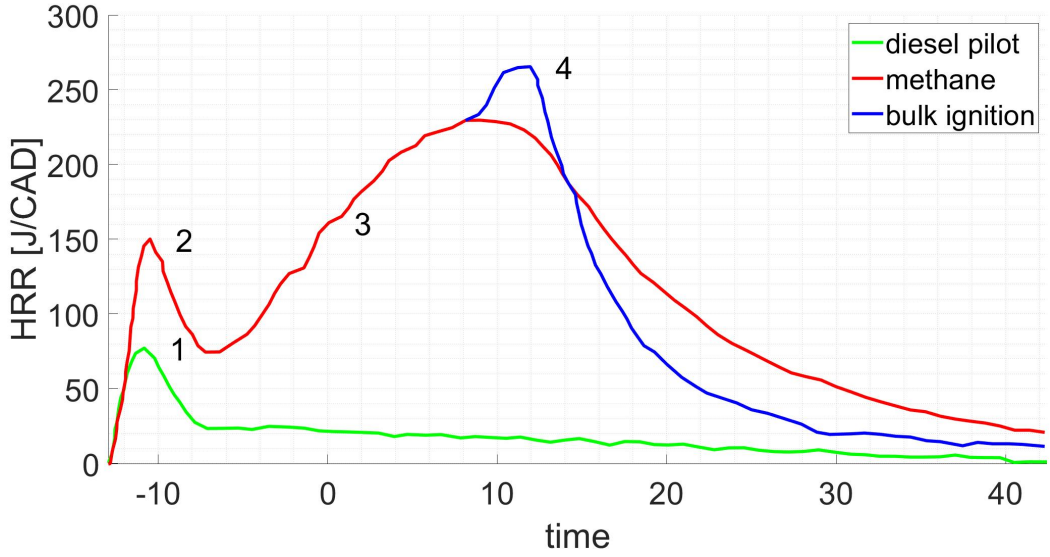

Figure 3.2: Hypotetical HRR curve for a DDF engine: the four parts are indicated [37]

Alongside these positive aspects, methane DDF engines present some drawbacks: at first the in-cylinder pressure during the initial part of combustion is slight lower and a longer ignition delay is detected in DDF configuration; then the pressure peak is generally lower and delayed with respect to the conventional diesel engine. Besides the combustion phase is longer than the diesel one because of the slower flame propagation of methane. Injection parameters of diesel pilot injection greatly affect in-cylinder pressure peakand heat release rate in DDF configuration much more than in normal diesel mode. DDF engine power is lower than conventional diesel engines and the maximum decline is around 2.1%. The power loss can be reduced or recovered by modifying some operating parameters, especially by increasing the intake temperature, the intake pressure and the pilot diesel quantity. Generally, DF combustion is characterized by higher energy consumption than diesel operation but this drawback is compensated by the reduced fossil fuel consumption [45]. Another problem is the engine stability: DDF engines presents higher COV_{IMEP} and COV_{IMEP} increases with higher load; a solution to improve combustion stability can be found by increasing the intake charge temperature or by introducing an hot EGR at low engine load.
Considering pollutant emissions, diesel-methane DF mode can significantly reduce CO_2 because of the inherent H/C ratio. Same happens for NO_X and PM emissions but unfortunately HC and CO emissions greatly increase. A few good strategies in order to further reduce CO_2 emissions and fuel consumption are advanced injection strategies and EGR,

despite the higher NO_X and PM emissions. Therefore in these kind of CI engines, the only way to reduce all NO_X ,CO_2 and PM emissions and to improve fuel economy seems to be the development of new alternative fuels and of a new combustion concept for natural gas. One solution can be the increase of pilot fuel quantity or the increase of intake air temperature (solution also able to reduce UHC emissions) yet to increase the diesel pilot amount means more particulate matter emissions. In particular it is demonstrated that the partial premixing of natural gas reduces CO and soot emissions but it is responsible for the increase of NO_X emissions that can be reduced using EGR.
Another issue related to diesel engines is the formation of particulate matter whereby the main solution is the Diesel Particulate Filter (DPF), with an efficiency around 90%. Optical investigations have demonstrated that DF combustion presents lower in-cylinder soot formation and lower temperature, resulting in lower NO_X emissions [45]. However, when used in diesel-methane DF engine, the DPF efficiency is lower, around 60-70%. Moreover, it was demonstrated that methane, not diesel, plays the main role in particulate formation because of the diffusive combustion of natural gas [44]. This means that it is methane itself the main cause of particulate formation therefore it is difficult to reduce particulate emissions in diesel-methane DF engines. In HPDI mode particle show higher number, diameter and mass than in PPCI configuration. To reduce this negative effect, many researches have been done and it was found that several parameters affects the particulate formation: for example, lower compression ratio and lower diesel pilot quantity reduce particle number and diameter, same happens with higher injection pressure and higher EGR. A significant effect on particulate emissions is traced back to the natural gas and diesel injection pulse separation (PSEP). In fact shortening the PSEP leads to higher heat release rate peak, longer combustion duration, less particulate emissions but, unfortunately, to higher NO_X emissions. PSEP also affects HRR shape in both HPDI and PPCI configurations: a short PSEP leads to a single peak, while long PSEP produce a bimodal shape [44]. Analyzing the combustion process, it can be noticed that, when using short PSEP, injection and combustion are nearly simultaneous in HPDI configuration, while in PPCI mode the mixture is ignited at the end of the injection. With long PSEP, for HPDI combustion several injections are required while for PPCI the combustion is incomplete because the natural gas creates an over-lean mixture due to the early injection.
Injection timing is also important for pollutant emissions: delaying the methane injection timing with fixed diesel injection timing makes NO_X emissions drops. Considering HPDI mode, HC emissions decrease at first and then increase while during PPCI combustion, NO_X emissions increase and HC emissions decrease. The natural gas injection timing also affects particulate matter generation, especially for HPDI mode whereas in PPCI mode PM generation is only slightly affected [44].

Despite some drawbacks, DDF diesel-natural gas engines have a very widespread application, in present days, because they are an effective solution to reduce greenhouse gas emissions, especially CO_2, and other pollutants. It also results in large applications fields (trucks and passenger cars, marine engines) and many other studies.

3.2. Diesel-hydrogen dual fuel engines

DF engines employ two different fuels, one with high cetane number and one with low cetane number. In the analysed dual fuel configurations, the fuel with high cetane number is always diesel, while many possibilities are available for the second fuel and hydrogen can be one of them. Many properties make hydrogen a good alternative fuel: high LHV, carbon free structure, renewability, low emission, no-toxicity and a wide range of flammability limit. Unfortunately, hydrogen is characterized by a low density and its production and its distribution facilities are not well developed yet.
Using hydrogen as fuel for internal combustion engines has some great advantages on exhaust emissions with respect to conventional fossil fuels, especially for what concern CO_2 emissions. Nowadays the main fuels for power generation are the fossil ones. Therefore, if they are replaced by hydrogen in any percentages, the emission of a large amount of CO_2 can be avoided, such emission reduction is the main advantage offered by the use hydrogen. This is possible only if hydrogen production is based on renewable energy, making hydrogen a renewable, sustainable and carbon free fuel. Moreover, other solution for a clean energy future relies on the use of hydrogen in hydrogen fuel cells (H_2FC). However, hydrogen as engine fuel is more convenient than hydrogen fuel cells for many reasons. ICEs do not require high hydrogen purity level, as in the case of H_2FC. This least dependence from pure hydrogen means that ICEs can use hydrogen derived from various processes, such as various electrolysis, dehydrogenation of organic chemical hydrides or steam reforming. The implementation of hydrogen for ICEs mostly depends on multi-fuel combustion technologies in internal combustion engines. Another advantage related to hydrogen in ICE when compared to H_2FC is a lower cost because the use of existing components make it possible to avoid a large amount of specific material, such as materials made of rare-earth metals [46].
The final aim is to fuel engines with only hydrogen to definitely cancel CO_2 emissions: this is the concept that led to the development of a spark ignition engine fueled with hydrogen [46]. Looking at efficiency, compression ignition engines have higher efficiencies than spark ignition engines, thus hydrogen has been applied also to CI engine to achieve their typical higher efficiency.
The use of hydrogen and diesel in dual fuel applications is very promising because of the

good performance and the low emissions obtained. For example, experimental test shows that an hydrogen CI engine direct injection can increase the peak power by 14% [47]. By applying a suitable hydrogen ratio, in a hydrogen-diesel dual fuel (HDDF) engine, the break thermal efficiency can be maximized up to 32.5% at 70% engine loads [48][49] because of the improved gaseous combustion. At low loads, instead, HDDF engines have some difficulties which are related to poor fuel utilization, combustion efficiency and ignition delay because of lean hydrogen-air mixture and because of the deterioration of the combustion environment [48][50].

In addition to technical aspects, the economic implications must also be considered. Unfortunately, hydrogen is not economically superior than convenient fossil fuel at the moment and its supply system is not well established yet. These aspects mean that hydrogen will be introduced step by step while fossil fuels are still present, leading to a period of transition when multi-fuel combustion technologies are going to be more likely to be used [46]. Hydrogen DDF combustion technology is therefore the main procedure to fuel engine with hydrogen and the most common hydrogen DDF operation is based on indirect injection, supplying hydrogen into the intake port to mix it with intake air and introduce a premixed gas into the engine cylinder; after the compression, small amount of diesel fuel is injected to ignite the premixed hydrogen [50].

The main advantages of hydrogen in DDF applications are higher thermal efficiency and unburned gas reduction at exhaust [46]. Exhaust emissions are marked also by soot and CO_2 emissions reduction because of the associated decrease of carbon. In particular, the reduction of soot and CO_2 emissions increases with larger hydrogen energy shares. Unfortunately, operating conditions at high hydrogen energy shares and medium to high loads lead to larger NO_X emissions because of the well-mixed hydrogen combustion in all the chamber. Solutions for the high NO_X emissions at higher hydrogen energy shares are found in the adoption of low temperature combustion (LTC) approaches, such as utilization of EGR, reduction in compression ratio accompanied by water injection, homogeneous charge compression ignition (HCCI), premixed charge compression ignition (PCCI) and reactivity controlled compression ignition (RCCI). These LTC strategies have the drawback of carbon-based emissions increase [50]. Anyway, this NO_X emissions increase is not very significant for hydrogen port injection configurations because larger hydrogen energy fractions affect oxygen concentration during the intake phase with the final effect of a lower combustion temperature [46].

The last hydrogen DDF issue is the possibility of pre-ignition during compression stroke before the diesel pilot injection, introducing limitations for the engine operation range. The cause of pre-ignition is not well defined but it seems to be related to hydrogen fraction to total input energy (over 50%), to high engine loads, to the cylinder head temperature

and to the engine speed. Increasing hydrogen fraction, the relationship between engine speed and engine head temperature is affected as follows: when hydrogen fraction to total input energy is over 50%, cylinder head temperature strongly depends on hydrogen fraction, probably because of hydrogen flame propagation.
Despite all the problems listed above, hydrogen-diesel dual fuel engines can play a main role to achieve renewable future energy, improving performance of CI engines and performing a CO_2 emissions reduction.

3.3. Ammonia dual fuel system

As hydrogen and methane, ammonia can be an alternative fuel for DDF applications. Ammonia can be introduced inside the combustion chamber via port injection and or via direct injection: both the solutions have been considered as valid options [2][3]. Ammonia dual fuel engine can be implemented with diesel or with hydrogen (see Chapter 2).
This thesis work focuses on the simulation of different combustion modes available for the use of alternative fuels in DF applications, especially diesel-ammonia.

4 | Tabulated kinetics approach for combustion modeling

New combustion modes are becoming more important day by day, therefore new computational models are required to design these combustion systems. The improvement in combustion models regards mainly two aspects: time saving and accuracy.
The basic concept of tabulated kinetics model is to process results of auto-ignition calculations in a homogeneous reactor to generate lookup tables in which chemical composition and reaction rates are stored.
This work uses solvers developed by ICEGroup in Energy department of Politecnico di Milano [5][6]. These solvers are validated for many operating conditions, especially diesel and diesel-methane applications. This work makes such solvers face new operating conditions because they are tested in performing combustion of alternative fuels.

4.1. Chemistry table

Figure 4.1 shows the method used to tabulate chemistry properties. This method relies on a chemical mechanism with thermochemical initial conditions specified by the user. Calculations are performed in a constant pressure homogeneous reactor in a user-defined range of thermochemical conditions. For example, a range for each of the following thermochemical conditions is defined:

1. mixture fraction Z;
2. ambient pressure p;
3. initial reactor temperature T_u;
4. residual gas fraction EGR.

Once these initial quantities have been defined, it is possible to compute the initial chemical compositions and to start reactor calculation. There are two methods to define the initial reactor temperature:

1. the temperature is not related to the mixture fraction Z;
2. the temperature depends on the value of the mixture fraction Z, which ranges between 0 and 1. Equations (4.1) (4.2), where h_l represents the heat vaporization of the fuel, take into account the fuel evaporation effect.

$$h(Z) = (1 - Z) \cdot h(T_{Z=0}) + Z \cdot h(T_{Z=1}) - Z \cdot h_l(T_{Z=1}) \tag{4.1}$$

$$T_u(Z) = T(h(Z)) \tag{4.2}$$

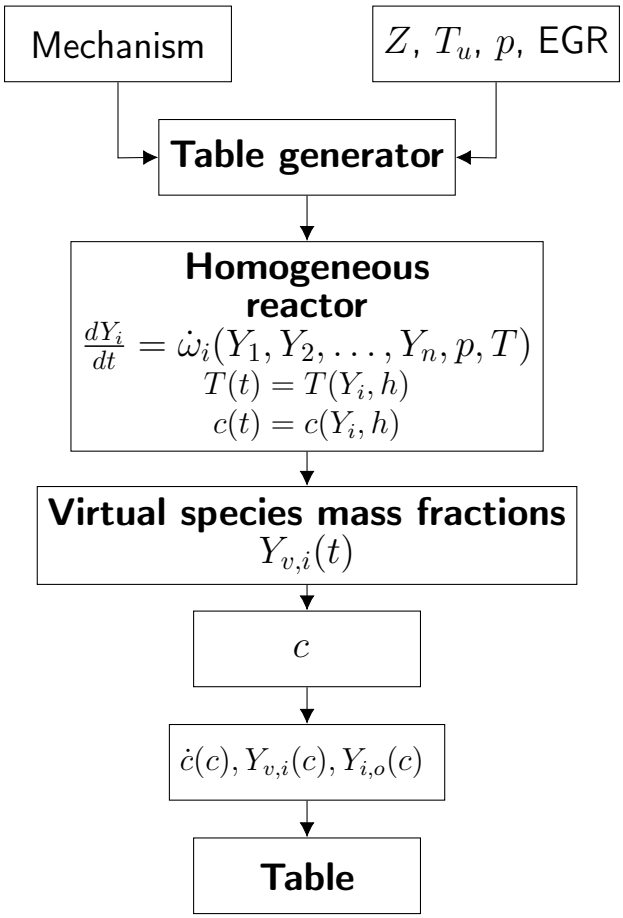

Figure 4.1: Chemistry table generation using homogeneous reactor assumption being Z the mixture fraction, p ambient pressure, T_u initial reactor temperature, EGR the residual gas fraction, h the mass specific enthalpy, c the progress variable, Y_i the mass fraction of species i and $\dot{\omega}_i$ the reaction rate of species i [6].

The thermodynamic accuracy is not affected by the dependence of the initial reactor temperature T_u on the mixture fraction because both methods can cover all the expected thermochemical states of the system and they lead to the same results. More precisely,

if thermochemical conditions include a very wide range, the two methods are no more similar but not in this case. If table discretization is made for diffusion combustion case, the approach n. 2 is expected to be the best one [6]. The value of the oxidizer temperature ($T_{Z=0}$), the value of the fuel temperature and the value of the evaporation heat are well known and they can be specified by the user.
The reaction rate $\dot{\omega}_i$ of chemical species i is defined in Equation (4.3) being Y_n the mass fraction of chemical species n, p the pressure value and T the temperature. The reaction rates are computed for any specified conditions. The reactor temperature T is directly computed from the initial enthalpy.

$$\frac{dY_i}{dt} = \dot{\omega}_i(Y_1, Y_2, \ldots, Y_n, p, T) \tag{4.3}$$

At each time step, two stages are performed:

1. the evaluation of progress variable C;
2. the computation of the chemical composition using the virtual species approach.

However, choosing the input progress variable C is not easy. This approach places the value equal to the heat released by combustion therefore C is defined in Equation (4.4) as the difference between the current and the initial value of the reactor enthalpy of formation h_{298}. Equation (4.4) involves all the N_s chemical species included in the user-specified mechanism.

$$C = \sum_{i=1}^{N_s} h_{298,i} \cdot Y_i(t) - \sum_{i=1}^{N_s} h_{298,i} \cdot Y_i(0) \tag{4.4}$$

The definition of C for each time i is important because it is the variable that uniquely defines each thermochemical quantity and it is suitable for a transport equation. Once each reactor calculation has been performed, the chemical composition and the reaction rate related to the progress variable are stored in tables as function of the discrete values of the normalized progress variable c_i specified by the user. The definition of c_i is specified in Equation (4.5), where C_{max} and C_{min} are respectively the maximum values of the progress variable C found after the auto-ignition event and the minimum value found at initial conditions. These maximum and minimum values are stored in the tables as function of Z, T_u and p.

$$c_i = \frac{C_i - C_{min}}{C_{max} - C_{min}} \tag{4.5}$$

Equation (4.6) computes the progress variable reaction rate $\dot{c}_i$, starting from the time value at which a specified c_i was found.

$$\dot{c}_i = \frac{c_{i+1} - c_i}{t_{i+1} - t_i} \tag{4.6}$$

To obtain the proper source term $\dot{C}$ in the progress variable transport equation, the next step is the solution of Equation (4.7).

$$\dot{C} = \dot{c}(C_{max} - C_{min}) \tag{4.7}$$

During these steps, the tables are updated with values of the progress variable c and with the chemical composition. To simplify the species storage and to gain tables characterised by an acceptable size only seven species - called virtual species - are tabulated. For them only, a mass fraction calculation is performed to preserve the main thermochemical properties of the full set used in the detailed mechanism. Lucchini at al.[6] explains the seven virtual species accounted in this approach. These virtual species follow: N_2, O_2, $fuel$, CO_2, CO, H_2O and H_2. Their composition is obtained for any values of c according to the following Equations (4.8)-(4.14).

$$\sigma_H = \sum_{i=1}^{N_s} N_{H,i} \cdot x_i = \sum_{k=1}^{N_v} N_{H,k} \cdot x_{v,i} \tag{4.8}$$

$$\sigma_C = \sum_{i=1}^{N_s} N_{C,i} \cdot x_i = \sum_{k=1}^{N_v} N_{C,k} \cdot x_{v,i} \tag{4.9}$$

$$\sigma_O = \sum_{i=1}^{N_s} N_{O,i} \cdot x_i = \sum_{k=1}^{N_v} N_{O,k} \cdot x_{v,i} \tag{4.10}$$

$$\sigma_N = \sum_{i=1}^{N_s} N_{N,i} \cdot x_i = \sum_{k=1}^{N_v} N_{N,k} \cdot x_{v,i} \tag{4.11}$$

$$h = \sum_{i=1}^{N_s} Yi \cdot h_i(T) = \sum_{k=1}^{N_v} Yi, v \cdot h_i(T) \tag{4.12}$$

$$c_p = \sum_{i=1}^{N_s} Yi \cdot c_{p,i}(T) = \sum_{k=1}^{N_v} Yi, v \cdot c_{p,k}(T) \tag{4.13}$$

$$\sum_{k=1}^{N_v} Yi, v = 1 \tag{4.14}$$

In Equations (4.8)-(4.13), σ is the total number of elements (C, H, O, N) in the reactor. N_s is the total number of species used by chemical reactor, N_v is the total number of virtual species, N is the total number of elements in each chemical species, x is the mole fraction, Y refers to mass fractions, h is the mass specific enthalpy and c_p is the mass specific heat.
The Y_O variable included in Fig. 4.1 is the mass fractions of the output chemical species defined by the user. These chemical species are specified by the user accordingly with the importance assumed by the user for a future analysis, e.g. for post-processing or exhaust emissions calculation.
The consistency of the model is proved by the calculations performed on a reactor at constant pressure and at different conditions.
The above-mentioned approach is designed to be flexible for spray combustion process simulation in ICEs and also for advanced combustion mode. In fact, it can handle multi-component fuel mixtures and it threats different fuel species as homogeneously mixed. The approach could also account for fuels relative variation for a good calculation of the ignition delay with engines operating on dual fuel mode. These last properties result from a transport equation including spray evaporation contribution.

4.2. Tabulated well mixed model

During the CFD domain solution, when the transport equations are solved for mixture fraction, enthalpy, unburned gas temperature and for the progress variable, the table is accessed. Furthermore, if necessary, an interpolation is performed by using the inverse distance-weighted technique. Figure. 4.2 shows all the operations.
Equation (4.15) is the transport equation of the mixture fraction and it includes the source term of evaporation $\dot{S}_Z$ which represents the fuel evaporation and it is included in the mixture fraction equation.

$$\frac{\partial \rho Z}{\partial t} + \nabla \left(\rho \mathbf{U} Z\right) - \nabla \left(\mu_t \nabla Z\right) = \dot{S}_Z \tag{4.15}$$

From Equation (4.6) and Equation (4.7) it is possible to derive the progress variable source term to be used in C transport equation:

$$\frac{\partial \rho C}{\partial t} + \nabla \left(\rho \mathbf{U} C\right) - \nabla \left(\frac{\mu_t}{Sc_t} \nabla C\right) = \rho \dot{C} \tag{4.16}$$

Equation (4.17) is used to compute the unburned gas temperature T_u which is a table independent variable:

$$\frac{\partial \rho h_u}{\partial t} + \nabla\left(\rho \mathbf{U} h_u\right) - \nabla\left(\alpha_t \nabla h_u\right) = \dot{Q}_s + \frac{\rho}{\rho_u} \cdot \frac{Dp}{Dt} \tag{4.17}$$

In Equation (4.17) the α_t variable represents the turbulent thermal diffusivity while ρ_u is the unburned gas density, calculated from T_u, cell pressure and chemical composition at $C = 0$. Lastly, $\dot{Q}_s$ is a term related to the spray evaporation.

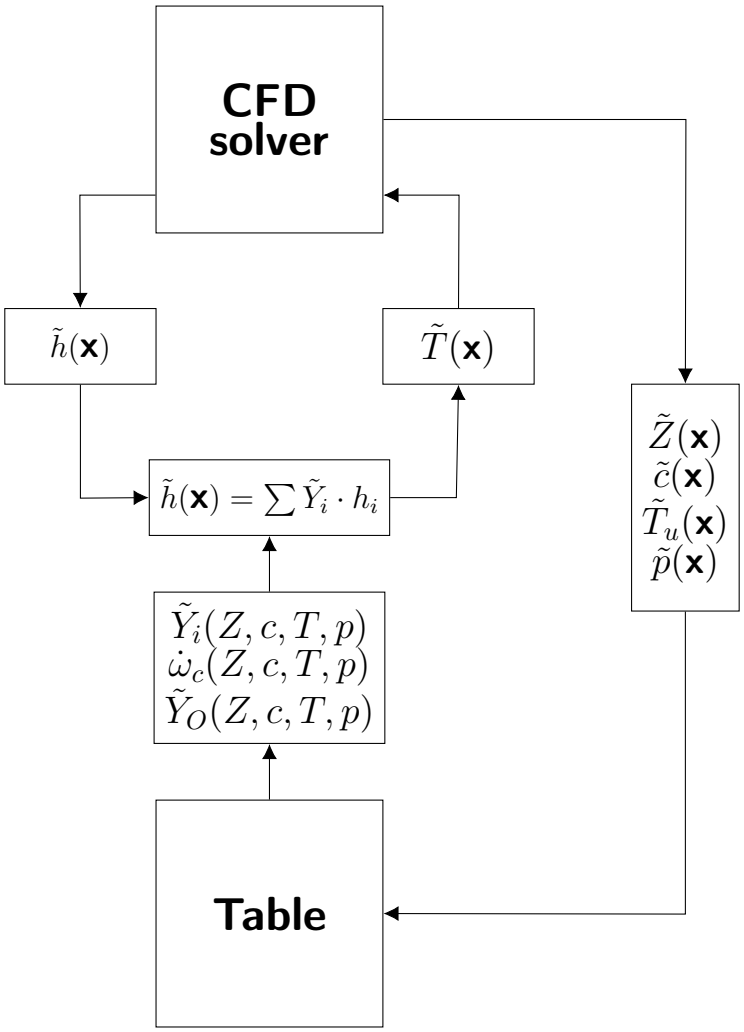

Figure 4.2: Procedure of the tabulated well mixed model, being Z the mixture fraction, p ambient pressure, T_u initial reactor temperature, h the mass specific enthalpy, c the progress variable, Y_i the mass fraction and $\dot{\omega}_c$ the progress variable reaction rate [6].

4.3. Dual fuel combustion

A simplified approach for modeling dual-fuel combustion assumes ignition as governed by local thermodynamic conditions and by the progress variable diffusion. Such approach relies on the use of separate tables for any fuel, without the need of intricate mechanism and with acceptable size tables.
The first step is to calculate the fuel mixture fraction for each fuel (Z_1 and Z_2) considering convection, diffusion and evaporation. With the assumption of an equal distribution of the oxidizer between the two fuels, it is possible to access both data tables with a global mixture fraction value. Starting from the weighted average of the corresponding value from each table, the progress variable reaction rate and the chemical composition are calculated with Equation (4.18) and (4.19).

$$\dot{\omega}_c = \frac{Z_1 \cdot \dot{\omega}_{c,fuel1} + Z_2 \cdot \dot{\omega}_{c,fuel2}}{Z_1 + Z_2} \tag{4.18}$$

$$\dot{Y}_i = \frac{Z_1 \cdot \dot{Y}_{i,fuel1} + Z_2 \cdot \dot{Y}_{i,fuel2}}{Z_1 + Z_2} \tag{4.19}$$

This approach for dual-fuel combustion simulation fits well with the high pressure direct injection operations, considering that in HPDI mode a small amount of pilot diesel injection happens before the top dead center and before the natural gas injection. Diesel auto-ignition happens in the time between the two injections or at the beginning of methane injection, initiating the natural gas combustion.

5 | Simulating premixed combustion with Weller combustion model

After being port injected, a fuel diffuses in all the cylinder before its ignition caused by diesel ignition. This dual fuel mode requires a computational approach able to manage the previous diffusive combustion of diesel and the premixed combustion of ammonia. Such model relies on the one-equation Weller model [4].
The combustion model of Weller is founded on the solution of a transport equation for a combustion regress variable b, which helps numerical stability in flame propagation description. In addition, the model counts on an algebraic expression of the flame wrinkling factor Ξ to control the reaction rate. The ignition event is described through a deposition model, performing transition from laminar to turbulent using a semi-empirical model[51].

5.1. Weller model

The regress variable b represents the unburned gas fraction in each computational cell and its transport equation is obtained conditionally averaging the continuity equation on the unburned gas state.

$$\frac{\partial \rho \tilde{b}}{\partial t} + \nabla \cdot \left(\rho \tilde{\mathbf{U}} \tilde{b}\right) - \nabla \cdot \left(\mu_t \nabla \tilde{b}\right) = \rho_u \tilde{S}_u \tilde{\Xi} |\nabla \tilde{b}| + \dot{\omega}_{ign} \tag{5.1}$$

$$\Xi = \frac{S_t}{S_u} \tag{5.2}$$

$$\Sigma = \Xi |\nabla \tilde{b}| \tag{5.3}$$

being μ_t the turbulent viscosity, S_u the unstrained laminar flame speed, ρ and ρ_u the mixture and the unburned mixture density, $\dot{\omega}_{ign}$ is the ignition source term and $\rho_u \tilde{S}_u \tilde{\Xi} |\nabla \tilde{b}|$ is the reaction rate due to turbulent flame propagation. The flame wrinkling factor Ξ is

the ratio between turbulent flame speed S_t and the unstrained one S_u, as defined in Equation (5.2). Equation (5.3) exposes the dependence between Ξ and the flame surface density Σ.
The regress variable b is set to 1 in any CFD cell until the combustion starts. This setup allows to solve fully implicitly the Equation (5.1), thanks to the exploitation of differential operator properties.

5.1.1. Ignition model

The ignition model aims to start the flame propagation process providing the initial distribution of the regress variable. To do this a simplified deposition model can be used. [52]
After the imposition by the user of an initial flame kernel diameter d_{ign} and a time interval Δt_{ign}, an ignition source term $\dot{\omega}_{ign}$ is imposed in any cell in a zone defined as a sphere with center in the spark plug and radius equal to r_{ign}.

$$r_{ign} = \frac{d_{ign}}{2} \tag{5.4}$$

$$\dot{\omega}_{ign} = \frac{C_s \rho_u b}{\Delta t_{ign}} \tag{5.5}$$

Equation (5.5) defines the ignition source term as function of a user-defined strength parameter C_s, a user-specified ignition duration Δt_{ign} and the unburned gas density ρ_u.
The deposition model is suitable for simplified SI combustion simulation because of two aspect above all:

1. user can calibrate the source term $\dot{\omega}_{ign}$ without large modifications for the heat release rate profile;
2. a gradual initialization of the regress variable b, going smoothly to zero only in the small volume around the spark plug.

In addition, in cells characterized by a null regress variable ($b = 0$) because of complete combustion no unphysical effects or results are obtained because of the implicit formulation. The model could be improved with other better ignition approaches.

5.1.2. Turbulent combustion model

The ignition model produces a regress variable distribution suitable for the propagation of a premixed flame. However, accordingly to the first term on the right side in Equa-

tion (5.1), an appropriate expression for Ξ is needed. This adequate expression for the wrinkling flame factor Ξ should account for the laminar to fully turbulent combustion transition. As a consequence of the one-equation Weller model, the distribution of Ξ depends on two aspects:

1. its equilibrium value Ξ^*_{eq},

$$\Xi^* = f\left(\Xi^*_{eq}\right) \tag{5.6}$$

2. the regress variable b as expressed by Equation (5.7).

$$\Xi = 1 + \left[1 + 2S_\Xi(0.5 - b)\right](\Xi^* - 1) \tag{5.7}$$

The laminar to turbulent transition ends when Ξ equals a value that depends on the equilibrium condition. The Ξ equilibrium value (Ξ^*_{eq}) affects the Ξ distribution in the domain. The equilibrium condition is the balance between productions and merging (destruction) of reaction layer corrugations; this condition is characterized by the maximum value of the wrinkling flame factor corresponding to the variable Ξ^*_{eq}.
Equation (5.7) links Ξ and b with a relation that represents the turbulence distribution across the flame; the user can calibrate this Ξ-b dependence by the tuning of the constant S_Ξ. Usually, as starting condition, S_Ξ is assumed as null to assume a constant value for Ξ^* across the flame.
Equation (5.6) is also the means of introducing a correct transition from laminar to turbulent regimes. More precisely the parameter Ξ^* is defined by Equation (5.8), where I_0 is the flame stretch coefficient and the parameter f models the flame evolution from laminar ($f = 0$) to turbulent ($f \to 1$).

$$\Xi^* = \frac{S_t}{S_u} = I_0 + I_0^{0.5} f\left(\Xi^*_{eq} - 1\right) \tag{5.8}$$

The f parameter is computed using the Herweg and Maly approach[51], on the basis of the following Equation (5.9) where t_{ign} is the time elapsed from spark timing, r_k is the flame kernel radius, u' is the turbulence intensity and L_t is the integral length scale.

$$f = \left[1 - exp\left(-\frac{r_k}{\langle L_t \rangle}\right)\right]^{0.5} \left[1 - exp\left(-\frac{\langle u' \rangle + \langle S_u \rangle}{\langle L_t \rangle} t_{ign}\right)\right]^{0.5} \tag{5.9}$$

The sign $\langle \cdot \rangle$ represents an operation field averaging on a spherical volume with radius $C_{vol} \cdot r_k$ around the spark-plug, with C_{vol} defined the user. Instead, the radius r_k is computed by Equation (5.10) with the assumption of laminar condition for r_k, employing

the burnt mixture density ρ_b and the laminar flame stretch parameter $I_{0,lam}$.

$$\frac{dr_k}{dt} = \frac{\rho_u}{\rho_b} I_{0,lam} S_u \tag{5.10}$$

the laminar flame stretch parameter $I_{0,lam}$ is defined by Equation (5.11), where $\mathcal{L}_u$ is the Markstein length referred to unburned gas. Equation (5.12) defines the flame strain rate κ with the hypothesis of a spherical geometry for the kernel.

$$I_{0,lam} = \left(1 - \frac{\mathcal{L}_u \kappa}{S_u}\right) \tag{5.11}$$

$$\kappa = \frac{2}{r}\frac{dr}{dt} \tag{5.12}$$

Turbulent combustion is assumed to start when the flame radius exceeds the threshold value $r_{k,trans}$. Equation (5.13) defines $r_{k,trans}$ as a multiple of Taylor turbulence micro-scale λ and the tuning parameter C_{Tay}. More specifically, λ depends on the kinematic viscosity ν, on the turbulent kinetic energy k and on the turbulent kinetic energy dissipation rate ϵ.

$$r_{k,trans} = C_{Tay} \cdot \lambda = C_{Tay} \cdot \sqrt{10 \cdot \nu \frac{k}{\epsilon}} \tag{5.13}$$

When the combustion reaches turbulent conditions, some equations are no more valid therefore other expressions are needed, for example to compute the flame kernel speed and to model laminar to turbulent transition. Equation (5.10) and Equation (5.9) are substituted by Equation (5.14) and Equation (5.15) to compute respectively flame kernel speed and the f' coefficient with respect to the kernel dimension relative to Taylor micro-scale.

$$\frac{dr_k}{dt} = \frac{\langle \rho_u \rangle}{\langle \rho_b \rangle} \left[I_0 + I_0^{0.5} f' \left(\left\langle \Xi_{eq}^* \right\rangle - 1\right)\right] \langle S_u \rangle \tag{5.14}$$

$$f' = \left[1 - exp\left(-\frac{r_k - C_{Tay}\lambda}{\langle L_t \rangle}\right)\right]^{0.5} \left[1 - exp\left(-\frac{\langle u' \rangle + \langle S_u \rangle}{\langle L_t \rangle} t_{ign}\right)\right]^{0.5} \tag{5.15}$$

As the flame kernel grows, there could be a continuity problem in Equation (5.14) between the $\frac{dr_k}{dt}$ fraction, the turbulence stretch effects and the laminar ones. The adoption of Equation (5.16) allows the solution of this continuity problem. All the remaining parameters are defined by the empirical relation in Equation (5.17) demonstrated by Bray [53], exploiting the Karlovitz number Ka.

$$I_0 = min\left(I_{0,lam}, I_{0-turb}\right) \tag{5.16}$$

$$I_{0,turb} = \frac{0.117}{1+\tau} Ka^{-0.784} \tag{5.17}$$

$$\tau = \frac{T_b}{T_u} - 1 \tag{5.18}$$

5.1.3. Equilibrium wrinkling factor correlation

Both Equation (5.8) and Equation (5.14) relies on the Ξ^*_{eq} parameter which are undefined until now. The introduction of the Gulder relation [54] by the use of Equation (5.19) allows to define Ξ^*_{eq}.$\mathcal{R}_\eta$ is the Kolmogorov Reynolds number and Ξ_{coef} is a parameter fixed to 0.62 on the basis of experimental data interpolation. [54]

$$\Xi^*_{eq} = 1 + \Xi_{coef}\sqrt{\frac{u'}{S_u}\mathcal{R}_\eta} \tag{5.19}$$

$$\begin{cases} \mathcal{R}_\eta = \frac{u'}{\eta \tau_\eta} \\ \\ \tau_\eta = \sqrt{\frac{\mu_u}{\rho_u \epsilon}} \end{cases} \tag{5.20}$$

In Equation (5.20) τ_η is the Kolmogorov time scale and μ_u is the dynamic viscosity of unburned mixture.

The lookup table can be accessed only after the solution the unburned gas enthalpy h_u transport equation. h_u is the starting point to compute the fresh charge temperature T_u. Equation (5.21) compute the burned gas enthalpy h_b by the use of h_u and of the mean cell value.

$$h_b = \frac{h - b \cdot h_u}{1 - b} \tag{5.21}$$

Finally, thanks to the knowledge of h_b and of the composition Y_i, it is possible to define the burned gas temperature T_b.

6 | Simulation of high-pressure dual-fuel engine

The first attempt to simulate dual fuel engine combustion concerns an high-pressure dual-fuel (HPDF) engine; the simulation solver is made on the base of the tabulated kinetics approach (see Chapter 4). This first approach consists of two parts: the first is the simulation of diesel-only, diesel-methane and diesel-hydrogen engine configurations. The model is validated with a comparison of simulated and experimental data found in research literature. After that, the ammonia combustion simulation is performed.
The experimental data for the validation are found in some recent works done by Frankl et al.[3] and Gleis et al.[55] on a dual fuel engine derived from MTU 4000 Diesel engine.

6.1. Engine geometry

The engine adopted for this analysis is a full optical accessible single cylinder engine in Bowditch design, with variable compression ratio, derived from a four strokes marine MTU 4000 diesel engine. A schematization is shown in Figure 6.1.
The main engine geometry parameters are summarized in Table 6.1. The cylinder head is flat with a valve masking for swirl generation and the adopted piston bowl has cylindrical shape for a better optical access. The connecting rood length is missing among the main geometry values therefore the value is assumed equal to 350 mm, resulting in a cranck-to-connecting rod length ratio of 0.3, which is a common value for this kind of engines.
The engine geometry is reproduced with the use of the GUI, a tools developed inernally to create engine and piston bowl mesh. Starting from some user-defined points, this tool creates the geometry mesh of an engine combustion chamber and it also applies some geometric correction to obtain the correct compression ratio on the base of bore, stroke and compression ratio values. The tool was originally developed to reproduce curved bowl shape and to consider only one injection event while this case is characterized by a flat bowl shape and two injections, one of diesel and one of methane performed. Because of the flat bowl shape and because of the injections geometry, a trade-off must be found

between the better mesh and the capability of the tools.

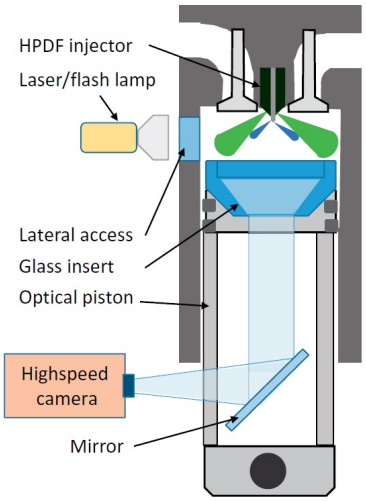

Figure 6.1: Single cylinder optical engine derived from MTU 4000 diesel marine engine: schematization [56].

MTU 4000 diesel engine	
Bore	170 mm
Stroke	210 mm
Compression ratio	17
IVC	240° bTDC
EVO	130° aTDC
Speed	750 rpm
Number of injector holes	9

Table 6.1: MTU 4000 marine diesel engine: main engine specifications.

The start time and the end time of the simulation are determined by the adopted valve timing for the intake and the exhaust valves (see Figure 6.2).
The chosen injector has 9 different injection holes. This characteristic allows to exploit the engine combustion chamber symmetry reducing the mesh to $\frac{1}{9}$ of the total volume, switching from the global combustion chamber domain to a 40° sector. Diesel-only simulation and initial diesel-methane simulations rely on this symmetry concept.

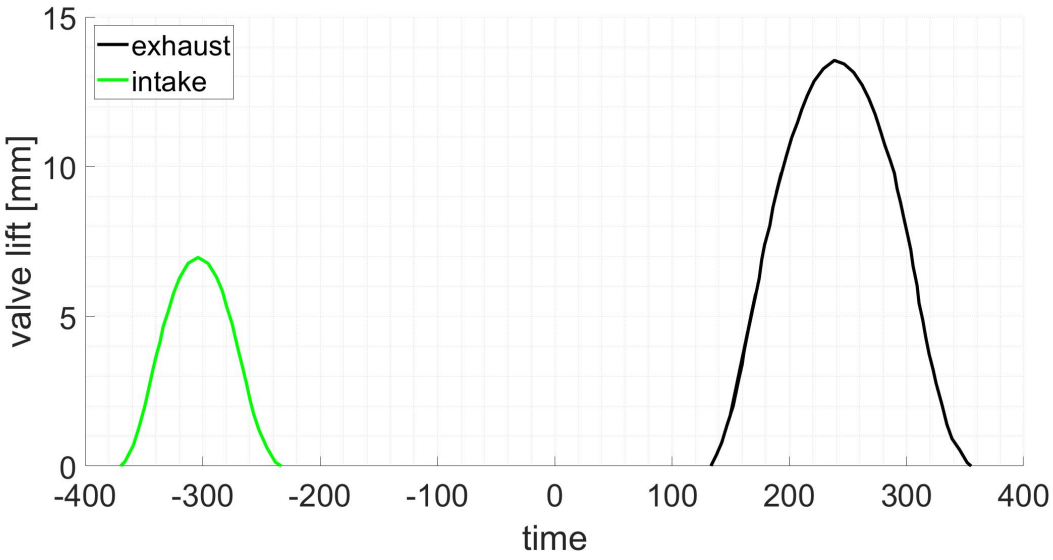

Figure 6.2: MTU 4000: valve timing representation [57]

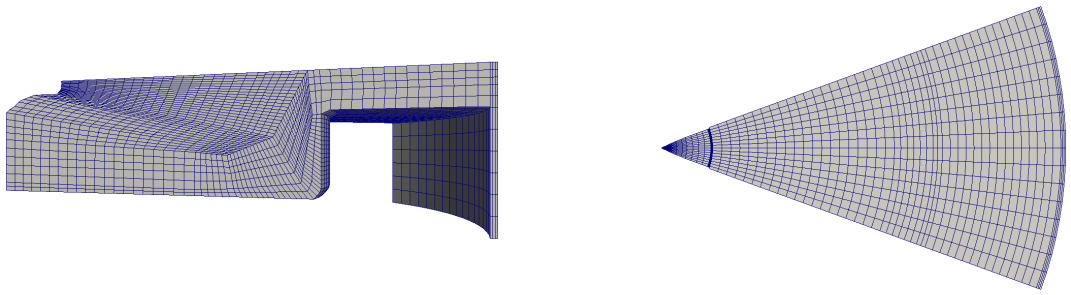

(a) (b)

Figure 6.3: MTU 4000 diesel marine engine: 40°sector engine mesh

6.2. Injection

In this case the engine is equipped with the Woodward L'Orange HPDI (high-pressure direct-injection) injector (see Figure 6.4a), centrally mounted in the cylinder head. The injector comes with nine holes for the pilot fuel and other nine holes for the main fuel. The injection system complexity is linked mainly to two aspects which are the high pressures adopted to inject the two fuels and the different values of these injection pressures. In diesel-methane case the fuels pressures are respectively 300 bar for the main injection and 1000 bar for the pilot injection, while for diesel-hydrogen case are respectively 500 bar and 1200 bar.

Figure 6.4 displays the injector tip and the injection geometry. Just looking at Figure 6.4b

it is evident that main and pilot injection direction are no aligned, except for the three couples of diesel and methane injections in radial direction.

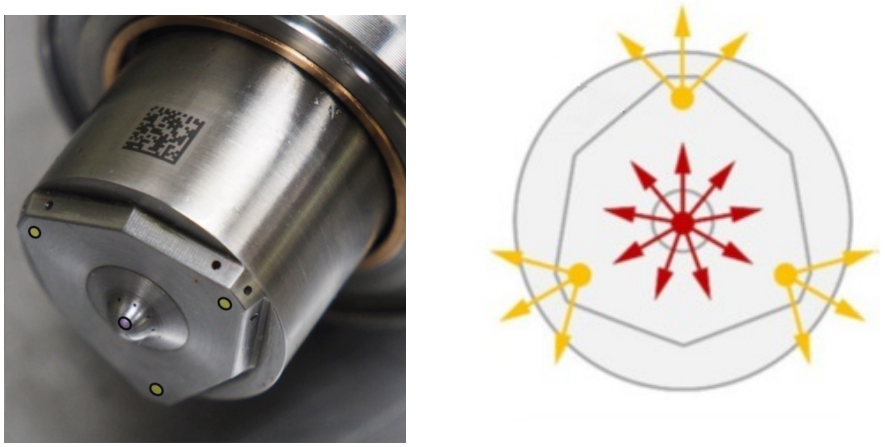

(a) Injector tip [58]

(b) Injection geometry: pilot injections in red and main injections in yellow [59]

Figure 6.4: Woodward L'Orange HPDI injector.

Each of the three couples of aligned injections is surrounded by a couple of diesel injections and a couple of methane injections and both these couples are symmetric with respect to the radial direction. This non-alignment is not compatible with the assumption of nine parts symmetry, therefore simulating combustion by considering only $\frac{1}{9}$ of the combustion chamber volume would lead to an error in simulation settings. A more complete CFD simulation thus requires a new mesh generated by the exploitation of a new symmetry based on three symmetric parts. The result is a mesh of a engine sector with an angle of 120° (see Figure 6.5).
This engine configuration is a methane - or hydrogen - DDF characterized by a diesel pilot injection followed by a methane injection: the adopted injections sequence leads to a methane diffusion flame, not a premixed one. The methane diffusive combustion is greatly affected by the injection sprays interaction, leading to the need of a precise injections geometry representation to properly simulate the combustion. Hence three-part mesh is more appropriate.
Table 6.1 lists the injections masses and Figure 6.6 displayes the injection laws.
Injector holes diameters are not specified therefore they are calculated from injections laws, injections masses and formulas available in literature [60]. Holes diameters are fixed to 0.53 mm for the main fuel hole and 0.14 mm for the pilot one.

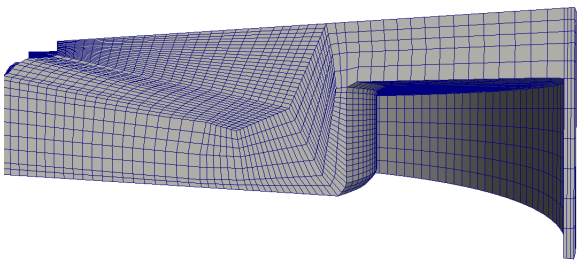

(a)

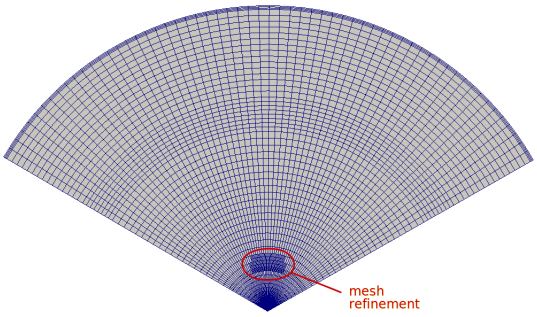

(b)

Figure 6.5: MTU 4000 diesel marine engine: 120° sector engine mesh.

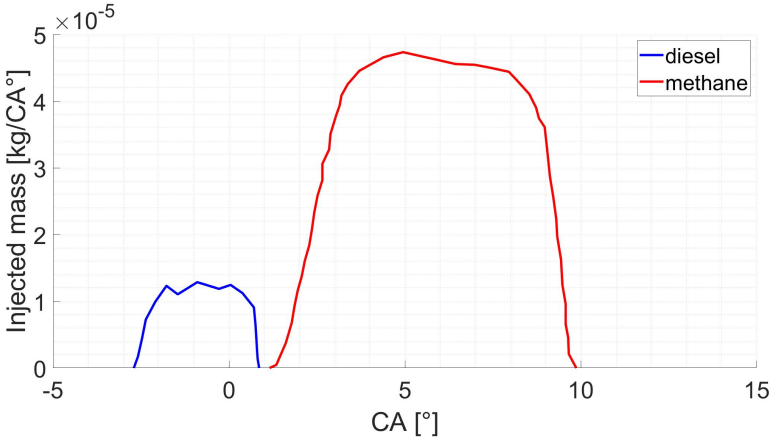

Figure 6.6: MTU 4000 diesel marine engine: diesel and methane injections laws

6.3. Virtual injector model

A Lagrangian approach suits the diesel injection because it allows to consider the liquid flow as a discontinuity phase, with the flow fragmentation in many particles. After evaporation, diesel is considered as n-heptane because of their similar thermochemical properties. However, the Lagrangian approach is not suitable for a gaseous phase injec-

tion because the injected gaseous flow cannot be characterized as an heterogeneous flow of particles. Shock waves and other phenomena feature a gas flow and such issues need an Eulerian approach because it is based on the continuum hypothesis.
The alternative approach is found in the so-called virtual injector model. The basic concept of this injection event modeling is the addition of a source term in the finite volume equation for a cells group defined by the user. Equation (6.1) is the resulting finite volume equation. With this step, the injection boundary conditions of the incoming gaseous fuel are substituted by the source cells and the wall replaces the inlet [61].

$$\frac{\partial}{\partial t}\int_{V_C}\rho\phi dV_C + \int_{\Omega_C}\vec{n}\cdot\left(\rho\vec{U}\phi - \Gamma\nabla\phi\right)d\Omega_C = \int_{V_C}\left(S_\phi + S_{\phi,add}\right)dV_C \tag{6.1}$$

$$S_{\phi,add} = \tilde{m}_{in}\phi_{in} \tag{6.2}$$

In Equation (6.1) the source term is added by the addition of the $S_{\phi,add}$ term. Equation (6.2) defines $S_{\phi,add}$ as the product of the mass flow rate of the injected stream per volume unit $\tilde{m}_{in}$ and the unitary value of the generic flow property, e.g. momentum, enthalpy and so on. All the injection properties are computed after the user-definition of injector diameter, start of injection (SOI), injected mass and injection law.
The main advantage of this injector model is the possibility to keep into account all the physical phenomena involved in a gaseous flow, among all shock waves and underexpansion [61]. Furthermore, the gaseous injection modeling is performed without any shaping of the injector internal geometry. Modeling gometry and events within the injector requires very small time-step and very tiny cells, resulting in larger computational time. The first step to use the virtual injector in a simulation is the definition of a mesh cells subset, a cellZone in OpenFOAM, where the source term will be applied.
The best cellZones definition for this case relies on the definition of three separate cellZones, on for each methane event, as shown in Figure 6.7. The three cellZones are placed on the cylinder wall because this configuration allows to avoid the recirculation of a small amount of the gaseous fuel from injector towards the combustion chamber center. The most probable cause for this recirculation is the momentum introduced by the virtual injector, because the source term applied in the cell zone introduces basically a mass quantity characterized by a velocity vector, thus introducing a momentum. This momentum, according to the action-reaction principle, leads to a force that generates an opposite flow field velocity which pushes methane in opposite direction. Moreover, each injections need a specific cellZone because the three injections are composed by three sprays with same mass, same injection timing but three different directions (one injection in radial direction and the other two in directions symmetric with respect to the radial one). The

imposition of all the sprays in the same cellZone means the introduction in the same cellZone of three momentum with same amplitude and three different directions. The symmetry of the two external directions leads to mutual annulment with the collapse of the two external injections on the central one.

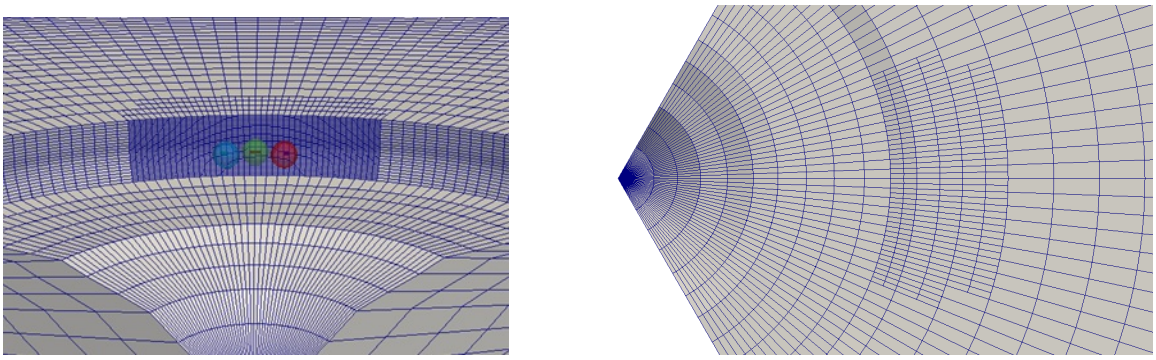

(a) Three cellZones configuration. The three coloured cyrcles represents the injector diameter

(b) Mesh refinement

Figure 6.7: Three different cellZones for virtual injector utility.

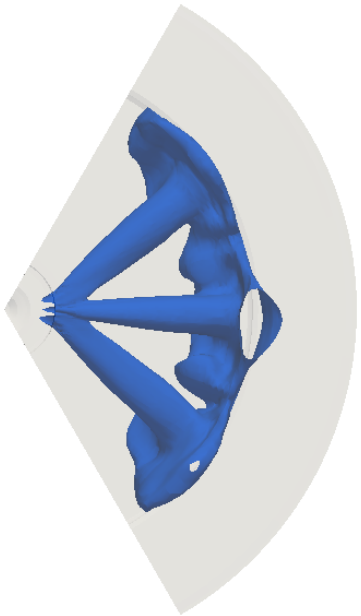

Figure 6.8: Final methane injection geometry: stoichiometric methane mass fraction at 8.5° aTDC.

The three cellZones are not in contact with each other to avoid any interaction between

the jets. Furthermore the distance between the cellZones represents the distance needed by the injector diameter for a better simulation of the injections.
The injector holes positions are assumed considering the geometry of the engine head and the injections directions. The main injection angle is 72.5° from the cylinder axis; for pilot injection is 74°.
To reach both the separation and distance conditions, a cell refinement shown in Figure 6.7b is performed near the injector hole. The original cells dimensions do not allow the separation between the cellZones leading to a wrong injections interaction, then to a wrong injection geometry.
After taking these measures, the resulting injection geometry is an injection with three different sprays and three different directions. This resulting injection shape is shown in Figure 6.8, where a tiny counter-current flow is still present but now its effect is negligible.

6.4. Simulation results

Experimental data are available for a MTU 4000 diesel marine engine in diesel-methane configuration [55] and in diesel-hydrogen configuration [3]. After the validation of the diesel-hydrogen modeling, the work done by Frankl et al.[3] simulates diesel-ammonia engine. This thesis work starts simulating with a diesel-only configuration for the MTU 4000 diesel marine engine to define some simulation parameters. Therefore diesel-methane and diesel-hydrogen modes are simulated to validate the model for a final diesel-ammonia simulation.

6.4.1. Diesel simulation

The first engine simulation is ran keeping the same energy content as diesel-methane configuration but using only diesel. The aim of this simulation is to check the basic parameters and made the needed corrections. The Representative Interactive Flamelet (RIF) combustion model is used for diesel-only simulations [7]. This method uses n-heptane to simulate diesel in vapour state because n-heptane has diesel-like ignition properties. However, diesel and n-heptane have different LHV (43 MJ/kg for diesel and 44.5 MJ/kg for n-heptane) therefore for keeping the same energy input the injected mass of n-heptane is scaled with respect to the injected mass of diesel.
The goal of the diesel-only simulation is to check the compression curve and to have a baseline case to allow comparison between single fuel and dual fuel operations. The adopted mesh for these tests are the 40° sector one (see Figure 6.3b) because diesel injections presents a axial-symmetric geometry with respect to the cylinder axis.

Different SOI for the diesel configuration are tested to obtain the diesel-only case with pressure peak at time close to the one of pressure peak of methane DDF case. For the diesel-only case the injection starts at 0° aTDC with a diesel injected mass of 43.28 mg for each hole. In the experimental setup the compression ratio is fixed to 17.15 and the inlet pressure is equal to 6 bar with a blow-by [55]. However, the higher (but undefined) pressure losses because of the optical engine structure cannot be neglected.

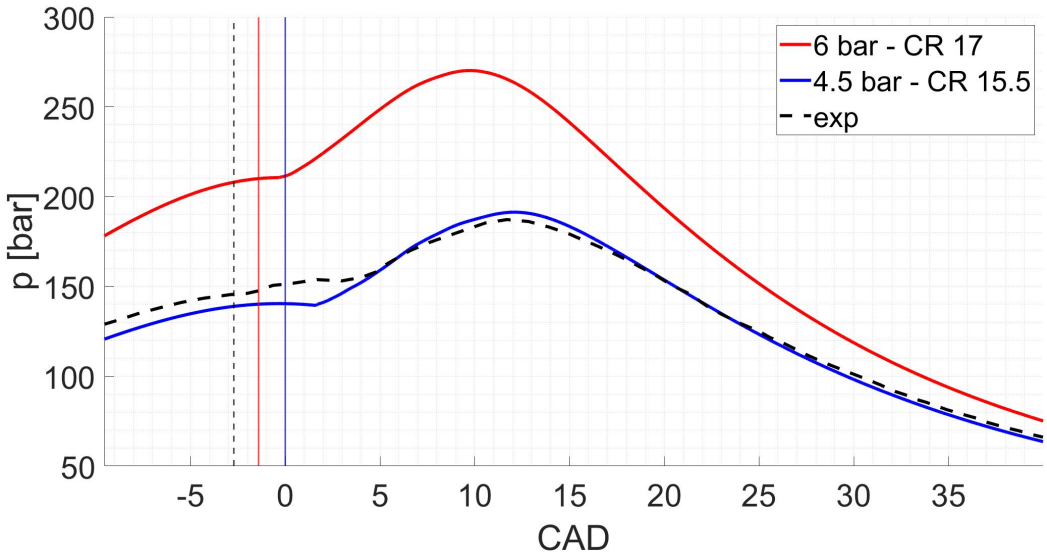

Figure 6.9: MTU 4000 : diesel-methane experimental and diesel-only simulated pressure curves with different IVC conditions.

Figure 6.9 displays the experimental pressure curve and the pressure curves resulting from simulations. Imposing a compression ratio equal to 17 and an inlet pressure of 6 bar leads to a condition very different from diesel-methane case SOI (2.7° bTDC). Therefore different conditions at IVC are tested to reach acceptable condition at SOI; the best one is an inlet pressure value equal to 4.5 bar and a compression ratio equal to 15.5. Lowering the inlet pressure allows to get closer to the experimental value of air mass flow inside the cylinder at IVC: this experimental value is equal to 16.4 mg/cycle. With 6 bar of inlet pressure and the compression ratio equal to 17 the air mass flow is equal to 25 mg/cycle; instead for an inlet pressure value of 4.5 bar and the compression ratio equal to 15.5 the air mass flow is around 16.8 mg/cycle. These new settings can be accepted because the comparison is done taking as reference conditions a point before the combustion event. The goal is to match the pressure condition of diesel SOI in diesel-methane mode with a diesel-only simulation and this comparison among configurations characterized by different fuels is acceptable because only fresh air compression event, not the combustion, is involved until the diesel SOI. The recap of the final simulation setup is done in Table 6.2.

The compression ratio and pressure lowering is supported also by looking at the pressure of diesel-hydrogen case. This engine configuration is set to a compression ratio equal to 17, with a bit higher inlet pressure, 6.5 bar. Figure 6.10 displays a comparison between the hydrogen DDF experimental conditions and diesel-only simulated ones. The first simulation with intake pressure fixed 6 bar and compression ratio equal to 17 shows higher pressure than the hydrogen DDF experimental configuration, set with 6.5 bar and 17.5 compression ratio. The higher pressure with respect to the case with higher inlet pressure and higher compression ratio is quite strange.

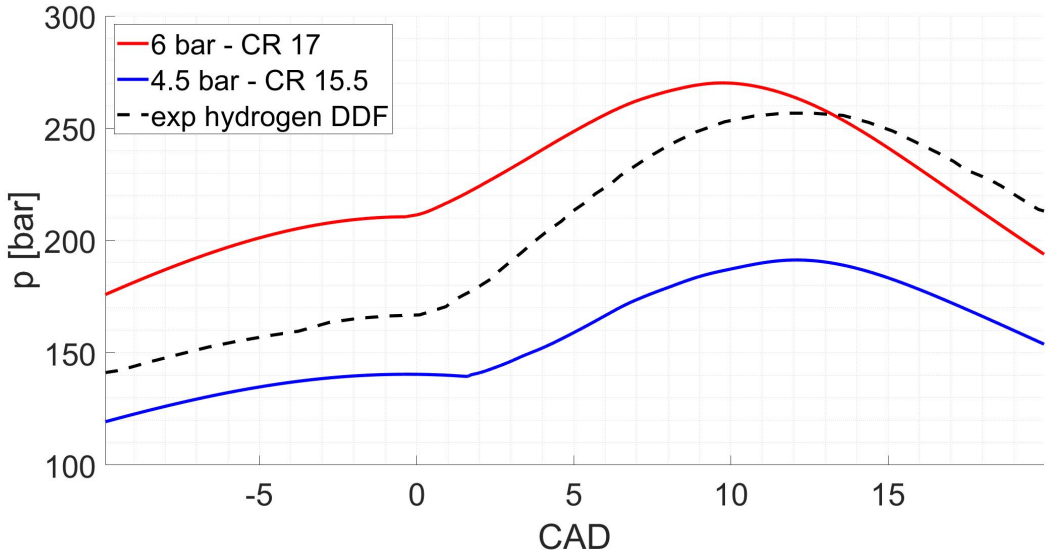

Figure 6.10: MTU 4000: diesel-hydrogen experimental pressure curve and diesel-only simulated ones.

The main unknown is a value for the blowby effect: the intake pressure and compression ratio modification helps to consider this effect.
After this correction of initial parameters, the diesel-methane dual fuel simulation can start with a more precise initial conditions.

6.4.2. Diesel-methane simulation

The methane DDF engine simulation is based on the tabulated kinetic method described in Chapter 4. Chemical composition and reaction rates are stored in two data tables, one for each fuel, generated using OpenSMOKE utility. The diesel spray is modeled by the use of the Lagrangian approach, introducing in the domain pockets of droplets with same properties, called parcels, and by the use of the blob cone injector model which computes the spray geometries, for example the spray angle. Many sub-models are used

for breakup, evaporation, injection and so on; in particular the simulation setup involves the KHRT model for the primary and secondary breakup and the standard $k-\epsilon$ model with the round jet correction for computing the vapor fuel jet penetration.

MTU 4000 diesel engine	
Compression ratio (exp)	17.15
Compression ratio (sim)	15.5
Pressure at IVC (exp)	6 bar
Pressure at IVC (sim)	4.5 bar
Diesel-only	
SOI	0° aTDC
Diesel mass	43.28 mg/cycle
Diesel-methane	
SOI diesel	2.7° bTDC
SOI methane	1.15° aTDC
Diesel mass	30 mg/cycle
Methane mass	320 mg/cycle

Table 6.2: MTU 4000 marine diesel engine: diesel-only and diesel-methane operating conditions.

The experimental data are taken from tests performed by Gleis at al.[55]. Injection data are summarized in Table 6.2 and in Figure 6.6.
A deeper analysis of the first simulations figures out a methane injection mass overestimation. The problem comes out looking at deltaMass.Cyl file and totFuel.Cyl output file. These two are both simulation output files about the mass quantity inside the domain. The first one reports the in-cylinder mass increase due to fuel injection in all the CFD domain; the second one reports the total fuel mass resulting from integral of mixture fraction over the CFD domain. The two values should be almost equal but in this case a large difference can be detected in Figure 6.11a. The integration in the CFD domain is not enough accurate, then the species and their properties are not so precise. The integration in CFD domain is improved increasing the number of outer correctors of the CFD solver from one to three; this new settings means that more iterations are performed then the error drops (see Figure 6.11b).
After the adjustment on simulation settings, the final simulation setup is run on 16 cores for a total time around 120 hours. Figure 6.12a shows the pressure curves in comparison

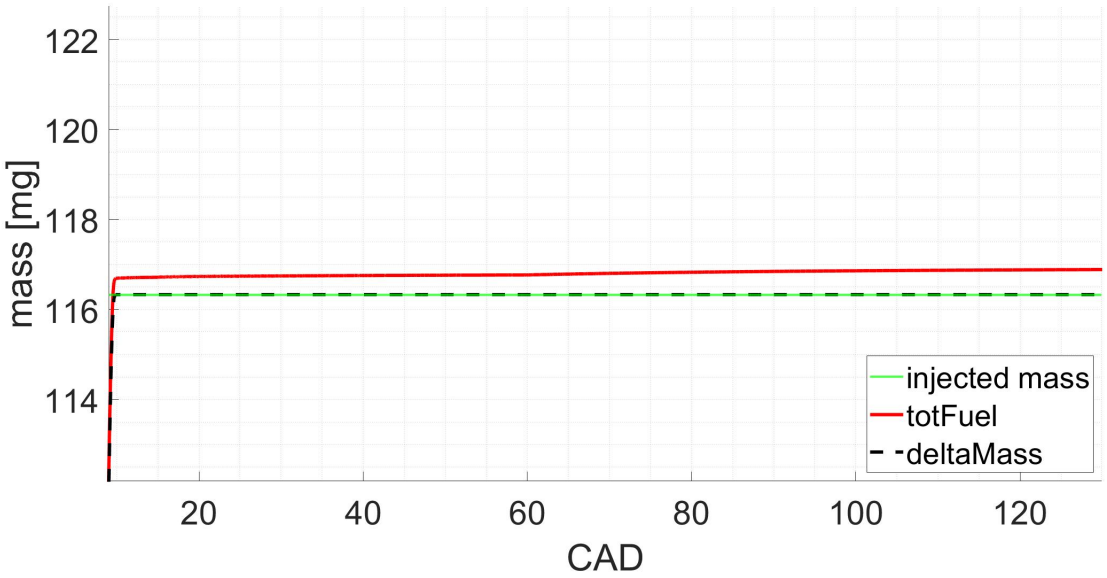

(a) Comparison between deltaMass.Cyl, totFuel.Cyl and injected mass: one outer corrector.

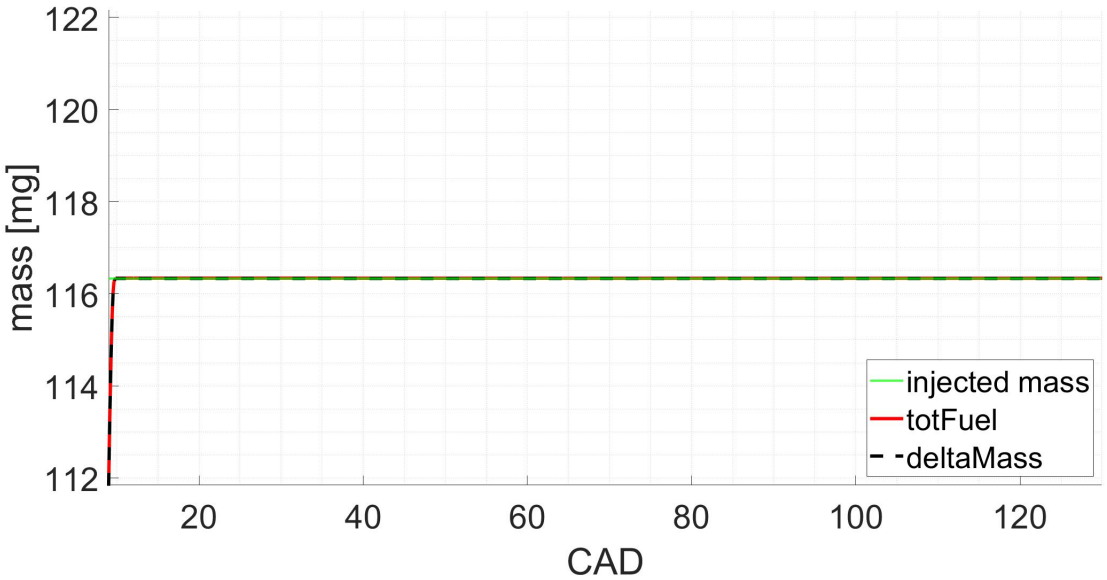

(b) Comparison between deltaMass.Cyl, totFuel.Cyl and injected mass: three outer corrector.

Figure 6.11: Comparison between deltaMass.Cyl, totFuel.Cyl and injected mass with different correctors number.

with the experimental one: simulated pressure matches quite well the experimental values until the methane injection start point. After that, the simulated curve overestimates the experimental one. The pressure raise is faster than the experimental one and to be precise the pressure peak overestimation is around 8.5%. However, the pressure overestimation regards only the natural gas combustion because the diesel pilot injection fits quite well.

Also the methane ignition delay is matched.

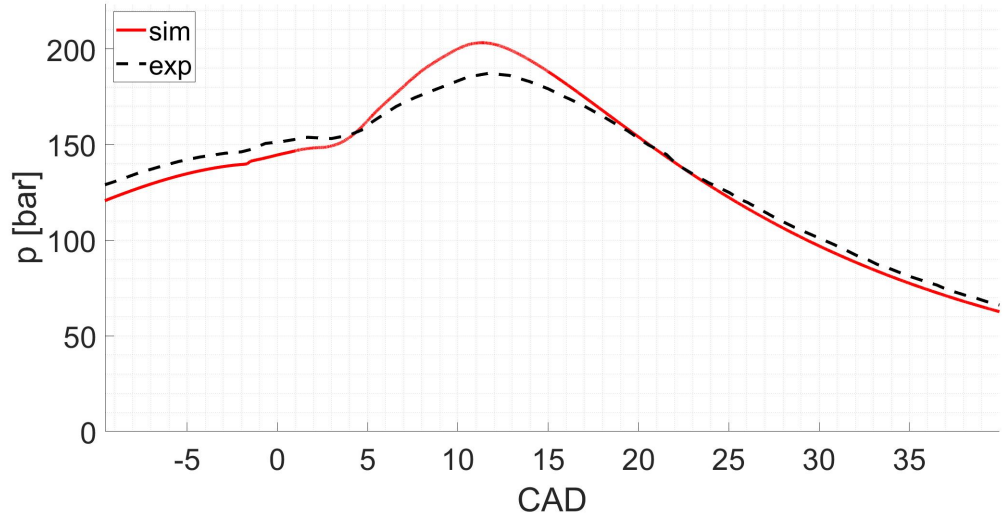

(a) Pressure curves: experimental and simulated

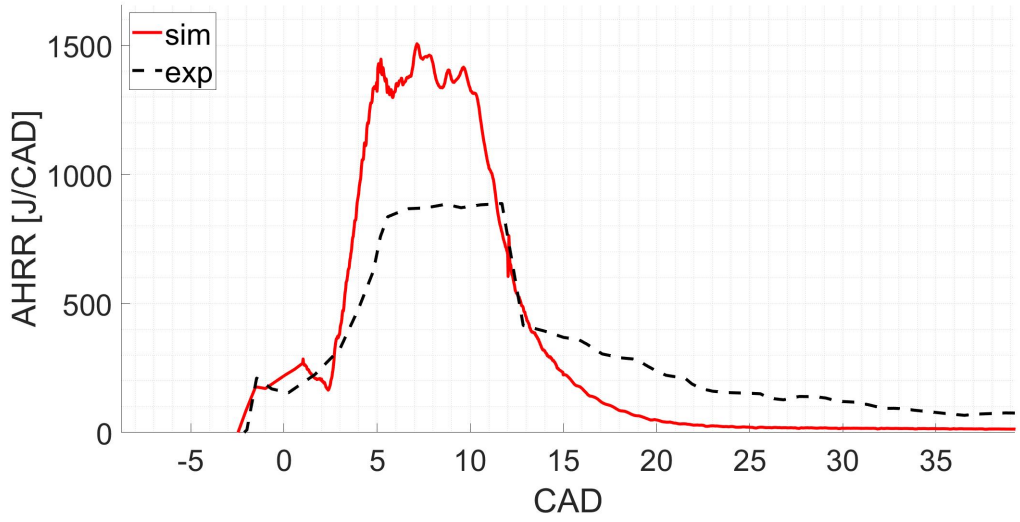

(b) AHRR curves: experimental and simulated.

Figure 6.12: MTU 4000 diesel-methane simulation: pressure and AHRR.

The AHRR curves are calculated starting from the pressure curve for both experimental and simulated cases. An AHRR curve is available in the experimental data [55] but the heat losses are undefined, therefore the simulated AHRR would consider different heat losses. Post-processing the pressure curves with the same method allows to compare the resulting AHRR. This comparison is done in Figure 6.12b: the obtained shapes are very different and the almost instantaneous simulated combustion of the injected methane stands out.

This instantaneous ignition is evidenced by looking at Figure 6.6 because of injection

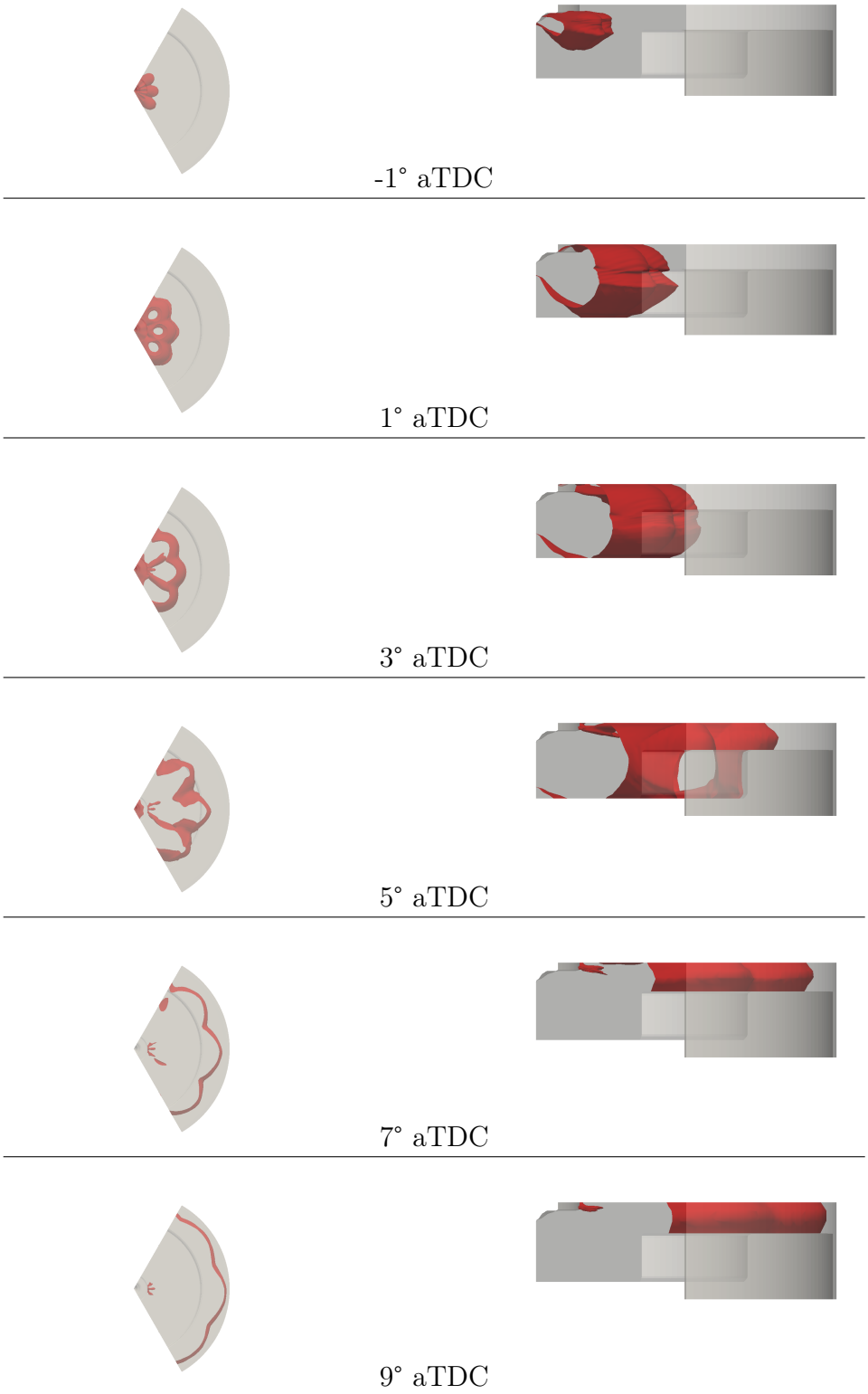

Figure 6.13: MTU 4000: diesel-methane combustion represented by $c = 0.5$.

law and AHRR curve similarity. The fast decrease of simulated AHRR is similar to the injection law shape except for the final part, where some methane still burns. For the

experimental AHRR curve, more methane still remains to burn. The fast methane combustion might be the main actor for the pressure overestimation but many factors might be the cause for this pressure error, especially considering the many assumptions made up to this point.

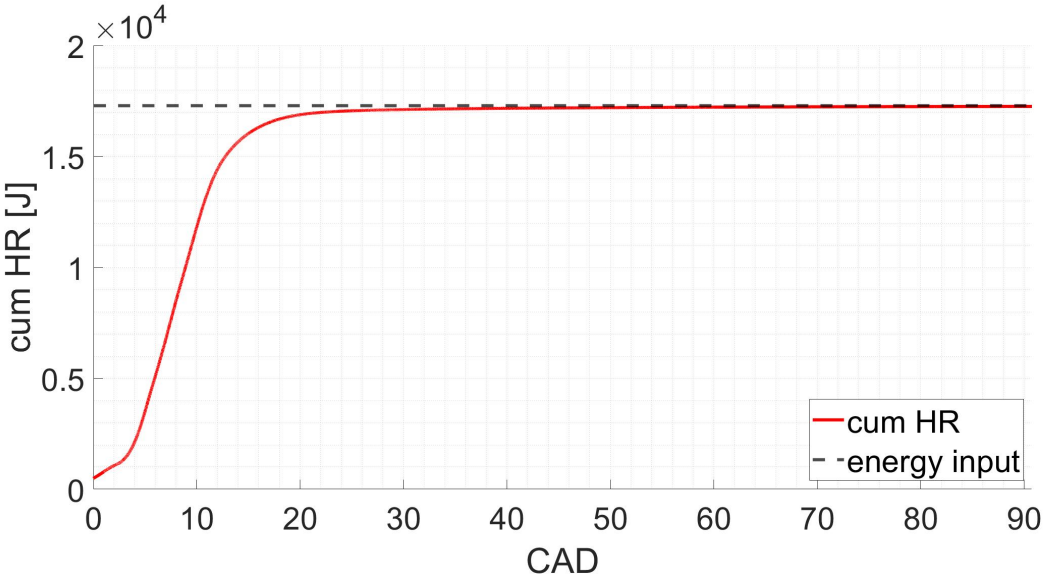

Figure 6.14: Cumulative HRR and energy input.

During the first simulation analysis, a second issue linked to the total energy input is found. The final value of the cumulative heat release rate was higher than the total energy input. After some modifications and simplifications on simulation models and sub-models, the energy input is correct, as demonstrated in Figure 6.14.
Figure 6.13 displays the methane combustion event for the diesel-methane mode by showing the behaviour of the isosurface for $c = 0.5$.
In conclusion, the adopted model fits quite well the experimental results whereas many aspects are suggested or assumed. Many improvements could be made, such as a better injector geometry, more specific IVC conditions and finer mesh. However, overcoming problems with hypotheses leave many uncertainties that hamper investigations about the simulations problems.

6.4.3. Diesel-hydrogen simulation

After the diesel-methane DF configuration, the same engine is tested in hydrogen diesel dual fuel mode.
The first problem to be dealt with is the lack of information about the injection because neither the fuel quantities nor the injection laws are defined, except for the SOI at -4.5 for

diesel and at 0° aTDC for hydrogen. [3] Figure 6.15 displays the AHRR curve available in experimental data [3] which helps to overcome the fuels quantities problem. The integral of the AHRR depends on the energy released by the combustion and this energy is related to the fuel amount by the Lower Heating Value (LHV). Working on the energy released during the pilot injection and the one released in the remaining time, the injected diesel mass and the methane one are computed accordingly to Equations (6.3)-(6.6).

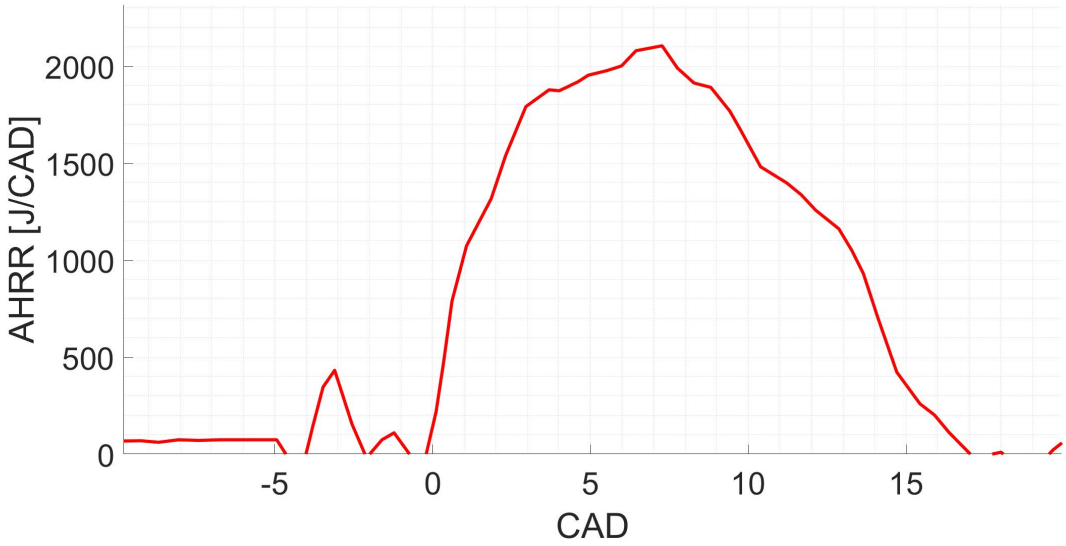

Figure 6.15: Diesel-hydrogen experimental test: AHRR. [3]

$$AHR_{diesel} = \int_{SOI_{diesel}}^{EOI_{diesel}} AHRR = 480.6\ J \tag{6.3}$$

$$mass_{diesel} = \frac{AHR_{diesel}}{LHV_{diesel} \cdot \#holes} = 1.24\ mg \tag{6.4}$$

$$AHR_{hydrogen} = \int_{SOI_{hydrogen}}^{EOI_{hydrogen}} AHRR = 22760\ J \tag{6.5}$$

$$mass_{hydrogen} = \frac{AHR_{hydrogen}}{LHV_{hydrogen} \cdot \#holes} = 21.1\ mg \tag{6.6}$$

These last operations are useful for having an approximate value of fuels quantity; however the real quantities are certainly greater because of combustion and heat losses. The missing diesel pilot injection laws is assumed as the one of methane DDF case. Instead the missing hydrogen injection law is assumed as a trapezoidal shape and it is computed by knowing the injection pressure, the injector diameter (equal to the one adopted in the

methane DDF case) and by using formulas that can be found in literature [60]. Figure 6.16 shows the obtained hydrogen injection law.
The adoption of three outer correctors main has the drawback of larger simulation time: in this case simulation time is about 107 hours.

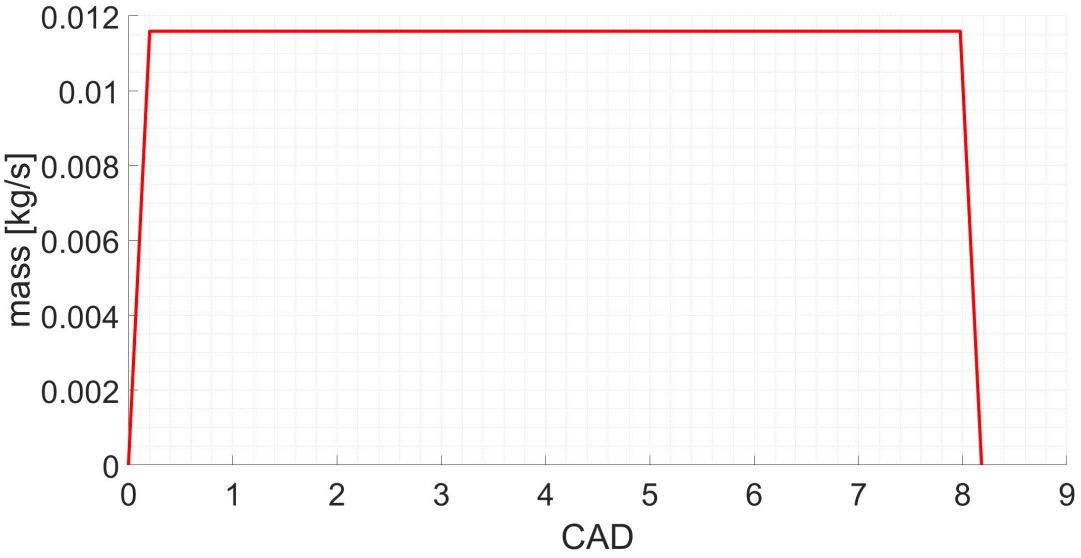

Figure 6.16: Injection law for hydrogen DDF case.

Figure 6.17a shows the pressure curves. The adoption of a compression ratio equal to 17 leads to a good estimation of pressure behaviour until the start of combustion. Simulated pressure has a good agreement with the experimental results until the start of hydrogen injection because simulated pressure values are very similar to the experimental ones, until the start of hydrogen combustion. However, an acceptable result is obtained until 2° aTDC. After this time, the simulated curve does not follow the experimental pressure behaviour, with a very large underestimation. The peak pressure error is about 40 bar, with an underestimation of 16%, and this value is not acceptable.
As expected, AHRR curves are not similar because they are both result of a pressure curve post-processing. The experimental case is characterised by a much faster combustion that leads to a higher pressure increase rate then to higher pressure peak. The simulated one instead, after a good fit for diesel combustion event, shows a small ignition delay of about 1° aTDC and then a good match only for a first small time. The incompatibility of these simulation results with respect to the experimental data are evident.
The main cause for the pressure difference might be the many parameters assumed before the simulation as for example the injection law.
Many attempts are done, assuming different injection masses, different injection pressures, different injector diameter and so on. However, none of these attempts leads to a good

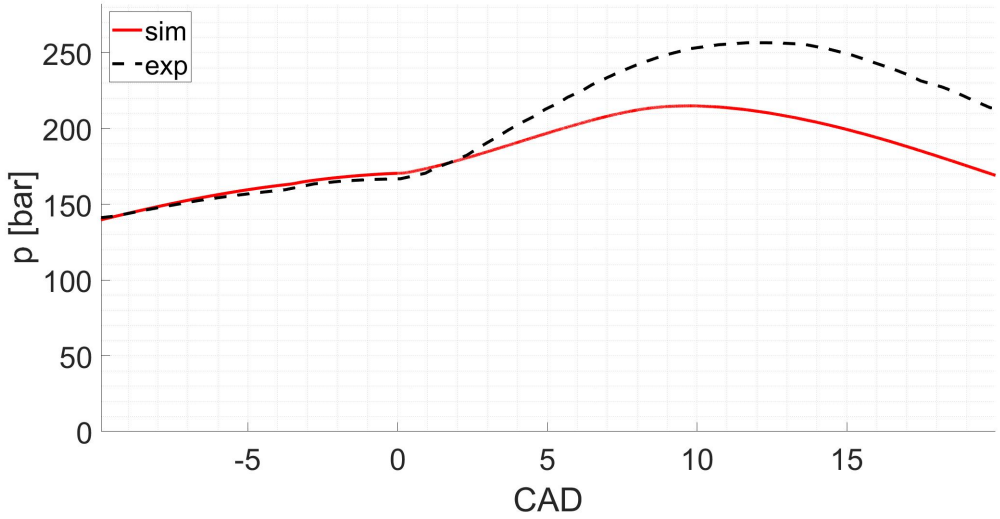

(a) Pressure curves: experimental and simulated.

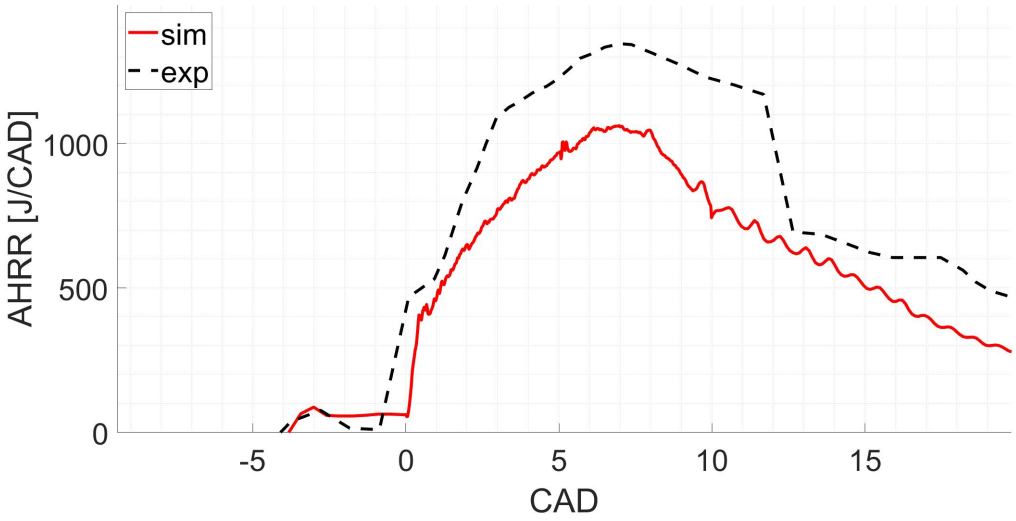

(b) AHRR curves: experimental and simulated.

Figure 6.17: MTU 4000 diesel-hydrogen simulation: pressure and AHRR.

pressure curve trend. An example of one these trials of simulation setting is shown in Figure 6.18. This attempt starts at diesel SOI and its number of correctors is fixed to one to reduce the simulation time. The lower correctors number explains the slightly different pressure value at SOI. In this example, larger diameter and larger hydrogen mass are adopted and the new injection law leads to a better representation of the combustion, with acceptable pressure increase rate and AHRR in the initial phase. However, after some CAD, the curves are no longer similar. The initial similarity lets think that the main problem is the unknown injection parameters. To reach acceptable injection conditions, geometry and pressure should be modified but doing that brings far from the experimental

case.

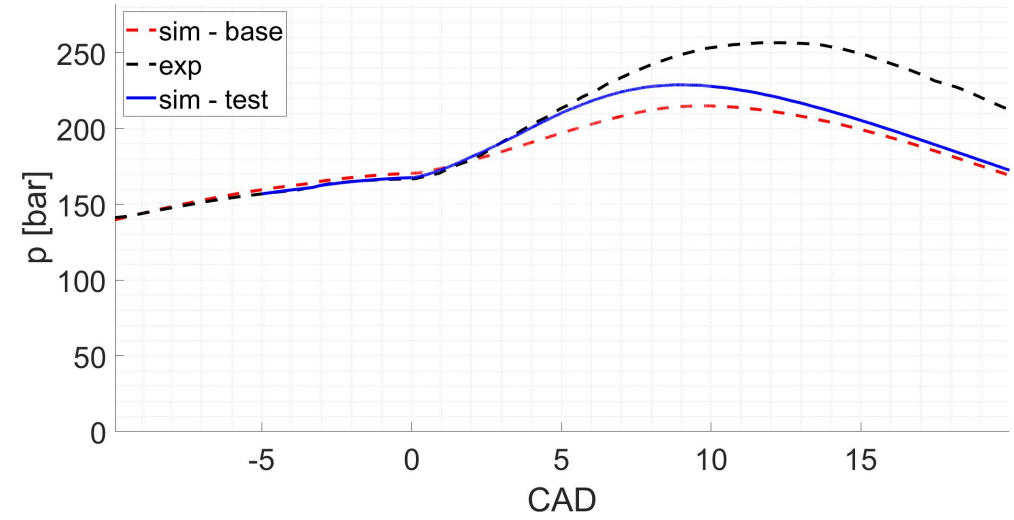

(a) Test on simulation settings: experimental and simulated pressure curves.

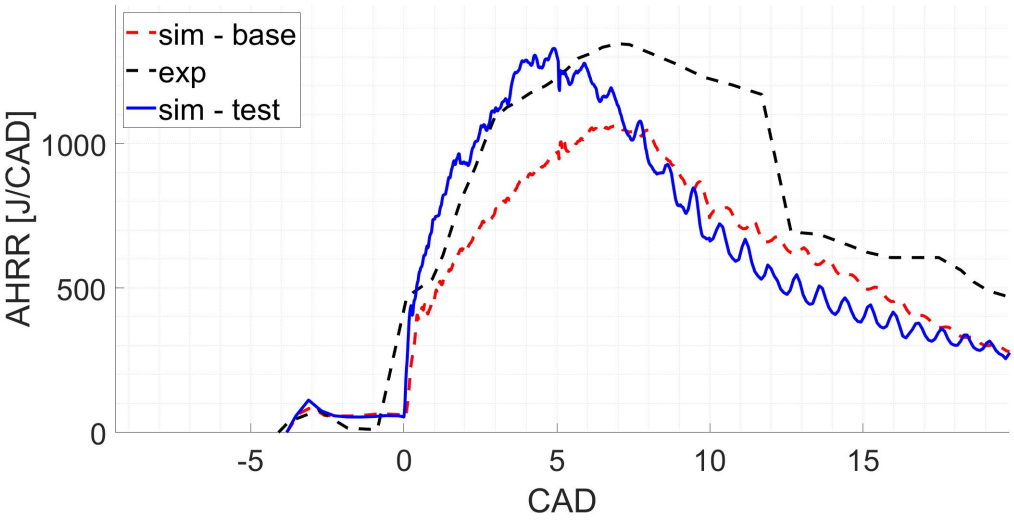

(b) Test on simulation settings: experimental and simulated AHRR.

Figure 6.18: MTU 4000 diesel-hydrogen simulation: test on new simulation settings

6.4.4. Conclusions

Both the diesel-methane and the diesel-hydrogen cases are preliminary tests to check the reliability of the simulation approach for a diesel-ammonia case. The simulation results of diesel-methane mode are satisfactory but the diesel-hydrogen case simulation is not enough accurate because of a large pressure underestimation. Furthermore, the shape of simulated pressure of the diesel-hydrogen engine implies something wrong during

the hydrogen combustion simulation because the pressure rise rate is never similar and because, despite the different assumptions, no setup is able to obtain minimally admissible results. The simulated AHRR curves are always far from the experimental ones and also this difference points out a failure in the diesel-hydrogen combustion simulation. Furthermore, the use of assumptions to overcome the lack of experimental setup leaves a global uncertainty about the error cause. The number of attempts done, the number of remaining possibilities and the time required by simulations makes a trial and errors approach quite unfeasible for defining the missing parameters.
In conclusion, the adopted approach cannot simulate diesel-ammonia engine on the basis of the diesel-hydrogen case because the premise of a good modeling performance is not fulfilled.

7 | Diesel-ammonia simulations with premixed ammonia

The final attempt to simulate ammonia combustion is done with a new configuration, taking as reference point data of experiment carried out by Yousefi et al.[2]. The engine configuration is now quite different from the previous one analyzed in Chapter 6. Ammonia is port injected in the intake manifold, no more directly injected inside the cylinder with a HPDI injector, thus leading to a premixed combustion.
For a correct approach to a premixed combustion, the chosen combustion solver is based on a hybrid model: tabulated kinetics is used to perform the diesel ignition therefore the premixed combustion of port injected ammonia is simulated by the Weller combustion model, explained in Chapter 5 [4]. The model equations are solved with RANS approach with $k - \epsilon$ model; the injection setup is kept consistent with what used in the previous chapters.

7.1. Engine geometry

The simulated engine is a single cylinder, four stroke, heavy duty (HD) engine derived from a Caterpillar 3401 diesel engine, which was adapted to work in dual fuel operations using diesel and ammonia. The main engine specifications are listed in Table 7.1.
The diesel injection system is composed by a common rail system with pressure up to 525 bar [2]. The ammonia port fuel injection (PFI) system is made by two solenoid gas injector. Simulation focuses only on the combustion phase and on what happens inside the cylinder when both intake and exhaust valves are close. The ammonia injection is not included and the assumption of ammonia as homogeneously distributed in the CFD domain substitutes the intake phase calculations.
The mesh domain is created using the GUI utility, presented in Chapter 6, starting from a CAT 3401 piston bowl profile and injection angle found in literature [62]. The total number of injector holes are six and they are placed in axial-symmetric position: this property allows to exploit the symmetry of the combustion chamber. The CFD mesh is

then reduced to a $\frac{1}{6}$ of the total cylinder volume, decreasing the simulation time; Figure 7.1 shows the mesh sector of 60°. The injection geometry is quite simple for this case because only diesel injector holes are present. Therefore there is no problem in the domain simplification on the base of geometry. The injector hole diameter is assumed equal to 0.23 mm, according to a data for a CAT 3400 engine found in literature [63].

Engine model	Caterpillar 3401
Number of cylinders	1
Bore	137.2 mm
Stroke	165.1 mm
Connecting rod	261.62
Compression ratio	16.25
Displacement	2.44 L
IVO	358.3° bTDC
IVC	169.7° bTDC
EVO	145.3° aTDC
EVC	348.3° aTDC
Speed	910 rpm
Number of injector holes	6

Table 7.1: Caterpillar 3401: main engine specifications [2].

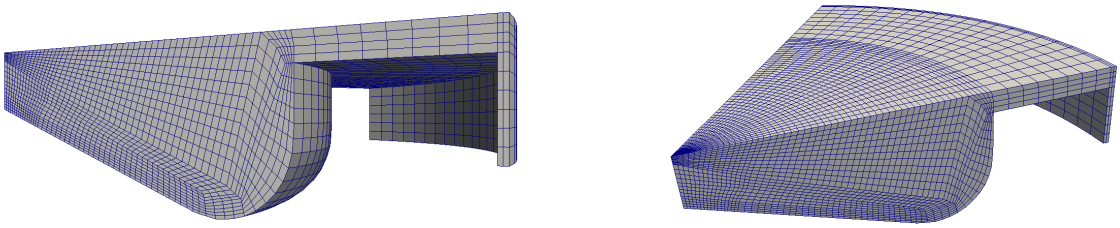

(a) (b)

Figure 7.1: Caterpillar 3401: engine mesh.

The experimental approach consists of two parts: the first one tests different ammonia quantities at constant energy input; the second one focuses on different diesel SOI effects,

keeping the same energy ammonia input. The main experimental conditions are summarized in Table 7.2 and Table 7.3. These tables list diesel, air and ammonia flow rates, diesel SOI and EOI and total energy fraction replaced by ammonia. This last parameter is computed according to Equation (7.1).

$$\%NH_3 = \frac{\dot{m}_{NH_3} \cdot LHV_{NH_3}}{\dot{m}_d \cdot LHV_d + \dot{m}_{NH_3} \cdot LHV_{NH_3}} \cdot 100 \tag{7.1}$$

NH_3 energy fraction	Diesel SOI (° aTDC)	Diesel EOI (° aTDC)	Diesel mass (kg/h)	NH_3 mass (kg/h)	Air mass (kg/h)
0	-14.2	2.28	3.38	0	83.26
20	-14.2	0.11	2.73	1.56	80.81
40	-14.2	-2.18	2.08	3.18	78.11

Table 7.2: Caterpillar 3401 engine test 1: main injection parameters [2].

The experimental settings report only the start and the end of the diesel injection, without other specifications about injection laws shape. Therefore the injection laws for each simulated condition is assumed as a square wave included in respectively SOI and EOI.

7.2. Diesel simulation

The first simulation is performed fueling the CAT 3401 engine with only diesel to get a baseline case. The simulations relies on condition listed in the first row of Table 7.2 and the RIF combustion model is used. As done in Section 6.4.1, the diesel-only engine simulation is useful also to set some initial conditions.
Figure 7.2 shows the results of the first simulation. These results are a good starting point because the simulation pressure trend matches quite well the experimental trend. The initial IVC pressure is computed starting from the mass flow value defined in Table 7.2. The compression ratio seems to be similar to the experimental one. Fixing the IVC pressure equal to 1.35 bar is in accordance with the trapped mass per cycle. The pressure peak is a bit higher (about 4 bar) and a bit advanced (about 5° CAD) but during the expansion phase the pressure trends are quite similar. The pressure peak advance is related to an early pressure increase, which starts right after the diesel injection while the experimental case shows a different pressure behaviour, with a large delayed pressure increase with respect to diesel SOI provided by Table 7.2.

The AHRR curves in Figure 7.2b are computed from the pressure curves. It is evident that the diesel ignition in the simulation case is advanced with respect to the experimental one. The thermochemical properties of diesel, or n-heptane as used in simulation case, are well-known and a so large ignition delay, up to 8° aTDC can not be explained as a computational problem. Furthermore the simulation solver is well established, therefore such delay cannot be related to the simulation solver or simulation settings.

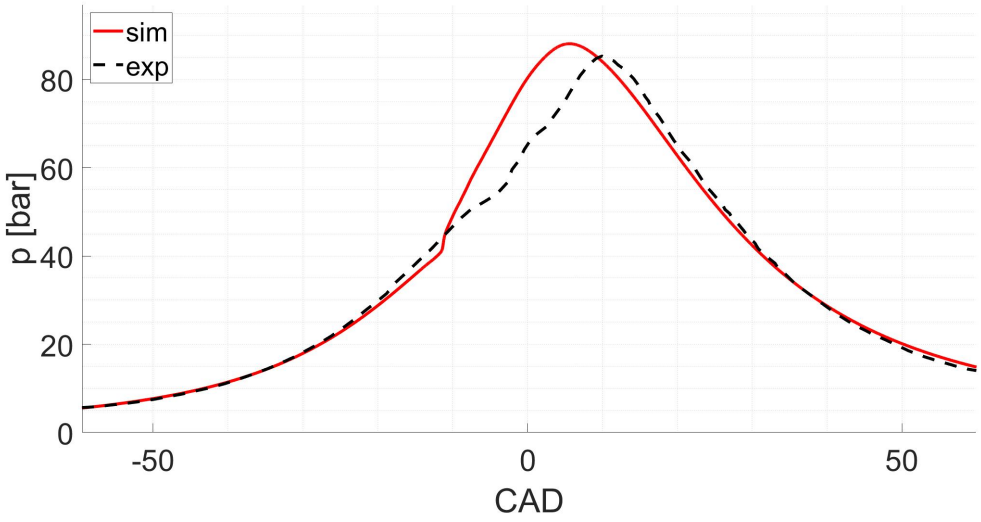

(a) Pressure curves: experimental and simulated.

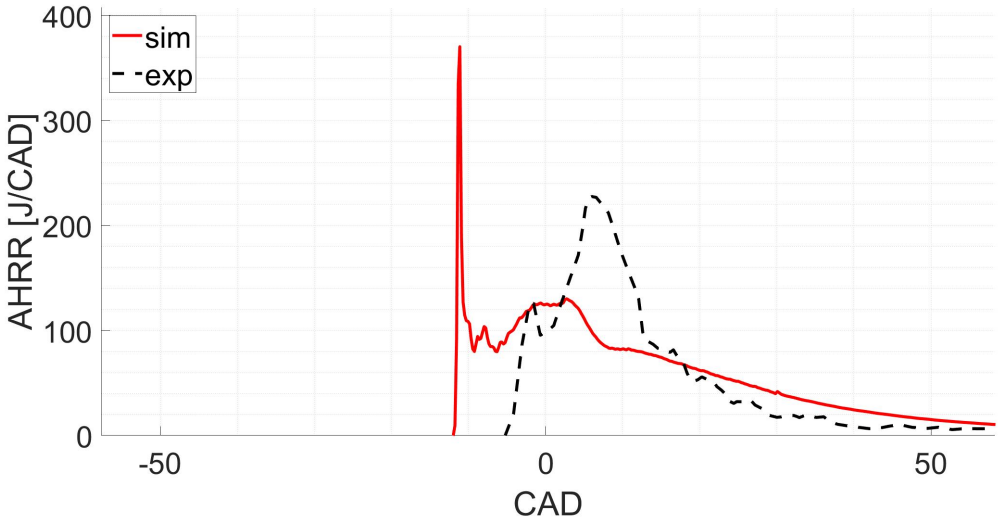

(b) AHRR curves: experimental and simulated.

Figure 7.2: CAT 3401 only diesel first simulation: pressure and AHRR.

The most likely cause for the diesel ignition delay is identified in an undefined hydraulic delay of the injector : SOI at 14.2° bTDC might be the start for the electric signal for the system to start injecting the fuel. On the other hand, it seems very improbable that

the diesel ignition takes up to 8° aTDC to start whereas in other cases it usually starts instantaneously. Because of the introduction of the injection delay, the new SOI is placed at 6.2° bTDC. A delay is assumed also for the EOI and the best result is obtained assuming a EOI delay equal to 5. Figure 7.3 displays the adopted injection law and the experimental one.

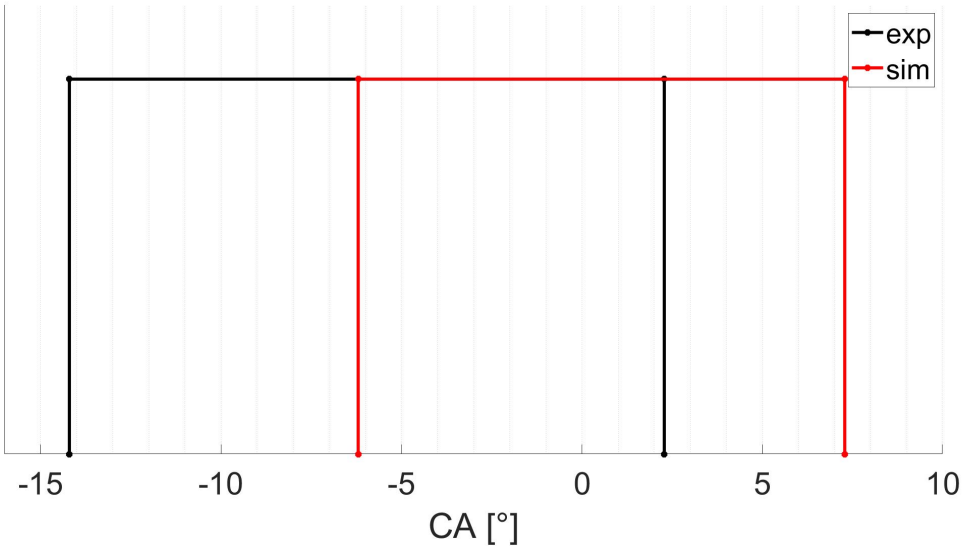

Figure 7.3: Diesel case injection laws: experimental one and one adopted for the simulation.

The final attempt for a diesel-only simulation is done with the new SOI and with a slightly higher compression ratio, up to 16.5, to compensate for the lower pressure at the SOI. Figure 7.5 reports the obtained simulation results. The pressure prediction improves a lot for both shape and values, with pressure peaks equal respectively 85.3 bar at 9.93° aTDC for experimental curve and 85.8 bar at 8.85° aTDC for the simulated one. Pressure trends are very similar and often overlapping, such as before SOI and during the expansion phase. The two curves are slightly different only during the combustion event because the simulated pressure curves grows with a constant trend after SOI timing and ignition; on the contrary the experimental one is characterized by a wave-like behaviour. The adoption of a square wave for injection law is a big assumption and it reduces the reliability on correct pressure curve details because small pressure rate variations can not be provided by any calculations.
Figure 7.5b displays the AHRR curves, computed as before from pressure curves. The experimental AHRR shows a slightly slower increase but globally the results are satisfactory.
Figure 7.4 shows the combustion event displaying an isosurface for Z stoichiometric value

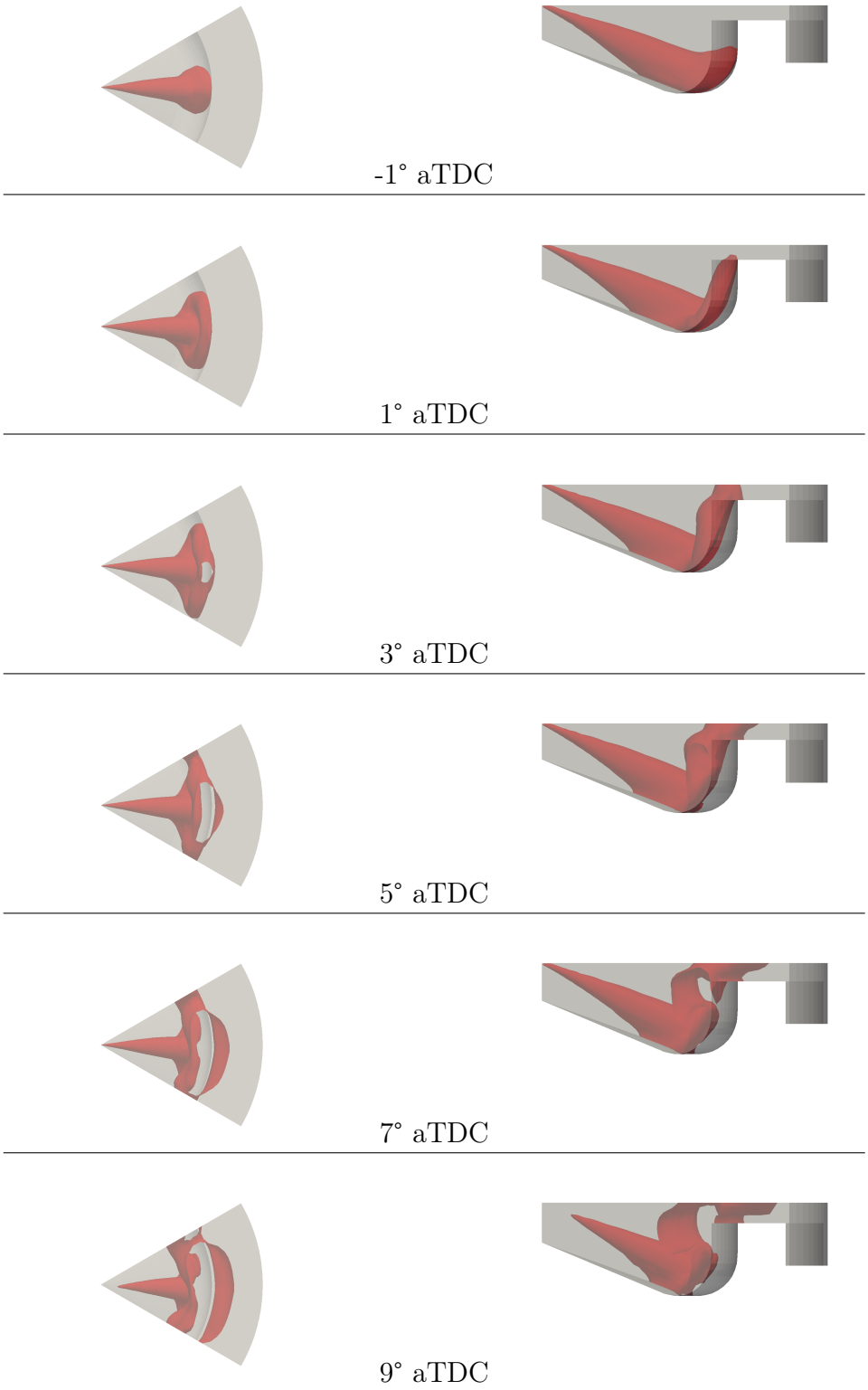

Figure 7.4: CAT 3401: diesel combustion represented by stoichiometric mass fraction value ($Z = 0.062$).

behaviour. With a comparison of Figure 7.4 and Figure 7.5b it can noticed that the decreasing behaviour of AHRR in Figure 7.5b between 1° bTDC and 0° aTDC could be related to the contact and interaction between flame and piston bowl wall in Figure 7.4. After 1° aTDC the Z stoichiometric diffuses in all the combustion chamber, with a simultaneous increase of combustion rate and of AHRR.

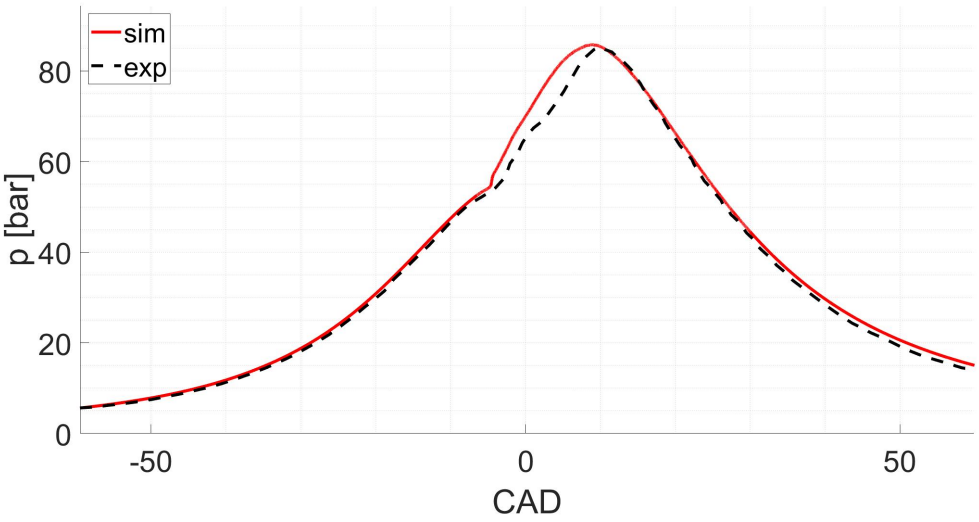

(a) Pressure curves: experimental and simulated.

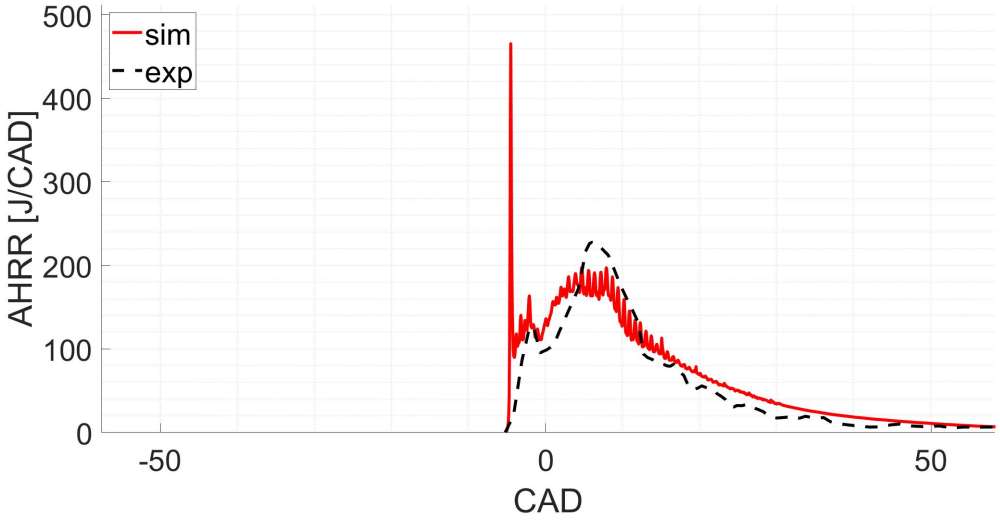

(b) AHRR curves: experimental and simulated.

Figure 7.5: CAT 3401 only diesel second simulation: pressure and AHRR.

7.3. Diesel-ammonia simulations

The diesel simulation helps to set more precisely the simulations conditions. After this step, the ammonia DDF simulation can start with the adoption of the ammonia injection specifications listed in Table 7.2. As done before with diesel simulation, the listed diesel SOI is advanced from 14.2° bTDC to 6.2° bTDC and the listed diesel EOI is delayed by 5 CAD. Also for the ammonia DDF cases the diesel injection laws are undefined so they are assumed as a square-like curve included between the modified SOI and EOI. Figure 7.6 shows diesel injection laws for each ammonia energy fraction case.

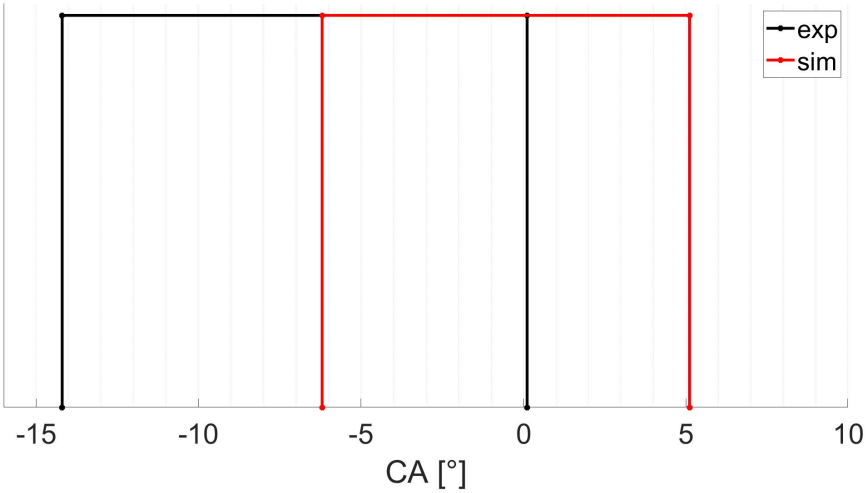

(a) Ammonia energy fraction: 20%.

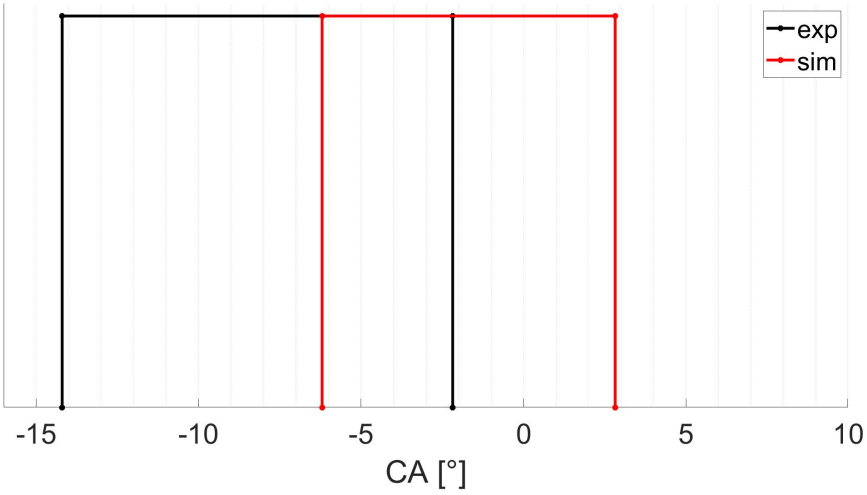

(b) Ammonia energy fraction: 40%.

Figure 7.6: CAT 3401: experimental diesel injection laws for ammonia DDF and the ones adopted for the simulation on ammonia energy fraction equal to 20% and 40%.

The simulation starts at IVC and it ends at EVO, without considering the intake phase and the mixture distribution inside the cylinder. Because of this simplification, ammonia mass is considered as equally distributed in all the CFD domain.
Diesel-ammonia simulations are performed accordingly to the condition listed in Table 7.2: ammonia energy fractions equal to 20% and to 40% are simulated and compared with experimental data. After these simulations, the effects of diesel SOI advancing are investigated at ammonia energy fraction fixed to 40%.

7.3.1. Diesel-ammonia simulation with 20% of ammonia energy fraction

The first ammonia DDF simulation is finally carried out with an ammonia energy fraction equal to 20%. Figure 7.7 shows the resulting pressure and AHRR curves. This attempt to simulate diesel ammonia combustion is the first attempt done using this solver.
The comparison between the simulated and the experimental pressure curves in Figure 7.7a shows similar trends and more specifically the SOI conditions are matched. Globally, experimental curve and simulated one are quite analogous. The simulated pressure peak and the experimental one are very close, respectively 83.8 bar at 8.3° aTDC and 83.6 bar at 9.1 aTDC. After the diesel ignition, simulated pressure starts to grow in a different way compared to diesel simulation (see Figure 7.5a): the different pressure increase rate between ammonia DDF and diesel-only mode is related to the ammonia-diesel interaction and the slower ammonia combustion with respect to the diesel one. The experimental pressure curve after diesel ignition does not grow constantly but substantially with two steps. This shape can be due to a fast diesel combustion during the injection and a slow flame propagation in ammonia. The adoption of a square wave as injection law is quite a rough assumption but it is needed to complete the simulation setup believing that a simplification is acceptable to obtain a results.
The experimental and simulated AHRR curves displayed in Figure 7.7b are computed from pressure curves, as done in other simulations. They have similar shape with both of them showing two peaks. The first one is overestimated by the simulation and a small delay is visible; also the second one is overestimated but a bit advanced. After diesel ignition, the simulation AHRR curve starts to grow at a fast rate but a change of growing rate is present around 0° aTDC. This change in slope is linked to the Weller combustion model because this discontinuity point is a side effect of the occurring transition from diffusive to premixed combustion. After the end of the transition to premixed combustion, the simulated curve has a steeper course. A deeper investigation about model parameters and diffusive to premixed transition might help reducing the AHRR peak delay, resulting

a steeper growing.

A small delay in the fuel ignition is detected by looking at Figure 7.7b because the experimental curve starts to grow a little earlier and with a steeper behaviour with respect to the simulated one; same happens in Figure 7.7a. However, the assumptions about SOI timing and about injection law undermine the foundations of any considerations about ignition delay. The general combustion event for this configuration is displayed in Figure 7.8 through the visualization of an isosurface of the normalized progress variable c,

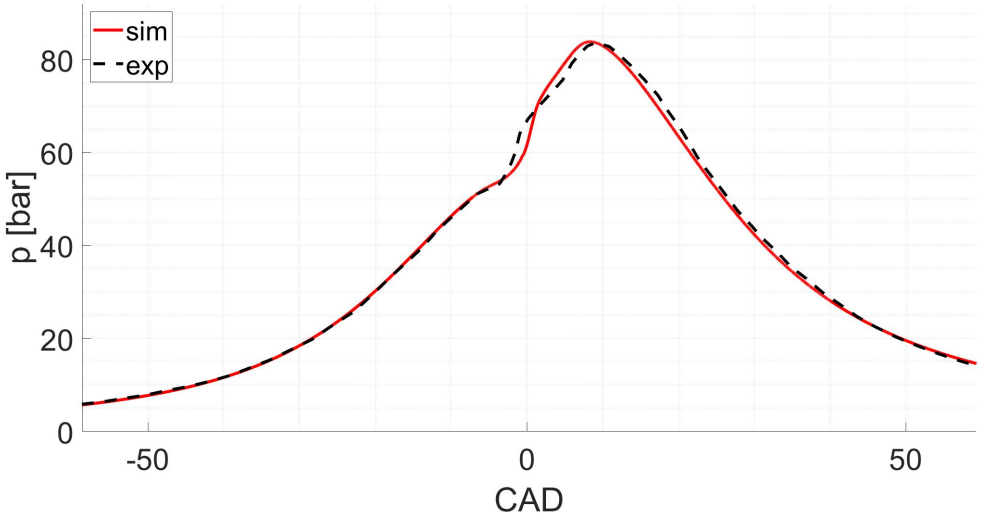

(a) Pressure curves: experimental and simulated.

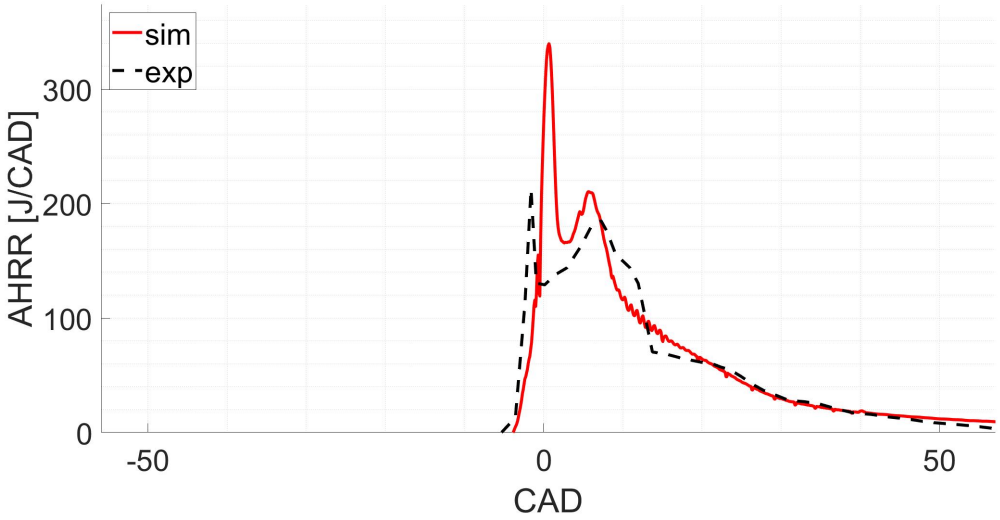

(b) AHRR curves: experimental and simulated.

Figure 7.7: CAT 3401 diesel-ammonia simulation: pressure and AHRR for the 20% ammonia energy fraction case.

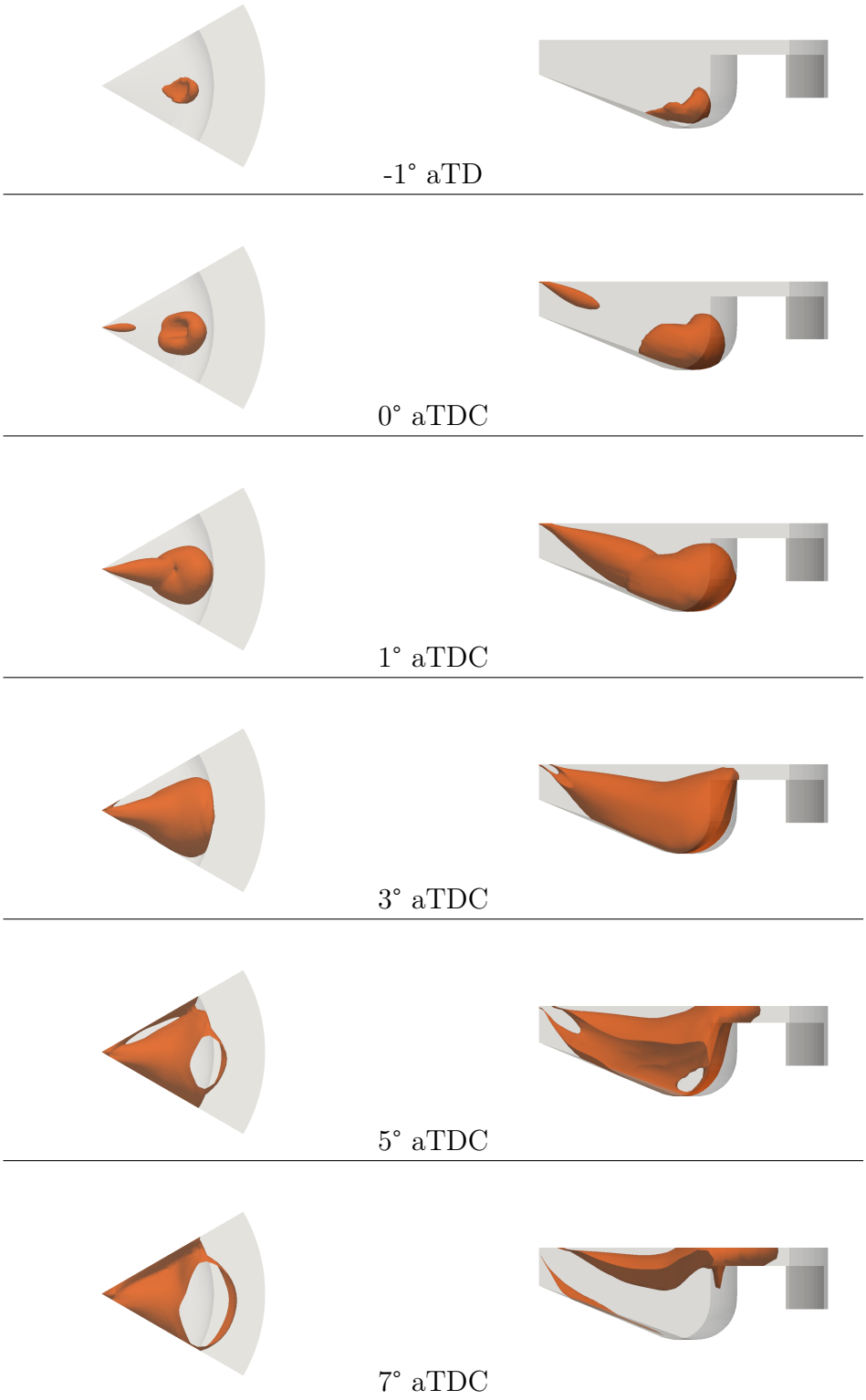

Figure 7.8: CAT 3401: ammonia DDF combustion (20% ammonia energy fraction) represented using an isosurface of the normalized progress variable $c = 0.5$.

defined in Equation (4.5), with $c = 0.5$. The presence of a ignition event near the injector hole is unexpected; some considerations about it are done in Section 7.3.2.

7.3.2. Diesel-ammonia simulation with 40% of ammonia energy fraction

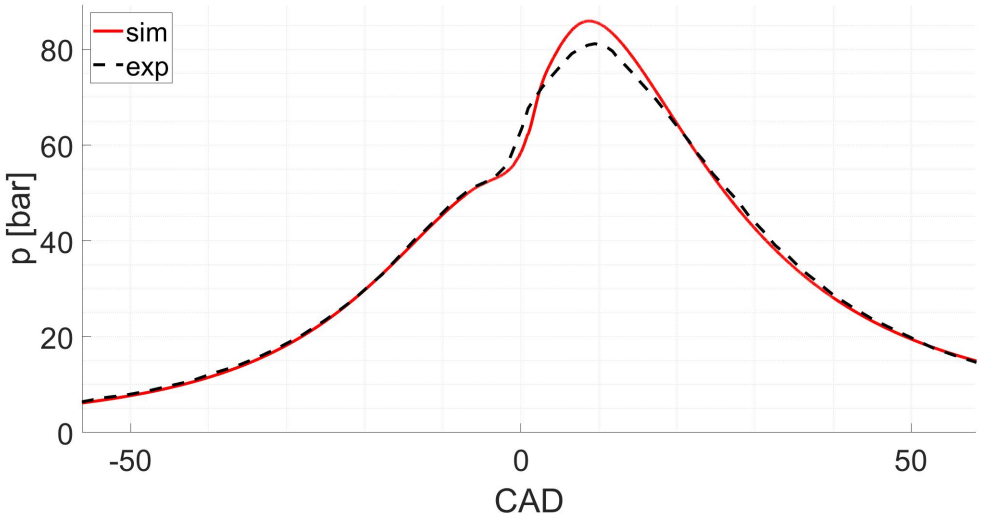

(a) Pressure curves: experimental and simulated.

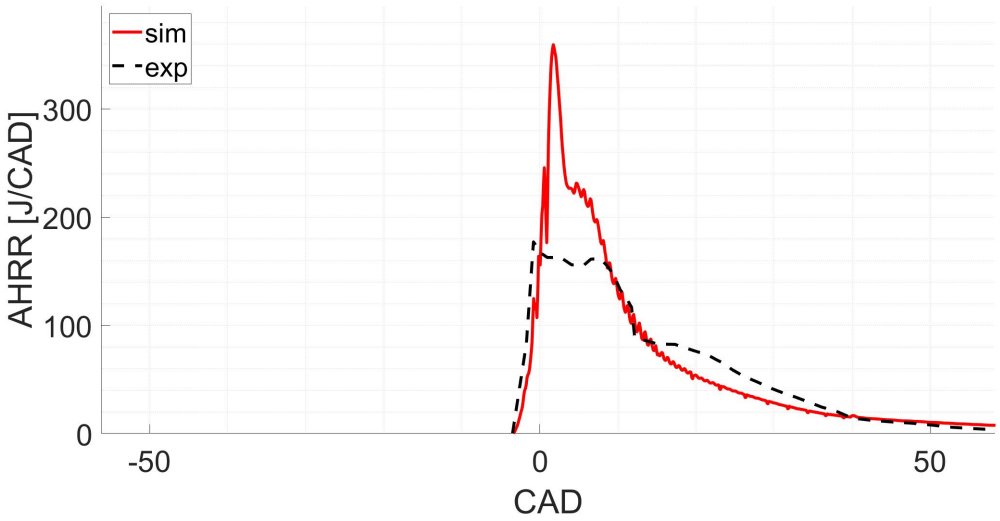

(b) AHRR curves: experimental and simulated.

Figure 7.9: CAT 3401 diesel-ammonia simulation: pressure and AHRR for the 40% ammonia energy fraction case.

The second ammonia DDF configuration is the 40% ammonia energy fraction configuration: pressure and AHRR curves can be found in Figure 7.9. These settings are

characterized by higher ammonia quantity, same SOI but shorter diesel injection duration than the previous configuration in Section 7.3.1. The diesel injection law is displayed in Figure 7.6b.

Pressure curves comparison in Figure 7.9a shows a pressure overestimation by the simulation; the difference is not very large, around 5 bar, with a percentage error about 6%. The simulated pressure peak is located at 8.6° aTDC with a value of 85.9 bar and the experimental one is 81.2 bar at 9.5 aTDC. The simulation results are acceptable for a first attempt, also because of the done assumptions. The SOI conditions are well matched by the simulation because at SOI the two curves are overlapped. After SOI, the experimental pressure curve starts growing before the simulated curve and a small ignition delay is detected by the simulation. After the ignition, the simulated pressure grows faster and exceeds the experimental values. Considerations about the ignition delays are not suitable for this case because of the assumed ignition delay. After the validation performed by engine simulations with diesel-only, SOI and EOI timings are modified with respect to the experimental data setup and they are assumed as in Figure 7.6b. SOI assumption, together with the assumption about the injection law shape, reduces the simulation reliability around the ignition event timing.

However, AHRR curves are quite different because the experimental one is characterized by a almost constant section after a bit higher peak. The diffusive to premixed combustion transition can be noticed also here because of the large simulated AHRR discontinuity around 1° aTDC. The global AHRR behaviour suggests that simulation presents slightly faster combustion than the experimental case: simulated AHRR presents higher peak, basically no constant section and faster decrease. More specifically, at about 20-25° aTDC the experimental curve shows higher AHRR, meaning larger fuel quantity is still burning.

A representation of the combustion event is displayed in Figure 7.10 representing an isosurface of $c = 0$. Figure 7.10 at 1° aTDC time shows a second ignition near the injector hole and this event is quite strange.

This unexpected event depends on diffusive to premixed combustion transition, which ends slightly before 1° aTDC (more precisely at 0.855° aTDC). Figure 7.11 shows the generation of this second premixed combustion by displaying the c behaviour. c field does not present any particular distribution at 0.75° aTDC, just before the transition. Just after the transition, a second premixed combustion begins near the injection hole. This widespread combustion might be the main cause for the faster combustion and the peak overestimation. Figure 7.11c shows the behaviour of this second ignition at 1.75° aTDC: after its generation, the second ignition diffuses and it tends to join with the other main combustion. More detailed investigations should be done to understand the cause of this second ignition near the injector hole and all the therefrom deriving effects.

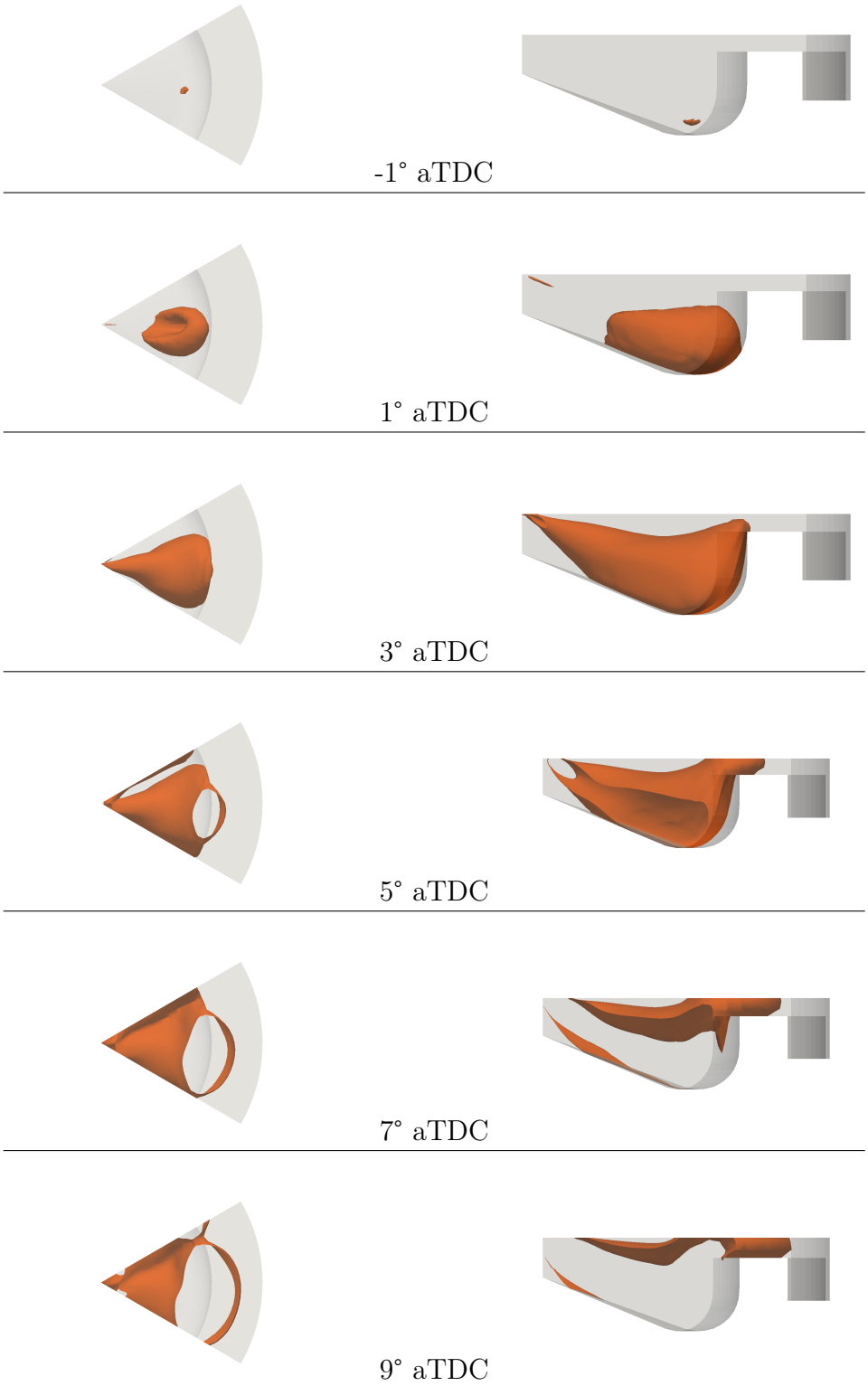

Figure 7.10: CAT 3401: ammonia DDF combustion (40% ammonia energy fraction) represented using normalized progress variable = 0.5.

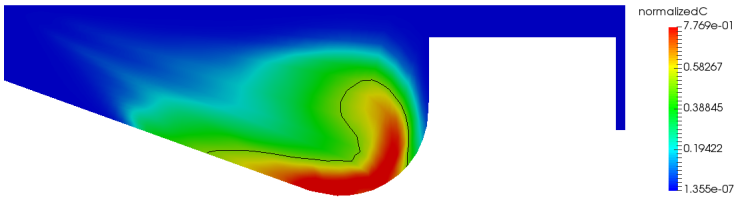

(a) Normalized progress variable at 0.75° aTDC .

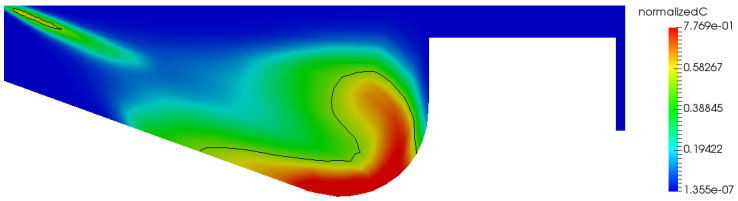

(b) Normalized progress variable at 1° aTDC . A second ignition can be noticed near the injection hole.

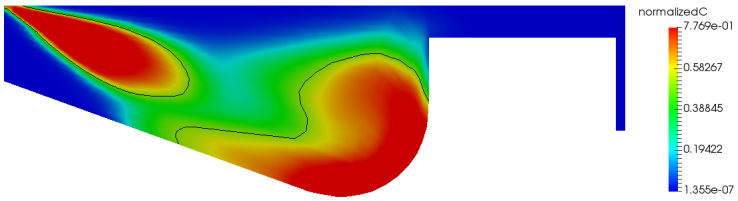

(c) Normalized progress variable at 1.75° aTDC . The second ignition joins the first one injection hole.

Figure 7.11: CAT 3401 diesel-ammonia simulation: normalized progress variable c at 0.75°, 1.00° and 1.75° aTDC in a slice on the injection axis. The dark line represents $c = 0.5$.

The representations of the two combustion event in Figure 7.8 and Figure 7.10 are useful also to understand the effect of ammonia quantity and ammonia burning difficulties on the ignition time.
In Figure 7.10 higher ammonia quantity is spread inside the cylinder and the combustion is slower with respect to the case of Figure 7.8. The SOI is the same for both of them but the ignition happens much before in the 20% ammonia energy fraction case. The normalized progress variable c of the 40% ammonia energy fraction case spreads inside the combustion chamber later than the 20% ammonia energy fraction case, leading to a slower c values growth. For example, the unexpected second ignition near the injection hole is present in Figure 7.8 already at 0° aTDC while it is barely visible at 1° aTDC in Figure 7.10. The longer ignition delay at increasing ammonia quantity can be detected also in Figure 7.12 which compares pressure curves at 0%, 20% and 40% ammonia energy fractions. Another important aspect that can be detected in Figure 7.12 is that diesel-ammonia DF engines can reach pressure values very similar to the diesel-only one. In addition, pressure curves at 0% and 40% ammonia energy fractions show similar pressure peak but the curve at 40% is overestimated with respect to the experimental one (see Figure 7.9a).

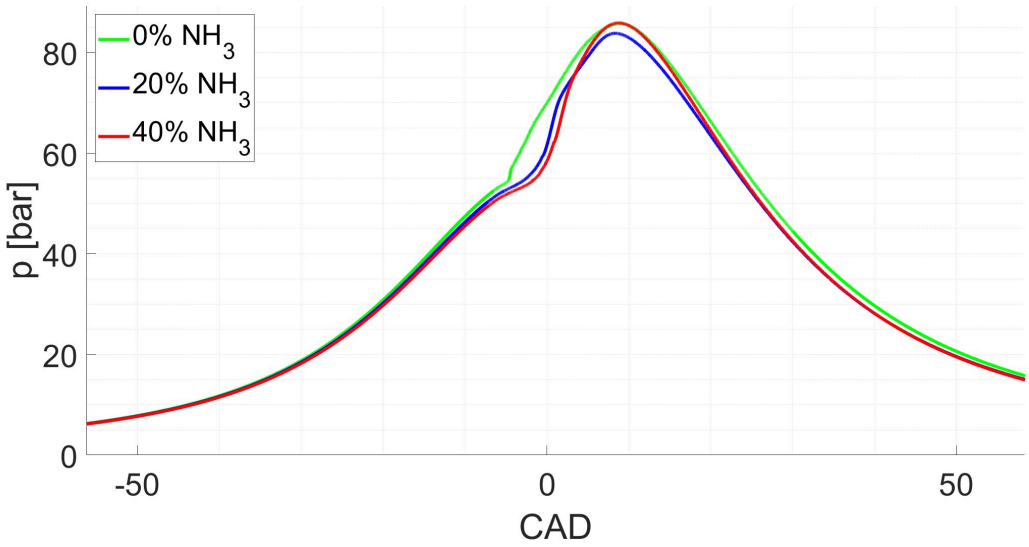

Figure 7.12: CAT 3401 diesel-ammonia simulation: simulated pressure curves for for 0%, 20% and 40% ammonia energy fraction cases.

A further consideration should be done about the ammonia quantity effect on the simulation results. The 20% ammonia energy fraction simulation presents a practically perfect overlap in Figure 7.7a between the simulated pressure curve and the experimental one. Instead a pressure overestimation is present in the case characterized by higher ammonia

energy fraction (which means larger ammonia quantity), as it is evident in Figure 7.9a. For a better model validation it would be useful to have the possibility to compare simulation and experimental tests with other amounts of ammonia, both larger and lower, focusing on the possible dependence of pressure overestimation from the ammonia amount. If simulated combustion is faster because of some inaccuracies in the ammonia combustion, larger ammonia quantity will lead to larger error.

7.3.3. Diesel-ammonia simulation: diesel SOI advancing in diesel-ammonia engine with 40% of ammonia energy fraction

A second series of experimental data are available in the work done by Yousefi et al.[2]. These tests focus on the SOI timing effects on engine performance, keeping the ammonia energy fraction fixed to 40%. The experimental conditions are listed in Table 7.3. In the simulations the SOI and the EOI values listed in table are delayed respectively by 8 and 5° aTDC to be coherent with the previous analysis.

NH_3 energy fraction	**Diesel SOI (° bTDC)**	**Diesel EOI (° aTDC)**	**Diesel mass (kg/h)**	**NH_3 mass (kg/h)**	**Air mass (kg/h)**
40	-14.2	-2.18	2.08	3.18	78.11
40	-16	-4.25	2	3.06	78.56
40	-18	-6.41	1.98	3.02	78.47
40	-20	-8.38	1.97	3.04	78.37
40	-22	-10.42	1.93	2.98	78.41
40	-24	-12.31	1.96	3.01	77.78

Table 7.3: Caterpillar 3401 engine test 2: main injection parameters [2].

Among all the CI engine parameters, the injection start time is one of the most important because it greatly affects engine performance. The optimal SOI is the basic requirement for a good combustion process, for an high efficiency and for the optimal pollutant emissions. In conventional diesel engine advancing the SOI implies advanced start of combustion, higher cylinder peak pressure and higher efficiency because of better diesel-air premixing. However, an excessive SOI advancing does not lead to much higher efficiency, but instead it leads to combustion instability then to engine instability.
Figure 7.12 displays simulated and experimental pressure and AHRR curves obtained by the simulation of each SOI conditions.

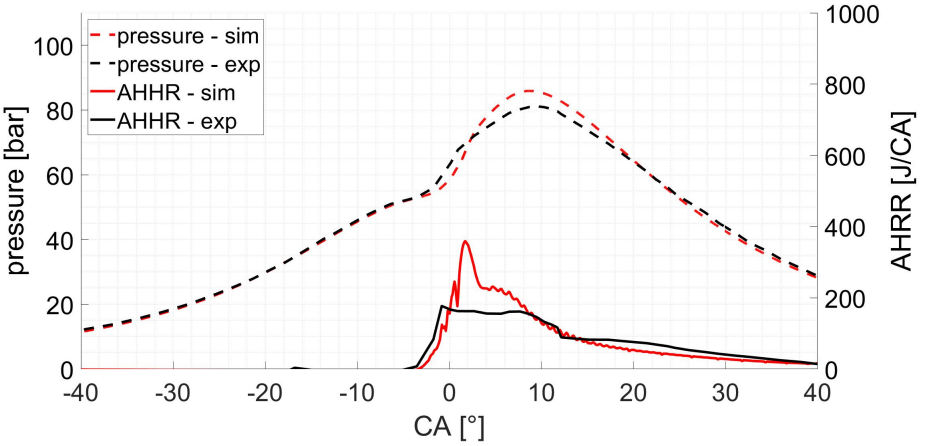

(a) SOI at 14.2° bTDC: experimental and simulated pressure curves.

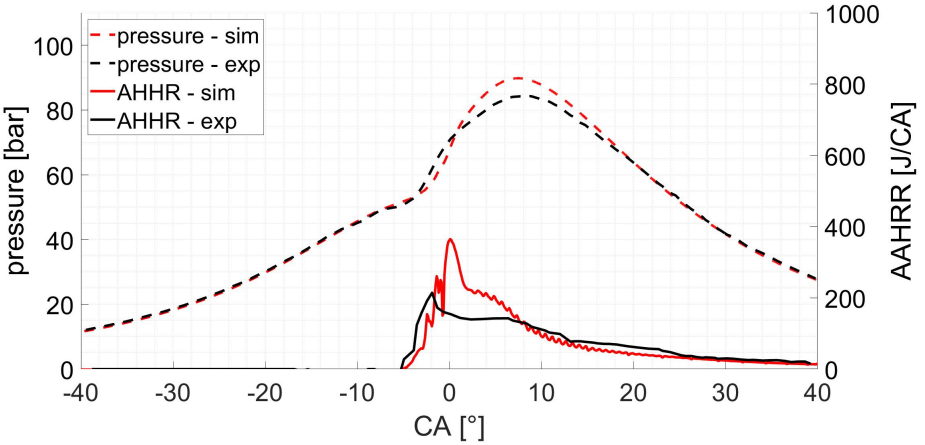

(b) SOI at 16° bTDC: experimental and simulated pressure curves.

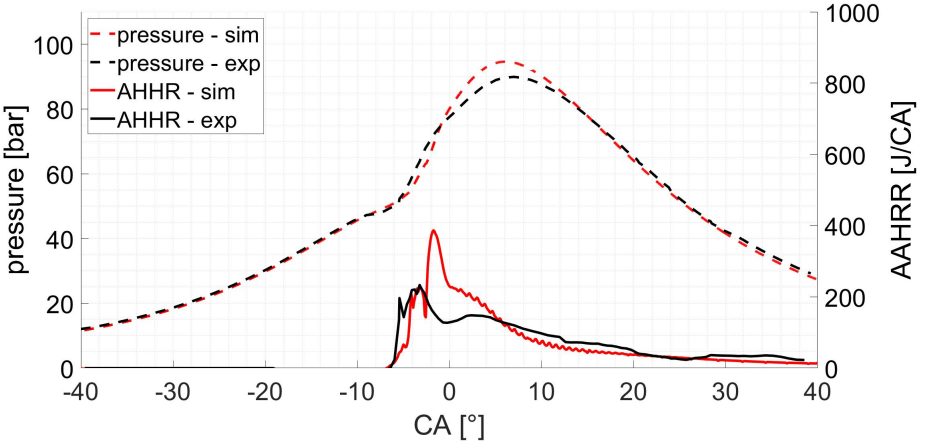

(c) SOI at 18° bTDC: experimental and simulated pressure curves.

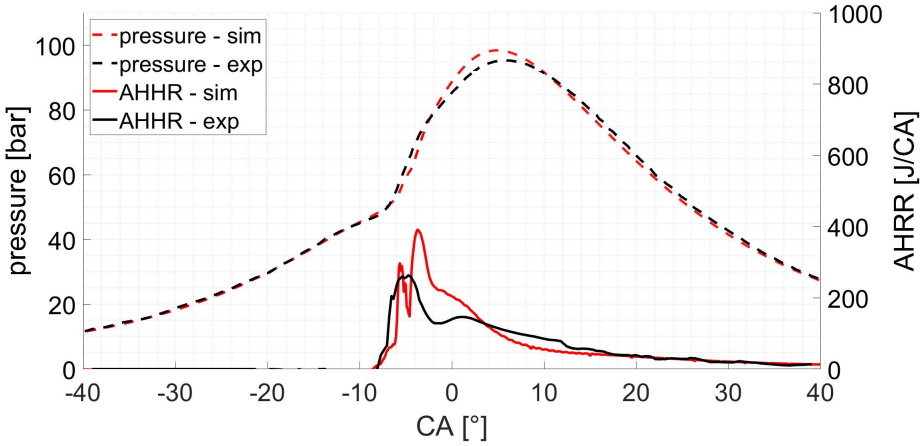

(d) SOI at 20° bTDC: experimental and simulated pressure curves.

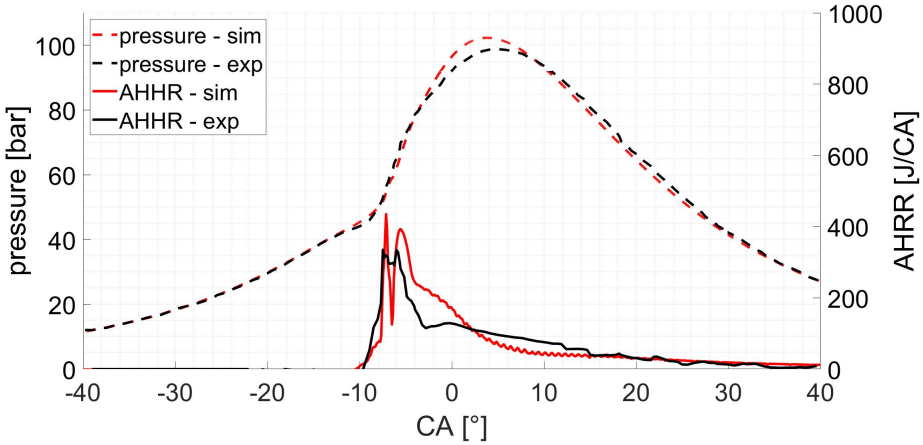

(e) SOI at 22° bTDC: experimental and simulated pressure curves.

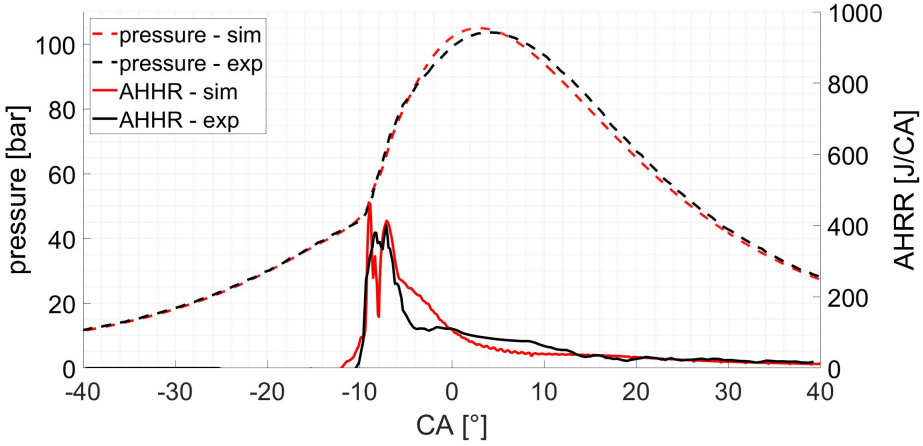

(f) SOI at 24° bTDC: experimental and simulated pressure curves.

Figure 7.12: CAT 3401 diesel-ammonia simulation: comparison between experimental and simulates pressure curves for different SOI values.

$$p_{error} = 100 \cdot \frac{max(p_{sim}) - max(p_{exp})}{max(p_{sim})} \tag{7.2}$$

Experimental pressure curves are matched quite well by simulations because, for example, all the pressure peaks are quite precisely estimated by simulations. Figure 7.13 shows the pressure peak value error, computed as in Equation 7.2 for the corresponding SOI. Globally, p_{error} has a general decreasing trend as the SOI is advance but all the error values are quite low because they are included in an interval between 1% and 6%.
Beside the lower peak pressure error, pressure curves in Figure 7.12 display better performance about the mixture ignition as the SOI is advanced. In fact, just by looking at the plots, it can be noticed that experimental pressure data at high SOI advance are better matched when the pressure starts to rise. This means also more precision of results close to the ignition event. This considerations concerns only the shape of the curves, not the curve timing because of the assumption about the injection. As said before, advancing SOI affects the diesel-ammonia mixture, improving premixing for more homogeneous mixture then improving combustion. The effect of the diesel-ammonia mixture homogeneity on the computational model should be studied carefully, especially to understand if the better diesel-ammonia mixing caused by SOI advance affects the simulation results.

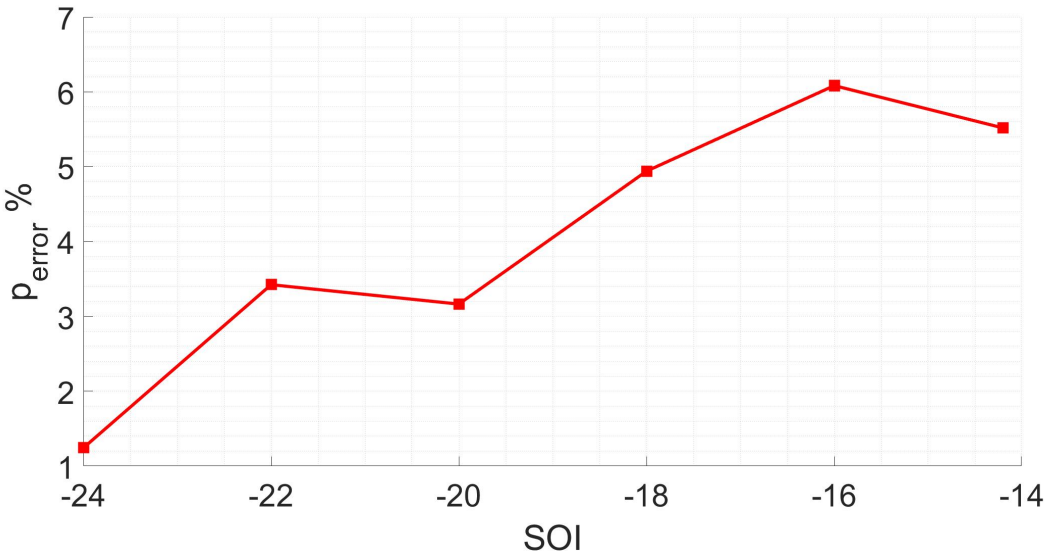

Figure 7.13: Pressure peak value error and corresponding SOI.

A focus on the engine efficiency is done by comparing experimental and simulated gross efficiency. Equation 7.4 computes efficiency starting from the gross work computed by Equation 7.3. Experimental pressure curve is available only for the crank angles interval between 60° bTDC and 60° aTDC therefore a comparison concerning the complete cycle

can not be done.

$$W = \int_{-60}^{60} p \cdot dV \tag{7.3}$$

$$\eta_{gross} = \frac{W}{m_{diesel} \cdot LHV_{diesel} + m_{NH_3} \cdot LHV_{NH_3}} \tag{7.4}$$

As expected, the overall trend shows an efficiency increase as the SOI is advanced, except for the maximum SOI advance, which is characterized by a tiny gross efficiency decrease. The best operating condition seems to be the one with SOI fixed at 22° bTDC; however the values considered here are gross efficiencies therefore the global efficiencies might have different trend.

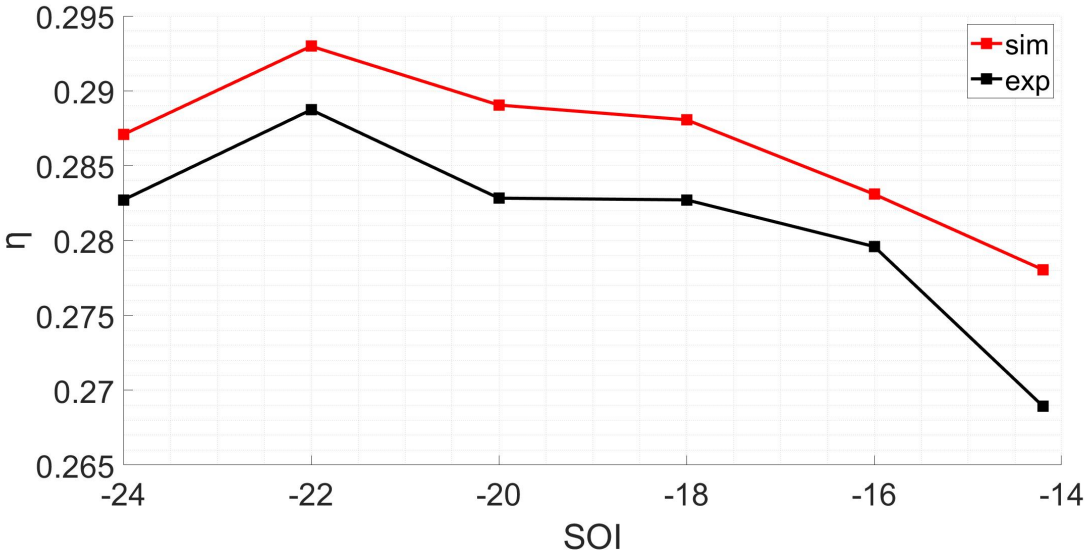

Figure 7.14: Gross efficiency values: experimental and simulated ones at corresponding SOI.

This work focuses only on the evaluation of the engine performances, without considering pollutants and greenhouse gases (GHG) emissions. However, nowadays the best operating condition analysis can not be detached from the pollutant and GHG emissions because of the nature itself of this analysis: the purpose of fueling engines with ammonia is to reduce emissions harmful for humans and for environment. Hence the focus should not be only on best efficiency point, but especially on the lower emission point. This emissions analysis should be a future development to understand which operating conditions make ammonia more beneficial with respect to common fuel.

8 | Conclusions and future developments

Among the proposed alternative fuels, ammonia stands out for its potential. Just as hydrogen, ammonia is marked by a carbon-free combustion because of its null carbon content. However, the use of ammonia instead of hydrogen as a fuel has many advantages, specially for internal combustion engines. Among all, ammonia is one of the most produced chemical compounds. Therefore, ammonia is cheaper and its production facilities, its storage system and its distribution infrastructure are more developed with respect to the hydrogen ones. Moreover, hydrogen density is much lower than ammonia thus hydrogen storage is more complex because of its high pressure and large volume. The use of ammonia as engine fuel for reducing CO_2 engine emissions relies on future improvements for a carbon-free production of ammonia, e.g. higher production efficiency and larger amount of green ammonia.

The use of ammonia for fueling internal combustion engines is not an invention of recent years because the first use dates back to 1822. Over the years the use of ammonia as engine fuel was put aside because of the propensity for gasoline and diesel fuels. Ammonia is usually considered as a non-flammable chemical compound because of its high auto-ignition temperature, because of the high energy level required by ammonia for auto-ignition and because of ammonia low cetane number. These properties are the main cause of the leaving of ammonia as engine fuel. After a short revival during the '60s, ammonia returned to the limelight a few years ago as a good solution to reach the increasingly strict greenhouse gases (GHG) emissions limitations.

Despite the long time passed since the first ammonia application, ammonia remains new in engine field therefore studies and tests are needed for a good implementation.

The purpose of this thesis work is to simulate ammonia combustion in engine field by the use of CFD tools available at Politecnico di Milano. The available CFD solvers are validated and widely used for common fuels (e.g. diesel and methane), but they are not tested for alternative fuels, such as ammonia. The simulation results are compared to experimental data available in literature with a focus on the simulated engine performances

analysis.
During the years, ammonia was tested as fuel for both compression ignition (CI) engine and spark ignition (SI) engine but CI engine is considered a better configuration because of its higher efficiency with respect to SI engine. Nowadays the best and more suitable configuration for an ammonia fueled engine is the ammonia-diesel dual fuel engine. Dual fuel configurations imply the use of two fuels: an high cetane fuel as pilot fuel (e.g. diesel) and a main fuel with low cetane number (e.g. methane, hydrogen or ammonia). Diesel dual fuel (DDF) engines allow both to exploit the benefits of higher efficiency of CI engine and to overcome the bad ignition properties of ammonia. The large nitrogen content of ammonia with respect to conventional fuels might increase the NO_X exhaust emissions, hence the adoption of selective catalytic reduction (SCR) system is essential.
Many configurations are available for DF engines and they mainly differ in the injections order, the injection system and the resulting combustion. This work focuses on two setups: the first one is a diesel dual fuel engine operating in high-pressure direct-injection (HPDI) mode; the second one is a DDF engine working with premixed ammonia.
The first application relies on a four strokes marine MTU 4000 diesel engine modified to be a full optical accessible single cylinder engine in Bowditch design. Experimental data are available for diesel-methane dual fuel mode and in diesel-hydrogen dual fuel mode. Furthermore, simulated data are available for diesel-ammonia DF mode. The basic idea is a simulation model validation through a comparison with experimental data, then the diesel-ammonia DF is simulated. An HPDI engine operates with a pilot injection of diesel and an injection of a low cetane fuel therefore, the result is a combustion diffusive that can be modeled through the tabulated kinetics model. After many assumptions, the experimental data for diesel-methane DF configurations are matched quite well, but simulations for diesel-hydrogen DF mode cannot be acceptable because of the results large error. Many data of the experimental setup of diesel-hydrogen test are missing, therefore, in order to overcome the problem, approximations are introduced on the basis of realistic assumptions. The model works quite well for diesel-methane case. However the error in diesel-hydrogen case implies to reconsider the assumptions on the boundary conditions. The large possibilities of new assumptions does not help in the error investigation, leaving large uncertainties. Thus the starting idea of model validation with diesel-hydrogen configuration then diesel-ammonia DF simulation is not feasible.
The second engine configuration is a single cylinder, four stroke, heavy duty engine derived from a Caterpillar 3401 diesel engine. In this setup, the ammonia is port injected and a diesel pilot injection ignites the ammonia-air mixture: the resulting ammonia combustion is a premixed-like one. The combustion is modeled by the use of an hybrid model which computes diesel ignition with the tabulated kinetics approach, then it switches to

the Weller combustion model for managing the ammonia premixed combustion. Experimental data are available for ammonia DDF under different operating conditions: at constant total energy input, different ammonia energy inputs are tested (0%, 20% and 40%); then the effects of advancing the diesel start of injection (SOI) are tested under ammonia energy input fixed to 40%.
For a first attempt with a tough fuel such as ammonia, the simulations results are very promising. In further studies a deeper analysis of the following aspects is recommended:

- Simulations match quite well the experimental data, with tiny differences in pressure curves. Ignition event needs a deeper analysis because of the unexpected presence of two different premixed combustion events inside the cylinder, one of them close to the injector. Studies about the setup of combustion model parameters and their effects on the combustion event is necessary.
- The first part of diesel-ammonia simulations basically consists in two different ammonia energy input: 20% and 40%. Simulation solver behaves good in both cases but simulation of the case with ammonia energy fraction equal to 40% features a pressure overestimation larger than the case with ammonia energy fraction equal to 20%. More ammonia energy input conditions should be tested to check how the ammonia percentage (then the ammonia quantity) affects the simulation of the diesel-ammonia combustion and if the specific ammonia properties are accurately matched by the model.
- Higher efficiency is one of the main benefits of SOI advance. Simulations are able to detect this increasing trend.
- Diesel SOI advance improves the diesel mixing with the homogeneous ammonia-air mixture, it then leads to an higher pressure peak. The solver features smaller peak pressure error as the SOI advance increases. Therefore, it should be useful to understand if a better mixing of diesel in an homogeneous ammonia-air mixtures affects the simulation reliability.
- Ammonia could be a turning point for a green energy future. A complete ammonia combustion analysis should then involve also pollutant and GHG emissions to determine the best operating condition. This work does not include exhaust emissions analysis because of the time limitations of the project but it can be considered as a preliminary step. Analysis and simulation of exhaust emissions should be done in future.

Bibliography

[1] J. S. Cardoso, V. Silva, R. C. Rocha, M. J. Hall, M. Costa, and D. Eusébio, "Ammonia as an energy vector: Current and future prospects for low-carbon fuel applications in internal combustion engines," *Journal of Cleaner Production*, vol. 296, p. 126562, 2021. [Online]. Available: https://www.sciencedirect.com/science/article/pii/S0959652621007824

[2] A. Yousefi, H. Guo, S. Dev, B. Liko, and S. Lafrance, "Effects of ammonia energy fraction and diesel injection timing on combustion and emissions of an ammonia/diesel dual-fuel engine," *Fuel*, vol. 314, p. 122723, 2022. [Online]. Available: https://www.sciencedirect.com/science/article/pii/S0016236121025886

[3] S. Frankl, S. Gleis, S. Karmann, M. Prager, and G. Wachtmeister, "Investigation of ammonia and hydrogen as co2-free fuels for heavy duty engines using a high pressure dual fuel combustion process," *International Journal of Engine Research*, vol. 22, no. 10, pp. 3196–3208, 2021. [Online]. Available: https://doi.org/10.1177/1468087420967873

[4] L. Sforza, T. Lucchini, G. Gianetti, and G. D'Errico, "Development and validation of si combustion models for natural-gas heavy-duty engines," 09 2019.

[5] T. Lucchini, G. D'Errico, A. Onorati, A. Frassoldati, A. Stagni, and G. Hardy, "Modeling non-premixed combustion using tabulated kinetics and different fame structure assumptions," *SAE International Journal of Engines*, vol. 10, no. 2, pp. 593–607, 2017. [Online]. Available: https://www.jstor.org/stable/26285068

[6] T. Lucchini, A. Della Torre, G. D'Errico, and A. Onorati, "Modeling advanced combustion modes in compression ignition engines with tabulated kinetics," *Applied Energy*, vol. 247, pp. 537–548, 2019. [Online]. Available: https://www.sciencedirect.com/science/article/pii/S0306261919307081

[7] H. Barths, C. Hasse, and N. Peters, "Computational fluid dynamics modelling of non-premixed combustion in direct injection diesel engines," *International Journal of Engine Research - INT J ENGINE RES*, vol. 1, pp. 249–267, 06 2000.

[8] G. D'Errico, T. Lucchini, F. Contino, M. Jangi, and X.-S. Bai, "Comparison of well-mixed and multiple representative interactive flamelet approaches for diesel spray combustion modelling," *Combustion Theory and Modelling*, 01 2014.

[9] T. Tsujimura and Y. Suzuki, "The utilization of hydrogen in hydrogen/diesel dual fuel engine," *International Journal of Hydrogen Energy*, vol. 42, no. 19, pp. 14 019–14 029, 2017, special Issue on The 21st World Hydrogen Energy Conference (WHEC 2016), 13-16 June 2016, Zaragoza, Spain. [Online]. Available: https://www.sciencedirect.com/science/article/pii/S036031991730318X

[10] C. Zamfirescu and I. Dincer, "Ammonia as a green fuel and hydrogen source for vehicular applications," *Fuel Processing Technology*, vol. 90, no. 5, pp. 729–737, 2009. [Online]. Available: https://www.sciencedirect.com/science/article/pii/S0378382009000241

[11] C. Lhuillier, P. Brequigny, F. Contino, and C. Mounaïm-Rousselle, "Combustion characteristics of ammonia in a modern spark-ignition engine," 10 2019.

[12] E. S. Starkman, H. K. Newhall, R. Sutton, T. Maguire, and L. Farbar, "Ammonia as a spark ignition engine fuel: Theory and application," *SAE Transactions*, vol. 75, pp. 765–784, 1967. [Online]. Available: http://www.jstor.org/stable/44563674

[13] S. Grannell, D. Assanis, S. Bohac, and D. Gillespie, "The fuel mix limits and efficiency of a stoichiometric, ammonia, and gasoline dual fueled spark ignition engine," *Journal of Engineering for Gas Turbines and Power-transactions of The Asme - J ENG GAS TURB POWER-T ASME*, vol. 130, 07 2008.

[14] D. Miura and T. Tezuka, "A comparative study of ammonia energy systems as a future energy carrier, with particular reference to vehicle use in japan," *Energy*, vol. 68, pp. 428–436, 2014. [Online]. Available: https://www.sciencedirect.com/science/article/pii/S0360544214002679

[15] P. Dimitriou and R. Javaid, "A review of ammonia as a compression ignition engine fuel," *International Journal of Hydrogen Energy*, vol. 45, no. 11, pp. 7098–7118, 2020. [Online]. Available: https://www.sciencedirect.com/science/article/pii/S0360319920300124

[16] W. Cornelius, L. W. Huellmantel, and H. R. Mitchell, "Ammonia as an engine fuel," *SAE Transactions*, vol. 74, pp. 300–326, 1966. [Online]. Available: http://www.jstor.org/stable/44460524

[17] J. T. Gray, E. Dimitroff, N. T. Meckel, and R. D. Quillian, "Ammonia fuel —

engine compatibility and combustion," *SAE Transactions*, vol. 75, pp. 785–807, 1967. [Online]. Available: http://www.jstor.org/stable/44563675

[18] H. Newhall and C. U. B. D. of MECHANICAL ENGINEERING., *CALCULATION OF ENGINE PERFORMANCE USING AMMONIA FUEL. 2. DIESEL CYCLE.* Defense Technical Information Center, 1965. [Online]. Available: https://books.google.it/books?id=4GwBkAEACAAJ

[19] E. S. Starkman, G. E. James, and H. K. Newhall, "Ammonia as a diesel engine fuel: Theory and application," *SAE Transactions*, vol. 76, pp. 3193–3212, 1968. [Online]. Available: http://www.jstor.org/stable/44562852

[20] T. J. Pearsall and C. G. Garabedian, "Combustion of anhydrous ammonia in diesel engines," *SAE Transactions*, vol. 76, pp. 3213–3221, 1968. [Online]. Available: http://www.jstor.org/stable/44562853

[21] C. G. Garabedian and J. H. Johnson, "The theory of operation of an ammonia burning internal combustion engine," ARMY TANK-AUTOMOTIVE CENTER WARREN MI, Tech. Rep., 1966.

[22] A. Reiter and S.-C. Kong, "Demonstration of compression-ignition engine combustion using ammonia in reducing greenhouse gas emissions," *Energy & Fuels - ENERG FUEL*, vol. 22, 07 2008.

[23] S. Gill, G. Chatha, A. Tsolakis, S. Golunski, and A. York, "Assessing the effects of partially decarbonising a diesel engine by co-fuelling with dissociated ammonia," *International Journal of Hydrogen Energy*, vol. 37, no. 7, pp. 6074–6083, 2012, xII International Symposium on Polymer Electrolytes: New Materials for Application in Proton Exchange Membrane Fuel Cells. [Online]. Available: https://www.sciencedirect.com/science/article/pii/S0360319911028710

[24] A. A. Boretti, "Novel heavy duty engine concept for operation dual fuel h2–nh3," *International Journal of Hydrogen Energy*, vol. 37, no. 9, pp. 7869–7876, 2012, 7th Petite Workshop on the Defect Chemical Nature of Energy Materials, 14-17 March 2011, Storaas, Kongsberg, Norway. [Online]. Available: https://www.sciencedirect.com/science/article/pii/S0360319912001875

[25] A. Boretti, "Novel dual fuel diesel-ammonia combustion system in advanced tdi engines," *International Journal of Hydrogen Energy*, vol. 42, no. 10, pp. 7071–7076, 2017. [Online]. Available: https://www.sciencedirect.com/science/article/pii/S0360319916335820

[26] C. W. Gross and S.-C. Kong, "Performance characteristics of a compression-ignition engine using direct-injection ammonia–dme mixtures," *Fuel*, vol. 103, pp. 1069–1079, 2013. [Online]. Available: https://www.sciencedirect.com/science/article/pii/S001623611200662X

[27] J. Lasocki, M. Bednarski, and M. Sikora, "Simulation of ammonia combustion in dual-fuel compression-ignition engine," *IOP Conference Series: Earth and Environmental Science*, vol. 214, p. 012081, 01 2019.

[28] M. I. Lamas Galdo, L. Castro-Santos, and C. G. Rodriguez Vidal, "Numerical analysis of nox reduction using ammonia injection and comparison with water injection," *Journal of Marine Science and Engineering*, vol. 8, no. 2, 2020. [Online]. Available: https://www.mdpi.com/2077-1312/8/2/109

[29] ——, "Numerical analysis of nox reduction using ammonia injection and comparison with water injection," *Journal of Marine Science and Engineering*, vol. 8, no. 2, 2020. [Online]. Available: https://www.mdpi.com/2077-1312/8/2/109

[30] S. Grannell, D. Assanis, S. Bohac, and D. Gillespie, "The operating features of a stoichiometric, ammonia and gasoline dual fueled spark ignition engine," *2006 ASME International Mechanical Engineering Congress and Exposition, IMECE2006 - Energy*, 01 2006.

[31] C. Mørch, A. Bjerre, M. Gøttrup, S. Sorenson, and J. Schramm, "Ammonia/hydrogen mixtures in an si-engine: Engine performance and analysis of a proposed fuel system," *Fuel*, vol. 90, no. 2, pp. 854–864, 2011. [Online]. Available: https://www.sciencedirect.com/science/article/pii/S0016236110005132

[32] M. I. Lamas Galdo, L. Castro-Santos, and C. G. Rodriguez Vidal, "Numerical analysis of nox reduction using ammonia injection and comparison with water injection," *Journal of Marine Science and Engineering*, vol. 8, no. 2, 2020. [Online]. Available: https://www.mdpi.com/2077-1312/8/2/109

[33] S. Frigo, R. Gentili, and F. Angelis, "Further insight into the possibility to fuel a si engine with ammonia plus hydrogen," *SAE Technical Papers*, vol. 2014, 11 2014.

[34] S. Haputhanthri, "Ammonia gasoline fuel blends: Feasibility study of commercially available emulsifiers and effects on stability and engine performance," *SAE Technical Papers*, vol. 2014, 10 2014.

[35] S. O. Haputhanthri, T. T. Maxwell, J. Fleming, and C. Austin, "Ammonia and Gasoline Fuel Blends for Spark Ignited Internal Combustion Engines," *Journal of*

Energy Resources Technology, vol. 137, no. 6, 11 2015, 062201. [Online]. Available: https://doi.org/10.1115/1.4030443

[36] F. R. Westlye, A. Ivarsson, and J. Schramm, "Experimental investigation of nitrogen based emissions from an ammonia fueled si-engine," *Fuel*, vol. 111, pp. 239–247, 2013. [Online]. Available: https://www.sciencedirect.com/science/article/pii/S0016236113002433

[37] G. D'Errico, "Advanced combustion modes for ic engines," 2020-2021.

[38] M. Pochet, V. Dias, H. Jeanmart, S. Verhelst, and F. Contino, "Multifuel chp hcci engine towards flexible power-to-fuel: Numerical study of operating range," *Energy Procedia*, vol. 105, pp. 1532–1538, 2017, 8th International Conference on Applied Energy, ICAE2016, 8-11 October 2016, Beijing, China. [Online]. Available: https://www.sciencedirect.com/science/article/pii/S187661021730509X

[39] M. Pochet, I. Truedsson, F. Foucher, H. Jeanmart, and F. Contino, "Ammonia-hydrogen blends in homogeneous-charge compression-ignition engine," *SAE Technical Papers*, vol. 2017-24-0087, 09 2017.

[40] D. Lee and H. Song, "Development of combustion strategy for the internal combustion engine fueled by ammonia and its operating characteristics," *Journal of Mechanical Science and Technology*, vol. 32, pp. 1905–1925, 04 2018.

[41] H. Park, E. Shim, and C. Bae, "Injection strategy in natural gas–diesel dual-fuel premixed charge compression ignition combustion under low load conditions," *Engineering*, vol. 5, no. 3, pp. 548–557, 2019. [Online]. Available: https://www.sciencedirect.com/science/article/pii/S2095809918303515

[42] B. S. Brown, S. N. Rogak, and S. Munshi, "Multiple injection strategy in a direct-injection natural gas engine with entrained diesel," *SAE International Journal of Fuels and Lubricants*, vol. 2, no. 1, pp. 953–965, 2009. [Online]. Available: http://www.jstor.org/stable/26273442

[43] H. Jaaskelainen, "Heavy-duty natural gas engines," 11 2019.

[44] S. Jin, J. Li, L. Deng, and B. Wu, "Effect of the hpdi and ppci combustion modes of direct-injection natural gas engine on combustion and emissions," *Energies*, vol. 14, p. 1957, 04 2021.

[45] S. Iorio, A. Magno, E. Mancaruso, and B. Vaglieco, "Diesel/methane dual fuel strategy to improve environmental performance of energy power systems," *International Journal of Heat and Technology*, vol. 34, pp. S581–S588, 10 2016.

[46] T. Tsujimura and Y. Suzuki, "The utilization of hydrogen in hydrogen/diesel dual fuel engine," *International Journal of Hydrogen Energy*, vol. 42, no. 19, pp. 14 019–14 029, 2017, special Issue on The 21st World Hydrogen Energy Conference (WHEC 2016), 13-16 June 2016, Zaragoza, Spain. [Online]. Available: https://www.sciencedirect.com/science/article/pii/S036031991730318X

[47] J. Gomes Antunes, R. Mikalsen, and A. Roskilly, "An experimental study of a direct injection compression ignition hydrogen engine," *International Journal of Hydrogen Energy*, vol. 34, no. 15, pp. 6516–6522, 2009. [Online]. Available: https://www.sciencedirect.com/science/article/pii/S0360319909008647

[48] S. Ouchikh, M. Lounici, L. Tarabet, K. Loubar, and M. Tazerout, "Effect of natural gas enrichment with hydrogen on combustion characteristics of a dual fuel diesel engine," *International Journal of Hydrogen Energy*, vol. 44, no. 26, p. 13974 – 13987, 2019, cited by: 52. [Online]. Available: https://www.scopus.com/inward/record.uri?eid=2-s2.0-85064081675&doi=10.1016%2fj.ijhydene.2019.03.179&partnerID=40&md5=23d8da6eef560ad21165e098dc91911a

[49] A. Gholami, S. A. Jazayeri, and Q. Esmaili, "A detail performance and co2 emission analysis of a very large crude carrier propulsion system with the main engine running on dual fuel mode using hydrogen/diesel versus natural gas/diesel and conventional diesel engines," *Process Safety and Environmental Protection*, vol. 163, pp. 621–635, 2022. [Online]. Available: https://www.sciencedirect.com/science/article/pii/S0957582022004748

[50] M. Karimi, X. Wang, J. Hamilton, and M. Negnevitsky, "Numerical investigation on hydrogen-diesel dual-fuel engine improvements by oxygen enrichment," *International Journal of Hydrogen Energy*, vol. 47, no. 60, pp. 25 418–25 432, 2022. [Online]. Available: https://www.sciencedirect.com/science/article/pii/S0360319922024739

[51] R. Herweg and R. R. Maly, "A fundamental model for flame kernel formation in s. i. engines," in *International Fuels & Lubricants Meeting & Exposition*. SAE International, oct 1992. [Online]. Available: https://doi.org/10.4271/922243

[52] X. Yang, A. Solomon, and T.-w. Kuo, "Ignition and combustion simulations of spray-guided sidi engine using arrhenius combustion with spark-energy deposition model," *SAE Technical Papers*, 04 2012.

[53] C. R. Choi and K. Y. Huh, "Development of a coherent flamelet model for a spark-ignited turbulent premixed flame in a closed vessel," *Combustion*

and Flame, vol. 114, no. 3, pp. 336–348, 1998. [Online]. Available: https://www.sciencedirect.com/science/article/pii/S0010218097001946

[54] Ömer L. Gülder, "Turbulent premixed flame propagation models for different combustion regimes," *Symposium (International) on Combustion*, vol. 23, no. 1, pp. 743–750, 1991, twenty-Third Symposium (International) on Combustion. [Online]. Available: https://www.sciencedirect.com/science/article/pii/S0082078406803255

[55] S. Gleis, S. Frankl, D. Waligorski, M. Prager, and G. Wachtmeister, "Investigation of the high-pressure-dual-fuel (hpdf) combustion process of natural gas on a fully optically accessible research engine," 08 2019.

[56] S. Frankl and S. Gleis, "Development of a 3d-cfd model for a full optical high-pressure dual-fuel engine," *SAE International Journal of Engines*, vol. 13, 01 2020.

[57] ——, "Development of a 3d-computational fluid dynamics model for a full optical high-pressure dual-fuel engine," *SAE International Journal of Engines*, vol. 13, no. 2, pp. 241–252, jan 2020. [Online]. Available: https://doi.org/10.4271/03-13-02-0017

[58] S. Gleis, S. Frankl, M. Prager, and G. Wachtmeister, "Optical analysis of the combustion of potential future e-fuels with a high pressure dual fuel injection system," 06 2020.

[59] H. Winter, K. Aßmus, C. Redtenbacher, D. Dimitrov, and A. Wimmer, "Cfd simulation-based predesign of an advanced gas-diesel combustion concept," *International Journal of Engine Research*, vol. 22, no. 12, pp. 3460–3474, 2021. [Online]. Available: https://doi.org/10.1177/14680874211035017

[60] G. Ferrari, *Motori a combustione interna*. Esculapio, 2016. [Online]. Available: https://books.google.it/books?id=UOoWxwEACAAJ

[61] Q. Zhou, "Brief review on direct gaseous fuel injection modeling," 2020.

[62] A. Yousefi, H. Guo, and M. Birouk, "Split diesel injection effect on knocking of natural gas/diesel dual-fuel engine at high load conditions," *Applied Energy*, vol. 279, p. 115828, 2020. [Online]. Available: https://www.sciencedirect.com/science/article/pii/S0306261920313064

[63] ——, "Effect of diesel injection timing on the combustion of natural gas/diesel dual-fuel engine at low-high load and low-high speed conditions," *Fuel*, vol. 235, pp. 838–846, 2019. [Online]. Available: https://www.sciencedirect.com/science/article/pii/S0016236118314340

List of Figures

List of Tables

Acknowledgements

I would like to express my heartfelt thanks to Andrea Schirru and to prof. Tommaso Lucchini for assisting and for recommending me during this thesis work.
Thanks also to my family for always supporting me.